Single and Double Beta Decay in Deformed Nuclei

D I S S E R T A T I O N

Zur Erlangung des Grades eines Doktors
der Naturwissenschaften

der Fakultät für Physik
der Eberhard-Karls-Universität zu Tübingen

vorgelegt von

Larisa Pacearescu
aus Târgu-Jiu, Rumänien

2004

Contents

Chapter 1

Introduction

1.1   Early History of the Neutrino

The neutrino was first postulated to exist by Wolfgang Pauli in 1930 [139]. In an attempt to explain the observed continous energy spectrum of the β-electron in β-decay, he proposed the existence of new, light, chargeless, spin 1/2 particles called *neutrons*, which exist in nuclei and are also emitted in the β-decay process. In a legendary letter to a conference in Tübingen,[1] Pauli wrote: "...Nämlich die Möglichkeit, es könnten elektrisch neutrale Teilchen, die ich Neutronen nennen will, in den Kernen existieren..."

In February 1932, James Chadwick discovered the particle we presently call the neutron. Neutrons, however, are heavy and could not correspond to the particle imagined by Pauli. At the Solvay conference in Bruxelles in October 1933, Pauli said, speaking about 'his' particles: "...their mass can not be very much more than the electron mass. In order to distinguish them from heavy neutrons, Mr. Fermi has proposed to name them 'neutrinos'. It is possible that the proper mass of neutrinos be zero... It seems to me plausible that neutrinos have spin 1/2. We know nothing about the interaction of neutrinos with the other particles of matter and with photons..."

Officially, the neutrino was christened by Enrico Fermi to their familiar name, which means 'little neutrons' in Italian. Fermi wrote [66]: "....nach dem Vorschlag von W. Pauli kann man z.B. annehmen, daß beim β-Zerfall nicht nur ein Elektron, sondern auch ein neues Teilchen, das sogenannte 'Neutrino' emittiert wird..."

Carl Anderson, in 1933, discovered the positron. This was the first observed particle of anti-matter. Also in that year, Frederic Joliot-Curie discovered $\beta+$ radioactivity, which is characterized by the emission of a positron instead of an electron as in β radioactivity.

The first calculations of the half-life of double beta decay were performed by Maria Goeppert-Mayer in 1935 while she studied the stability of even-even nuclei over geological time [120]. Applying the new Fermi theory of β-decay to two neutrino double beta decay, a second order process of the weak interaction

$$(A, Z) \rightarrow (A, Z + 2) + 2e^- + 2\bar{\nu}, \tag{1.1}$$

she obtained a lifetime on the order of 10^{17} years.

In 1939, W.H. Furry, following a theory proposed by Majorana, showed that another process, which had not yet been observed, might arise. This process, neutrinoless double beta decay,

$$(A, Z) \rightarrow (A, Z + 2) + 2e^-, \tag{1.2}$$

---

[1]The entire letter can be found in the Appendix.

would have a lifetime longer than that of two neutrino double beta decay "by a factor which ranges from 10^5 to 10^{15} or more" [73]. In this decay, the neutrino would be a virtual particle. Also, the signature would differ in the $2e^-$ energy spectrum by having a sharp peak, in contrast to the continuous spectrum of the neutrino accompanied process.

On July 16, 1945, mankind detonated the first nuclear bomb at the Trinity test range in New Mexico. For physicists, nuclear explosions represented a new and remarkably powerful source of neutrinos. Frederick Reines, who worked at Los Alamos, spoke to Fermi in 1951 about his project to place a neutrino detector near a nuclear explosion. In 1952, Reines met with Clyde Cowan and they agreed to use a more *pacific* source of neutrinos: the nuclear power plant in Hanford, Washington. Their detector was quickly built. The experiment was proposed in February 1953, realized in the spring, and their results came out during the summer of 1953. However, the data they obtained were not convincing. They repeated their experiment in 1956, this time more carefully, at the nuclear reactor in Savannah River, South Carolina. Their improvements to reduce the background noise worked; for the first time the neutrino was detected. Its signature was clearly visible in the detector, well above the background. Reines and Cowan's experimental setup consisted of using a target made from a mixture of roughly 400 liters of water and 80 kg of dissolved cadmium chloride. The anti-neutrino coming from the nuclear reactor interacts with a proton in the target, producing a positron and a neutron: $p + \overline{\nu} \longrightarrow n + e^+$. The positron then quickly annihilates with an electron of the surrounding material, simultaneously producing two 511 keV photons. The neutron slows down until it is eventually captured by a cadmium nucleus, which subsequently decays releasing a gamma-ray. If this gamma-ray and the two photons from the electron-positron annihilation were detected within a window of 15 microseconds, this was the signature to identify the neutrino.

In 1957-58, near the same nuclear power plant, another physicist, Ray Davis, tried to detect neutrinos using carbonate chloride solutions. In his experiment he searched for the process $\overline{\nu_e} + {}^{37}\text{Cl} \rightarrow \text{e}^- + {}^{37}\text{Ar}$ in which and the lepton number is violated. This process is only possible if the neutrino is a Majorana particle ($\nu = \overline{\nu}$). Since he did not find any reaction product ${}^{37}\text{Ar}$, he concluded that the neutrino is a Dirac particle ($\nu \neq \overline{\nu}$).

Furry realized that in neutrinoless double beta decay the neutrino did not necessarily have to be real as in the reactor process, but could be virtual. The virtual exchange in neutrinoless double beta decay has finally proved to be the more sensitive test for Majorana neutrinos ($\nu = \overline{\nu}$) mainly because the phase space of the virtual neutrino is much larger than for the real neutrino in the the Davis experiment. The alternative to the Majorana neutrino is the Dirac neutrino. The formal description of this process is done by introducing a "leptonic charge" which is conserved in beta decay and has a different sign for particle and antiparticle now known as leptonic

number. Electrons and neutrinos are assigned L=1, positrons and antineutrinos L=−1.

A rumor that R. Davis observed ^{37}Ar in his experiment, reached B. Pontecorvo . He came to the conclusion that neutrino oscillations ($\nu \leftrightarrow \bar{\nu}$) could be a possible and natural explanation of the "observed events" and published the first paper on neutrino oscillations [140]. B. Pontecorvo assumed that neutrino and antineutrino, produced in usual weak processes, are different particles and there exists an additional interaction, which transfers neutrinos into antineutrinos. He concluded that in this case "neutrino and antineutrino are *mixed* particles, i.e., a symmetric and antisymmetric combination of two truly neutral Majorana particles ν_1 and ν_2 of different combined parity" [2].

In 1956-57 the violation of parity in the β-decay was discovered by Wu et al. [210]. In 1956 T.D.Lee and C.N.Yang proposed a peculiarity of the neutrinos emitted in the beta-decay and weak interaction processes, namely the left handed chirality for neutrinos and right handed chirality for antineutrinos. If they were Dirac particles with absolutely no mass, neutrinos themselves would violate parity because their spin vectors would always be aligned along their direction of motion, while the spins of antineutrinos would point the opposite way. In the Wu experiment the β-decay of the polarized ^{60}Co was studied and the helicity of neutrinos was observed (1957). The helicity mismatch between the antineutrino emitted by one neutron and the neutrino absorbed by another neutron now forbids this process for a Majorana neutrino as long as the latter is massless, and as long as there are no right-handed currents. The phenomenological theory of weak interactions by Feynman and Gell-Mann [68] and Sudarshan and Marshak [181] in 1958 was based on the assumption that only the left-handed components of all fields are involved in the Hamiltonian of weak interactions. They showed that only a V-A interaction was compatible with parity nonconservation.

1.2 Neutrinos in the Standard Model

The Standard Model proposed by Glashow [79], Weinberg [208] and Salam [152] is the name given to the current theory of fundamental particles and how they interact. This theory includes the strong interactions due to the color charges of quarks and gluons and a combined theory of weak and electromagnetic interaction, known as electroweak theory, that introduces W and Z bosons as the carrier particles of weak processes, and photons as mediators to electromagnetic interactions (Figure 1.1). The theory does not include the effects of gravitational interactions. These effects are tiny under high-energy Physics situations, and can be neglected in describing the experiments. The Standard Model is divided into three sections: quarks, leptons

---

[2]In the first papers on neutrino oscillations B.Pontecorvo considered maximum mixing

and bosons. The quarks and leptons, which are fermions, possess non-integer spin, and in turn are divided into three generations. Each of the fermion particles come in pairs. Quarks are grouped up with down, charm with strange, and top with bottom. The experimental evidence for the top quark was just recently found at Fermilab in 1995. In nature, the quarks always combine together in triplets, called baryons, or in quark-antiquark pairs, called mesons. The two baryons found in nature are the proton and the neutron. The proton is composed of two up and one down quark, while the neutron has two down and one up quark.

The other type of fermions, the leptons, are paired such that the electron, muon and tau particles each have an associated low mass and chargeless neutrino. The electron, like the proton and the neutron (the neutron just in bounded nucleus) is a stable particle and the three compose almost all matter. The muon and tau particles, however, are unstable and are found primarily in decay processes.

The intermediate vector bosons, or force carriers, make up the third section of the Standard Model. The exchange of bosons is the mechanism for three of the four fundamental forces through which matter is known to interact. The gluon is responsible for the most powerful force, the strong force, which binds together quarks inside protons and neutrons, and holds protons and neutron together inside an atomic nucleus. The photon is the electromagnetic force carrier which governs electron orbits and is the dominant force in chemical processes. Lastly, the W and Z bosons mediate the weak force, which plays a role in radioactive decay. The weak force is the mechanism used in the study of neutrinos. Neutrinos are insensitive to the electromagnetic force (due to their lack of charge) and unaffected by the strong force (which governs nuclear interactions), leaving only the weak force to characterize their properties.

One part of the Standard Model is not yet well established. It is not known what causes the fundamental particles to have masses. A way around this deficiency is to introduce another type of intermediate vector boson called, the Higgs particle, Higgs boson, or Higgson. When W and Z particles interact with the Higgs particle, they acquire mass. The simplest idea is called the Higgs mechanism. The Higgs particle has not yet been observed. Today we can only say that if it exists, it must have a mass greater than about 80 GeV/c^2. Searches for a more massive Higgs boson are beyond the scope of the present facilities at SLAC or elsewhere. Future facilities, such as the Large Hadron Collider at CERN, or upgrades of present facilities to higher energies are intended to search for the Higgs particle and distinguish between competing concepts.

In the Standard Model, neutrinos are postulated as massless and left-handed. However, recent experimental observations indicate neutrinos oscillating between different flavors. This strongly implies that neutrinos, though very light, are not massless. In addition, some scientists suggested that the oscillations give a hint to a possible existence of a fourth neutrino: the sterile neutrino, called so because it

Figure 1.1: Elementary particles in the Standard Model.

does not appear to interact with any other particle.

The investigation of neutrino properties is a way to discover new physics beyond the Standard Model. The problem of neutrino masses and mixing is still far from being solved. The finite mass of neutrinos is related to the problem of lepton number violation. The Standard Model strictly conserves the lepton flavor but the Grand Unified Theories, which are extensions of the standard model, violate the lepton flavor conservation at some levels.

1.3   Neutrinos in Grand Unified Theories

In spite of the fact that the Standard Model represents the simplest and most economical fundamental theory which describes jointly weak and electromagnetic interactions, and in spite of the fact that it has been very successful wherever it has been tested, it can not answer many of the fundamental questions. For Example: are neutrinos really massless? If neutrinos have mass, why is this mass much smaller

than that of the corresponding charged leptons? What kind of particles are neutrinos: Dirac ($\nu \neq \overline{\nu}$) or Majorana ($\nu = \overline{\nu}$)? Does neutrino mixing take place? Unable to answer these questions, the Standard Model cannot be considered as the ultimate theory of nature. The theories which unify the electroweak and strong interaction are called Grand Unified Theories. Expectations arising from Grand Unified Theories (GUTs) are that the conservation laws of the Standard Model may be violated to some small degree. Embedding the Standard Model in Grand Unified models, or in supersymmetric or even superstring models, reduces the number of free parameters. In GUTs, the electroweak and the strong interaction are described by one single force with one coupling constant. Mostly , the neutrino has a finite mass and a slight right handed interaction, if the model is right-left symmetric. The non-zero neutrino masses and neutrino mixing appear naturally in many different variants of GUTs like the simplest SO(10) left-right symmetric model [124], minimal supersymmetric standard model (MSSM) and their extensions.

GUTs offer a variety of mechanisms which allow the neutrinoless double beta ($0\nu\beta\beta$) decay. One possibility is via the exchange of a Majorana neutrino between the two decaying neutrons [49, 93, 164, 198]. If the global symmetry associated with lepton number conservation is broken spontaneously, the models imply the existence of a physical Nambu-Goldstone boson, called a Majoron [37, 74, 76, 163], which couples to neutrinos. The Majoron might occur in the Majoron mode of the neutrinoless double beta decay [98]. There are also other possible mechanisms of $0\nu\beta\beta$–decay induced by lepton-number violating quark-lepton interactions of R-parity non-conserving extensions of the SM [123, 198]. A complete analysis of this mechanism within the MSSM for the case where the initial d-quarks are put inside the two initial neutrons (two-nucleon SUSY mode) was carried out in Ref. [98]. Recently, it has been found that a new contribution of the R-parity violating ($\not{R}_p$) supersymmetry (SUSY) to the $0\nu\beta\beta$-decay, via pion exchange, dominates over the two-nucleon $\not{R}_p$ SUSY mode [63]. The R-parity conserving SUSY mechanisms of $0\nu\beta\beta$-decay have been proposed and investigated in Ref. [98]. GUTs also predict a new type of gauge boson, called the leptoquark, which can transform quarks into leptons or vice versa [27]. A new mechanism for $0\nu\beta\beta$-decay based on leptoquark exchange has been discussed in Ref. [99].

1.4 $\beta\beta$-decay – General Aspects and Experimental Status

Double beta decay is a rare spontaneous nuclear transition in which the nuclear charge changes by two units while the mass number remains the same. For a long time, this process has been recognized as a powerful tool to study lepton number

conservation in general, and neutrino properties in particular. Because of the long lifetimes involved in double beta decay, the experiments to detect their occurance are very challenging and have led to the development of many new and broadly valuable techniques to achieve extremely low backgrounds.

The first experiments on double beta decay were undertaken even before the existence of the neutrino was proved directly in the reactor experiment of Reines and Cowan. In 1949, E. L. Fireman searched for electrons from the transition ^{124}Sn $\rightarrow$ ^{124}Te using coincidence counters and observed a signal which corresponds to a half life between 4×10^{15} and 9×10^{15} years. At the same time, M. G. Inghram and J. H. Reynolds looked for the final nucleus and exploited the fact that measurable amounts of the daughter nucleus might accumulate over geological time in ores which are rich in the corresponding parent nucleus. They analyzed a tellurium ore sample which was roughly 1.5 bilion years old and reported evidence for the transition ^{130}Te $\longrightarrow$ ^{130}Xe with a half-life of 1.4×10^{21} years. They attributed their result to the two-neutrino double beta decay of ^{130}Te.

For the $\beta\beta$-decay to proceed, the initial nucleus must be less bound than the final one, but more bound than the intermediate nucleus. These conditions are realized in nature for a number of even-even nuclei (but never for nuclei with an odd number of protons or neutrons). Since the lifetime for $\beta\beta$-decays are always much longer that the age of the universe, both the initial and final nuclei can be found in nature (some of the actinides being the only exceptions). In many of the *candidates*, the transition of two neutrons to two protons is energetically possible, with the largest Q value just above 4 MeV. In a few cases, the opposite transition, which decreases the nuclear charge, is possible but the Q values are typically smaller.

As was mentioned earlier, the double beta decay transition can proceed in several ways. One of them, the 2ν decay (equation 1.1) conserves lepton number, while the other one, the 0ν decay (equation 1.2) violates lepton number conservation and is therefore forbidden in the standard electroweak theory (Figure 1.2). The prospect of discovering the neutrinoless double beta decay mode is the driving force behind much of the interest in this field. It provides a potential window into physics 'beyond the Standard Model'.

Double beta decay, in all its modes, is a second order weak semileptonic process. Hence its lifetime, which is proportional to $(G_F \cos \theta_C)^{-4}$, is very long. (Here $G_F = 1.166 \times 10^{-5} \mathrm{GeV}^{-2}$ is the Fermi coupling constant, and θ_C is the Cabibbo angle.) The neutrinoless decay can be mediated by a variety of virtual particles; in particular by the exchange of light or heavy Majorana neutrinos. The decay amplitude then depends on the masses and coupling constants of these virtual particles. Independent of the actual mechanism of the $0\nu\beta\beta$ decay, its observation would imply that neutrinos necessarily have a nonvanishing Majorana mass [163]. In fact, if the 0ν decay is actually observed, and its rate is measured, one can obtain, at least in principle, a lower limit on that neutrino's mass [107].
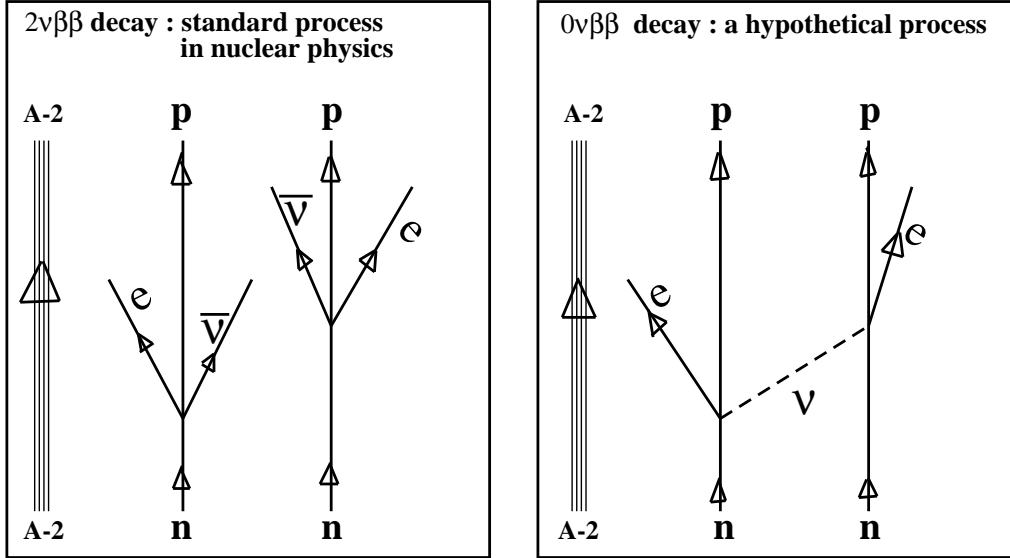
Figure 1.2: Diagrams for $2\nu\beta\beta$-decay (left) and $0\nu\beta\beta$-decay (right) with Majorana neutrinos. By having two particles in the final states in the continuum, the phase space increased by a factor of about 10^6 in the neutrinoless mode compared to the two-neutrino mode.

So far no $0\nu\beta\beta$-decay has been observed. This means (barring artificial complete cancellation of the amplitudes which we dismiss as unnatural) that the upper limit of the decay rate can be interpreted as an independent limit for each of the possible amplitudes of the decay. In particular, we can obtain the limit on the properties of light and heavy virtual Majorana neutrinos. (Other possibilities, e.g., the decays mediated by the new particles predicted by supersymmetry, are discussed in [109, 199].)

The $2\nu\beta\beta$-decay with the Majoron (χ) emission ($0\nu\chi$ mode),

$$(Z, A) \rightarrow (Z + 2, A) + e_1^- + e_2^- + \chi \, , \tag{1.3}$$

belongs to the category of lepton number violating decays, even though the lepton number is formally conserved when χ is assigned the lepton number -2. The hypothetical scalar particle χ, which must in this case be light enough to be emitted in the $2\nu\beta\beta$-decay, is usually associated with a spontaneous breaking of $B - L$ symmetry [36, 74].

Empirically, it is easy to distinguish between the three decay modes listed above, provided the electron energies are measured. The electron sum energy spectra are determined by the phase space of the outgoing leptons and clearly characterize the decay mode, as schematically illustrated in Figure 1.3. (Geochemical or milking experiments, however, cannot distinguish between the different $2\nu\beta\beta$ modes as they
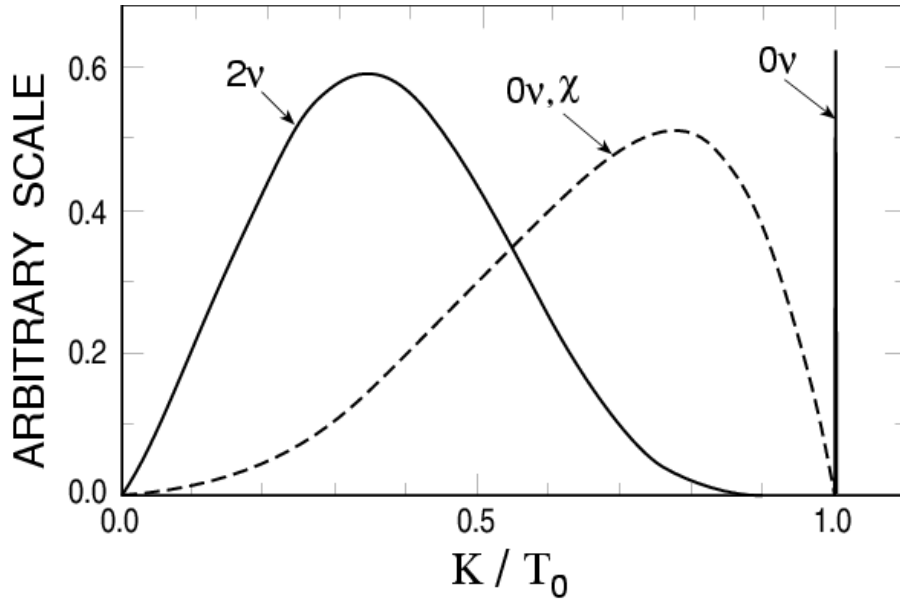
Figure 1.3: Schematic sum electron spectra of the three $\beta\beta$-decay modes. Each is normalized arbitrarily and independently of the others. The abscissa is the ratio K/T_0 of the sum-electron kinetic energy divided by its maximum value.

determine only the total decay rate.)

Both, the $2\nu\beta\beta$-decay and $0\nu\beta\beta\chi$-decay modes have continuous electron energy spectra which differ in the position of their maxima since different numbers of light particles are present in the final state. The signal of $0\nu\beta\beta$-decay will be a sharp peak at the end of the electron-electron coincidence spectrum, whose centroid is the sum of the energies of the two electrons, as long as they carry the full available kinetic energy of this process.

There are two distinct groups of theoretical issues associated with the interpretation of the $\beta\beta$-decay experiments. The particle physics issues deal with the expression of the decay rate in terms of the fundamental parameters, such as the neutrino masses and mixing angles, coupling constants in the weak interaction Hamiltonian, etc. This group of problems also involves the relation of $\beta\beta$-decay to other processes, such as neutrino oscillations, direct mass measurements, and searches for other lepton number violating processes.

The other, essentially decoupled, set of problems involves the nuclear structure issues associated with $\beta\beta$-decay. The decay rate is expressed in terms of nuclear matrix elements (NME) which have to be evaluated. One would like to know, first of all, their value and their uncertainty. This area of research has attracted much attention, and there are many, often conflicting, evaluations available in the literature. Unfortunately, there is no simple way of judging the correctness and the accuracy

of the evaluations of the nuclear matrix elements for the neutrinoless decay. Comparison to the experimentally known rate of the $2\nu\beta\beta$-decay rate is often invoked in that context as a test of the ability of the nuclear model to describe the related phenomena. It is not clear, however, if this is indeed a valid test. For example, if one assumes that the 0ν decay is mediated by the exchange of a heavy particle (whether this exchanged particle is a heavy neutrino or not), then the corresponding internucleon potential is of short range, and additional issues involving nucleon structure, irrelevant for the 2ν decay, play an important role. Another less fundamental but in praxi perhaps more important example deals with the dependence of the NME on the number of single nucleon subshells included in the calculation. For the 2ν decay, where only the Gamow-Teller operator ($\sigma\tau$) plays a role, it is clearly sufficient to include only the states within the valence oscillator shell. It is less clear, however, that the same truncation is sufficient for the correct description of the 0ν decay.

The experimental study of $\beta\beta$-decay presents a formidable challenge since the goal is to detect a process with a half-life on the order of 10^{25} years (the present best limit for the 0ν decay). $\beta\beta$-decay must be detected in the presence of an inevitable background of similar energy caused by trace radioisotopes with half-lives 15 or more orders of magnitude shorter. Thus, the optimum separation of the signal from the background, combined with the requirement of having kilogram quantities of the source isotopes, characterizes the present day experiments.

It is beyond the scope of this dissertation to describe in detail the experimental techniques developed to meet the challenge of background suppression and signal recognition needed to determine the rate (or an interesting limit) of $\beta\beta$–decay. Thus, only the briefest outline is given, and the most important experimental results are summarized in tables.

Historically, the existence of $\beta\beta$-decay was first established using the *geochemical* method. Here one takes advantage of geologic integration times by searching for daughter products accumulated in ancient minerals that are rich in the parent isotope. (The related *radiochemical* method is applicable if the daughter isotope is radioactive.) Since the energy information is long lost, the mode of the $\beta\beta$ decay responsible is not directly determined. Instead, the total decay rate is determined, and thus an upper limit of each mode as well.

One distinguishes directly the mode of decay by measuring the energies of electrons released in the decay in direct counting experiments. The 2ν and $0\nu\chi$ decay modes each result in a rather generic looking electron spectrum (see Figure 1.3), and the observation of these decays requires either extremely efficient background suppression or additional information, such as a tracking capability.

The measured half-lives of the 2ν mode are collected in Table 1.1. Many of them have been measured by several groups; only the results with the smallest claimed errors are shown. (The case of ^{130}Te where the two competing results have the same error but exclude each other is the only exception.) Also, the numerous half-life

Table 1.1: Recent $\beta\beta_{2\nu}$ results.
(Only positive results are listed. The most accurate published values are given, except for ^{130}Te where two conflicting results with the same claimed errors are quoted.)

Isotope	$T^{2\nu}_{1/2}$ (y)	Reference
^{48}Ca $\longrightarrow$ ^{48}Ti	$(4.3^{+2.4}_{-1.1} \pm 1.4) \times 10^{19}$	[10]
^{76}Ge $\longrightarrow$ ^{76}Se	$(1.77 \pm 0.01\ ^{+0.13}_{-0.11}) \times 10^{21}$	[92]
^{82} Se $\longrightarrow$ ^{82}Kr	$(8.3 \pm 1.0 \pm 0.7) \times 10^{19}$	[7]
^{96} Zr $\longrightarrow$ ^{96}Mo	$(3.9 \pm 0.9) \times 10^{19}\ ^{geoch}$	[105]
^{100} Mo $\longrightarrow$ ^{100}Ru	$(6.82^{+0.38}_{-0.53} \pm 0.68) \times 10^{18}$	[44]
^{116} Cd $\longrightarrow$ ^{116}Sn	$(3.75 \pm 0.35 \pm 0.21) \times 10^{19}$	[6]
^{128} Te $\longrightarrow$ ^{128}Xe	$(7.2 \pm 0.4) \times 10^{24}\ ^{geoch}$	[19]
^{130} Te $\longrightarrow$ ^{130}Xe	$(2.7 \pm 0.1) \times 10^{21}\ ^{geoch}$	[19]
	$(7.9 \pm 1.0) \times 10^{20}\ ^{geoch}$	[187]
^{150}Nd $\longrightarrow$ ^{150}Sm	$(6.75^{+0.37}_{-0.42} \pm 0.68) \times 10^{18}$	[44]
^{238}U $\longrightarrow$ ^{238}Pu	$(2.0 \pm 0.6) \times 10^{21}\ ^{radioch}$	[194]

^{geoch} geochemical determination; total decay rate.
^{radioch} radiochemical determination; total decay rate.

limits have been omitted. The 2ν mode is now well established; no doubt many more accurate results will become available soon.

In fact, $\beta\beta$-decay is becoming a valuable tool of nuclear spectroscopy. The decay of ^{100}Mo into the excited 0^+ state at 1130 keV in ^{100}Ru has been observed [13, 30]. The technique used, observation of the subsequent γ decay cascade, can be readily be applied to other nuclei as well. This development not only expands the scope of the experimental study of $\beta\beta$-decay, but also allows more detailed comparisons between theory and experiment (for an early attempt, see [89]).

The 0ν mode can be approached quite differently from 2ν and $0\nu\chi$ modes because of the distinctive character of the 0ν electron sum spectrum – a monoenergetic peak at the full Q–value (see Figure 1.3). Obviously, the narrow width of the peak in 0ν detection is a big advantage which will help to isolate the process from the background. As in the case of the 2ν decay, other capabilities, such as tracking, will naturally help as well.

The best reported limits for the neutrinoless $\beta\beta$ decay modes are collected in Tables 1.2 and 1.3. Again, only the most restrictive limits for the given transitions

Table 1.2: Best reported limits on $T_{1/2}^{0\nu}$ and $\langle m_\nu \rangle$.
The experimental result is listed first with its reference. This is followed by the limit on $\langle m_\nu \rangle$ followed by the reference to the employed nuclear matrix element (NME). Whenever possible the choice of the authors of the experimental paper regarding the NME is respected. See the text for the discussion of uncertainties associated with the evaluation of NME's.

Isotope	$T_{1/2}^{0\nu}$ (10^{22} y) (CL%)	exp. Ref.	$\langle m_\nu \rangle$ (eV)	NME Ref.
^{48}Ca	> 0.95 (76)	[211]	< 18.3	[93]
^{76}Ge	$> 1600(5700)$	[16]	$< 0.4(0.2)$	[179]
^{82}Se	> 2.7 (68)	[59]	< 5	[93]
^{100}Mo	> 5.2 (68)	[51]	< 6.6	[189]
^{116}Cd	> 2.9 (90)	[75]	< 4.6	[179]
$\frac{T_{1/2}(130)}{T_{1/2}(128)}$	$(3.52 \pm 0.11) \times 10^{-4}$	[19]	$< 1.1 - 1.5$	[179, 55]
^{136}Xe	> 44 (90)	[116]	$< 2.3 - 2.8$	[55]
^{150}Nd	> 0.12 (90)	[44]	< 4.0	[179]

are shown. The longest half-life limit, reported for ^{76}Ge by the Heidelberg-Moscow collaboration [16], is based on 24.16 kg·yr of exposure and uses pulse shape discrimination to suppress the background (in the relevant energy region the background is a mere (0.06 ± 0.02) events/(kg·yr·keV)). In that experiment, 7 events were observed in the 3σ region around the 0ν decay Q value, while from the background extrapolation one expects 13 events. Using this lack of background events, an even more stringent limit (the entry in parenthesis in Table 1.2) is obtained.

The limit based on the Te lifetime ratio in Table 1.2 is based on the different Q value dependence of the 0ν and 2ν modes. That this offers a valuable tool has been recognized already in the prophetic early paper by Pontecorvo [141]. Although the corresponding NME are not exactly equal, they are close enough to allow one to use the geochemical lifetime determination in Table 1.3.

1.5   Motivation and goals

As mentioned earlier, the question concerning the mass of neutrinos is still open. The recent experimental evidence that neutrinos are massive particles has considerable impact on different domains of physics: in particle physics, where the description of

Table 1.3: The most restrictive Majoron limits.

Isotope	$T_{1/2}^{0\nu,\chi}$ (y) and (CL %)	$\langle g_{\nu,\chi} \rangle$	Reference
^{48}Ca	$> 7.2 \times 10^{20}$ (90)	$< 5.3 \times 10^{-4}$	[12]
^{76}Ge	$> 1.66 \times 10^{22}$ (90)	$< 1.8 \times 10^{-4}$,	[20]
^{82}Se	$> 2.4 \times 10^{21}$ (68)	$< 2.3 \times 10^{-4}$	[7]
^{100}Mo	$> 5.4 \times 10^{21}$ (68)	$< 7.3 \times 10^{-5}$	[51]
^{116}Cd	$> 1.2 \times 10^{21}$ (90)	$< 2.1 \times 10^{-4}$	[42]
^{128}Te	$> 7.7 \times 10^{24\ geoch}$ (90)	$< 3 \times 10^{-5}$	[19]
^{136}Xe	$> 7.2 \times 10^{21}$ (90)	$< 1.6 \times 10^{-4}$	[116]
^{150}Nd	$> 2.8 \times 10^{20}$ (90)	$< 1 \times 10^{-4}$	[44]

^{geoch} geochemical determination; from total decay rate

non-zero masses and mixing requires the extension of the Standard Model of fundamental interactions; in astrophysics, for the comprehension of various phenomena such as nucleosynthesis; in cosmology with, for instance, the search for dark matter. However, from a quantitative point of view, the neutrino mass is still a research topic and so far the available theoretical and experimental techniques do not provide any exact solution, only qualitative descriptions and limit calculations. The first aim of this dissertation is to go one step further in the qualitative description of the double beta decay from a nuclear structure point of view. To show, on simple grounds, the applicability of commonly used approximations and to take into account new parameters, in particular the nuclear deformation.

The results which are gained using a Woods-Saxon basis (spherical and deformed) within a model incorporating apart from the pairing interaction, the residual particle-hole and particle-particle interaction in the charge-exchange channel. The model is supposed to reproduce the main properties of the nuclei, thus justifying phenomenological concepts. Although the model is simplified, it reveals valuable information on many body systems treated at, and beyond, the mean-field level. In particular, an interesting problem is the effect of the particle-hole and particle-particle correlations in the calculations of the Gamow-Teller transitions (the energy position of GT-giant resonance) and of the $2\nu\beta\beta$ matrix elements. Another interesting problem, which has been examined and treated explicitly, is the effect of deformation in those calculations. In the past, the nuclear structure community has devoted considerable theoretical and experimental efforts to study the single and double beta decay matrix elements. There are some theoretical indications that

taking into account the nuclear deformation will cause the $2\nu\beta\beta$ matrix elements to be strongly suppressed. The nuclear overlap between the mother and daughter nuclei is now very sensitive to the shape of the nuclei. In any case, in order to fix the strengths involved in $2\nu\beta\beta$ calculation, better knowledge about simple beta transitions is necessary. This study has been done, apart from mean field only, also for effective interaction in order to understand which approximation brings more reliable results. A great body of experimental information is also available, therefore, the second aim of this dissertation is to study and compare the theoretical results with the relevant experimental data which have been accumulated in recent years.

Chapter 2

Neutrinos

In the last few years positive oscillation signals have been found in a series of experiments using neutrinos produced with various sources [115, 185]. In view of the importance of this discovery and its implications, a number of projects are running, planned in the near future, or under study in order to address many still open questions about neutrinos. Among them are those concerning their Majorana or Dirac nature, the mass hierarchy and absolute mass scale, the knowledge of the mixing angle θ_{13}, the possible existence of sterile neutrinos and of CP violation in the leptonic sector.

2.1 Neutrino Mass -Theoretical Aspects

2.1.1 Majorana and Dirac neutrinos

Empirically, the neutrino masses are much smaller than the masses of the charged leptons with which they form weak isodoublets. Even the mass of the lightest charged lepton, the electron, is at least 10^5 times larger than the neutrino mass constrained by the tritium beta decay experiments. The existence of such large factors is difficult to explain, unless one invokes some symmetry principle. The assumption that neutrinos are Majorana particles is often used in this context. Moreover, many theoretical constructs invoked to explain neutrino masses lead to this conclusion.

The term "Majorana" is used for particles that are identical with their own antiparticles while Dirac particles can be distinguished from their antiparticles. This implies that the Majorana fermions are two-component objects while the Dirac fermions are four-component. It is worthwhile to discuss, briefly, the formalism needed to describe them. [49]

Massive fermions are usually described by the Dirac equation, where the chirality eigenstates Ψ_R and Ψ_L are coupled and form a four-component object of mass m,

$$i(\hat{\sigma}^\mu \partial_\mu)\Psi_R - m\Psi_L = 0, \qquad i(\hat{\sigma}^\mu \partial_\mu)\Psi_L - m\Psi_R = 0, \qquad (2.1)$$

where $\hat{\sigma}_\mu = (\sigma^0, \vec{\sigma})$, $\sigma_\mu = (\sigma^0, -\vec{\sigma})$ and $(\sigma^0, \vec{\sigma})$ are the Pauli matrices. As written, $\Psi_{L(R)}$ are two-component spinors; the usual four-component bispinors are defined as:

$$\Psi = \begin{pmatrix} \Psi_R \\ \Psi_L \end{pmatrix} \; ; \; \Psi_R = \begin{pmatrix} \Psi_R \\ 0 \end{pmatrix} \; ; \; \Psi_L = \begin{pmatrix} 0 \\ \Psi_L \end{pmatrix} , \qquad (2.2)$$

where $\Psi_{L(R)}$ are just the chiral projections of Ψ, i.e. the eigenstates of $P_{L(R)} = (1 \mp \gamma_5)/2$.

However, Majorana's suggestion [119] allows to use an alternative description of those massive fermions which do not have any additive quantum numbers as either

two-component ψ_R (mass m), or ψ_L (mass m'), which obey independent equations

$$i(\hat{\sigma}^\mu \partial_\mu)\psi_R - m\epsilon\psi_R^* = 0 \ ; \ i(\sigma^\mu \partial_\mu)\psi_L + m'\epsilon\psi_L^* = 0 \ , \tag{2.3}$$

where $\epsilon = i\sigma_y$. The Majorana fields can be also expressed in the four-component form

$$\Psi_L(x) = \left(\begin{array}{c} -\epsilon\psi_L^*(x) \\ \psi_L(x) \end{array} \right) \ , \ \text{and/or} \ \Psi_R(x) = \left(\begin{array}{c} \psi_R(x) \\ \epsilon\psi_R^*(x) \end{array} \right) \ . \tag{2.4}$$

Such a four-component notation is a convention useful to express the charged weak current in a compact form. It is then clear that the Dirac field Ψ, Equation 2.2, is equivalent to a pair of Majorana fields with $m = m'$ and $\psi_L = \epsilon\psi_R^*$. The Lorentz invariant mass term in the neutrino Langrangian can appear in three forms:

$$M_D[\bar{\nu}_R\nu_L \ + \ (\bar{\nu}_L)^c\nu_R^c] \ , \ M_L[(\bar{\nu}_L)^c\nu_L + \bar{\nu}_L\nu_L^c] \ , \ M_R[(\bar{\nu}_R)^c\nu_R + \bar{\nu}_R\nu_R^c] \ , \tag{2.5}$$

where $\nu_{L(R)}$ are the notation for the corresponding neutrino annihilation operators. The first expression in Equation 2.5 is the Dirac mass term (with the mass parameter M_D) which requires the existence of both chirality eigenstates ν_L and ν_R and conserves the lepton quantum number. The second (and third) mass terms are Majorana mass terms, which violate the lepton number and can be present even without the existence of ν_R (for the term with mass parameter M_L) or ν_L (for the term with mass parameter M_R). In general, all three terms might coexist, and then the mass Langrangian must be diagonalized resulting in two generally nondegenerate mass eigenvalues for each flavor. (That is the situation with the generic see-saw mass [212], where it is assumed that $M_R \gg M_D \gg M_L \sim 0$, and the light neutrino acquires the mass $m_\nu \sim M_D^2/M_R$.) In the general situation with N flavors of the left-handed neutrinos ν_L and in addition an equal number N of the right handed neutrinos ν_R, the most general Lorentz invariant mass term of the neutrino Langrangian has the form

$$\mathcal{L}_M = -\frac{1}{2} \left((\bar{\nu}_L)^c \ \ \bar{\nu}_R \right) \mathcal{M} \left(\begin{array}{c} \nu_L \\ \nu_R^c \end{array} \right) \ + \text{h.c.} \ , \ \mathcal{M} = \left(\begin{array}{cc} \mathcal{M}_L & \mathcal{M}_D^T \\ \mathcal{M}_D & \mathcal{M}_R \end{array} \right) \ , \tag{2.6}$$

where ν_L and ν_R are column vectors of dimension N. Here $\mathcal{M}_L$ and $\mathcal{M}_R$ are symmetric $N \times N$ matrices (Majorana masses for the left- and right-handed neutrinos) and $\mathcal{M}_D$ is an arbitrary and generally complex $N \times N$ matrix. The mass matrix $\mathcal{M}$, with real positive eigenvalues $m_1, \ldots, m_{2N}$, is diagonalized by the $2N \times 2N$ unitary matrix

$$\left(\begin{array}{c} \nu_L \\ \nu_R^c \end{array} \right) = \left(\begin{array}{c} U \\ V \end{array} \right) \Phi_L \ . \tag{2.7}$$

The general mixing matrices U and V have N rows and $2N$ columns and Φ_L is a column vector of dimension $2N$ of Majorana-like objects [111]. On the other hand, if

none of the states ν_R exist, or if $\mathcal{M}_R$ is so large that the corresponding states need not be considered, only $\mathcal{M}_L$ is relevant, and only the $N \times N$ mixing matrix U is needed to diagonalize the mass term (and Φ_L has then only N components, naturally). For $\mathcal{M}_L \neq 0$, the $N \times N$ unitary mixing matrix U contains N^2 real parameters. However, N of them correspond to unphysical phases; there are $N(N-1)/2$ angles and $N(N-1)/2$ physically relevant phases describing possible CP violations. (For a discussion of parameter counting, see [111].) In the oscillation experiments that violate only the flavor lepton number, but conserve the total lepton number (such as $\nu_e \rightarrow \nu_\mu$ or $\nu_\mu \rightarrow \nu_\tau$), one can determine, in principle, all angles and $(N-1)(N-2)/2$ phases. These phases, common to the Dirac and Majorana neutrinos, describe CP violation responsible for the possible differences of the oscillation probabilities $\nu_\ell \rightarrow \nu_{\ell'}$ and $\bar{\nu}_\ell \rightarrow \bar{\nu}_{\ell'}$. The remaining $N-1$ phases affect only neutrino oscillation-like processes (in which neutrinos are created in the charged current weak processes and absorbed again in charged current) that violate the total lepton number, such as the $0\nu\beta\beta$ decay. Such phases are physically significant only for Majorana neutrinos; they are unphysical for Dirac neutrinos. This is so because for Majorana neutrinos one cannot perform the transformation $\nu_i \rightarrow \nu_i' = e^{i\alpha_i}\nu_i$, which would violate the selfconjugation property.

2.1.2   Lepton number violation

With the usual assignment of the lepton number, $L(l^-) = L(\nu) = -L(l^+) = -L(\bar{\nu}) = +1$, $0\nu\beta\beta$ decay represents a change in the global lepton number by two units, $\Delta L = 2$. In that respect its observation would be related to the attempts to detect $\bar{\nu}_e$ from the sun, or of ν_e from nuclear reactors. Both of these latter processes represent a kind of "$\nu \leftrightarrow \bar{\nu}$ oscillations", and also are possible only for massive Majorana neutrinos.

For light Majorana neutrinos the lepton number conservation is irrelevant and the 0ν decay is hindered only by the helicity mismatch. However, the "antineutrino" born in association with one of the e^- in the 0ν decay is not fully righthanded, but has a lefthanded component of amplitude $\sim m_\nu/E_\nu$. This lefthanded piece can be absorbed by another neutron which is converted into a proton and the second e^- is emitted. Similar consideration would govern the above mentioned $\nu \leftrightarrow \bar{\nu}$ oscillations. The word "oscillations" in this context is a misnomer, however, since the process (if it exists) would proceed without an oscillatory behavior [72].

The expected branching ratio for the "wrong" neutrinos at low energies, relevant for the sun or nuclear reactors is [114]

$$R \sim \frac{m_\nu^2}{2E_\nu^2}\frac{\sigma^{\bar{\nu}N}}{\sigma^{\nu N}} \sim 10^{-14} , \qquad (2.8)$$

where the numerical factor was derived for $m_\nu \sim 1$ eV, $E_\nu \sim 5$ MeV, and the ratio

of cross sections put to unity. Since the $0\nu\beta\beta$ decay is presently sensitive to such neutrino masses, one cannot expect a signal for this kind of $\nu \leftrightarrow \bar{\nu}$ oscillations until similar sensitivity is achieved.

However, it is also possible that $\bar{\nu}_e$ from the sun are produced in a more complicated, but possibly more efficient way. Let us assume that a transition magnetic moment $\mu_{e,l}$ connects the lefthanded $\nu_{e,L}$ with a righthanded $\bar{\nu}_{l,R}$ of a different flavor, which can subsequently oscillate (by the vacuum or matter enhanced oscillations) into the righthanded and thus observable $\bar{\nu}_{e,R}$, i.e., when neutrinos propagate in a transverse solar magnetic field $B_\perp$ one or both of the sequences $\nu_{e,L} \rightarrow \bar{\nu}_{l,R} \rightarrow \bar{\nu}_{e,R}$ or $\nu_{eL} \rightarrow \nu_{l,L} \rightarrow \bar{\nu}_{eR}$ occurs. Such process requires that the magnetic conversion, which is possible only for the massive Majorana neutrinos and which depends on the product $\mu_{e,l}B_\perp$, and the flavor oscillation, which depends on Δm^2 and $\sin^2 2\theta$, are both present. There is no obvious relation between this process and the neutrinoless $\beta\beta$ decay, except that both require the existence of the neutrino Majorana mass term. (This brief discussion of the magnetic conversion is highly simplified. In reality, the transition magnetic moments ought to be written in terms of mass eigenstates [25].)

Finally, tight experimental limits exist on the total lepton number violating processes which involve both electrons and muons (see [29]), such as the muon conversion

$$\mu^- + (Z, A) \rightarrow (Z - 2, A) + e^+ \ , \tag{2.9}$$

and the muonium-antimuonium conversion

$$\mu^+ \ e^- \rightarrow \mu^- \ e^+ \ . \tag{2.10}$$

The relation of these processes to the $\beta\beta$ decay is, however, not well established.

2.2   Particle physics aspects

The rate of the neutrinoless $\beta\beta$ decay is related to the unknown parameters of the neutrino mass matrix and to the phenomenological parameters describing a generalized semileptonic charged current weak interactions H_W:

$$H_W \ = \ \frac{G_F}{\sqrt{2}} \left[J_L^\alpha (M_{L\alpha}^+ + \kappa M_{R\alpha}^+) \ + \ J_R^\alpha (\eta M_{L\alpha}^+ + \lambda M_{R\alpha}^+) \right] \ + \ \text{H.c.} \ , \tag{2.11}$$

where $J_{L(R)}$ and $M_{L(R)}$ are the lepton and quark left(right)-handed current four-vectors, respectively. The dimensionless parameters η, λ, and κ characterize deviations from the standard model. (Since κ gives a negligible contribution to double beta decay, we will not consider it from now on.) The coupling parameters η and

λ, modified by the neutrino mixing, and denoted then usually as $\langle \eta \rangle$ and $\langle \lambda \rangle$ are unknown (and presumably small).

The lepton sector of the theory contains in general n generations of charged leptons as well as n left- and n right-handed neutrinos. The neutrino mass matrix is the $2n \times 2n$ matrix M

$$M = \left(\begin{array}{cc} M_L & M_D^T \\ M_D & M_R \end{array} \right) \, , \tag{2.12}$$

where M_D is the $n \times n$ lepton number conserving Dirac mass term, and the symmetric $n \times n$ matrices M_L and M_R are the lepton number violating Majorana mass terms. The matrix M has $2n$ real, but not necessarily positive, eigenvalues. Writing the eigenvalues as $m_j \epsilon_j$, one can impose the physically reasonable condition that $m_j \geq 0$. The sign of the eigenvalues of the mass matrix is contained in the phases $\epsilon_j = \pm 1$ which are the intrinsic CP parities of the neutrinos j.

Neutrino oscillation phenomena arise because the "mass eigenstates" of M or, more precisely their chiral projections N_j^L and N_j^R, are not necessarily the familiar weak interaction neutrinos that couple to the known intermediate vector boson W_L and to the hypothetical right-handed boson W_R. The physical "weak eigenstate" or current neutrinos, the n left-handed neutrinos ν_L and the n right-handed ones ν_R' (the prime has been added in order to stress that they are *different* particles), are related to the neutrinos of definite mass by the $n \times 2n$ mixing matrices U and V

$$\nu_L \; = \; U N^L \;\; , \;\; \nu_R' \; = \; V N^R \, . \tag{2.13}$$

The mixing matrices U and V obey the normalization and orthogonality conditions

$$\sum_{j=1}^{2n} U_{lj}^* U_{l'j} \; = \; \delta_{ll'} \; , \;\; \sum_{j=1}^{2n} V_{lj}^* V_{l'j} \; = \; \delta_{ll'} \; , \;\; \sum_{j=1}^{2n} U_{lj}^* V_{l'j} \; = \; 0 \, . \tag{2.14}$$

In the neutrinoless $\beta\beta$ decay the rate depends on the effective parameters which are expressed in terms of the mixing matrices U and V:

$$\begin{aligned} \langle m_\nu \rangle \;\; &= \;\; {\sum_j}' \epsilon_j m_j U_{e,j}^2 \, , \\ \langle \lambda \rangle \;\; &= \;\; \lambda {\sum_j}' \epsilon_j U_{e,j} V_{e,j} \, , \\ \langle \eta \rangle \;\; &= \;\; \eta {\sum_j}' \epsilon_j U_{e,j} V_{e,j} \, , \\ \langle g_{\nu,\chi} \rangle \;\; &= \;\; \frac{1}{2} {\sum_{i,j}}' \left(g_{i,j} \epsilon_i + g_{j,i} \epsilon_j \right) U_{e,i} U_{e,j} \, . \end{aligned} \tag{2.15}$$

Here the prime indicates that the summation is over only relatively light neutrinos. Also, λ and η are the dimensionless coupling constants for the right-handed current

weak interaction, equation(2.11), and $g_{i,j}$ are the coupling constants of interaction between the Majorana χ and the Majorana neutrinos N_i and N_j. For the heavy neutrino one obtains

$$\langle m_\nu^{-1} \rangle_H = \sum_j{}'' \epsilon_j m_j^{-1} U_{e,j}^2 \ , \qquad (2.16)$$

where the double prime indicates that the summation, involving the inverse neutrino masses m_j^{-1}, is over only the heavy neutrino mass eigenstates ($m_j \geq 1$ GeV).

It is now clear that, within the mechanism considered so far, there is no neutrinoless double beta decay if all neutrinos are massless. Not only $\langle m_\nu \rangle$ vanishes in such a case but also $\langle \lambda \rangle$ and $\langle \eta \rangle$ vanish due to the orthogonality condition equation (2.14). Moreover, $\langle \lambda \rangle$ and $\langle \eta \rangle$ vanish for the same reason even if some or all neutrinos are massive but light and therefore the summation in equation(2.15) contains all neutrino mass eigenstates. In that case, however, there is a smaller next order contribution from the mass dependence of the neutrino propagator, which for this purpose can be written as

$$\frac{\gamma_\mu q^\mu}{q^2 + m_j^2} \approx \frac{\gamma_\mu q^\mu}{q^2} \left(1 - \frac{m_j^2}{q^2} \right) \ . \qquad (2.17)$$

The expression for e.g., $\langle \lambda \rangle$ now contains $\sum_j{}' \epsilon_j U_{e,j} V_{e,j} m_j^2$ which clearly shows that a nonvanishing neutrino mass is required.

The presence of the phases ϵ_j in the expression for $\langle m_\nu \rangle$ means that cancellations are possible. In particular, for every Dirac neutrino there is an exact cancellation, since the Dirac neutrino is equivalent to a pair of Majorana neutrinos with the opposite sign of the phases ϵ_j and degenerate masses.

In the general case the neutrinoless double beta decay rate is a quadratic polynomial in the unknown parameters

$$\begin{aligned} [T_{1/2}^{0\nu}(0^+ \to 0^+)]^{-1} &= C_1 \frac{\langle m_\nu \rangle^2}{m_e^2} + C_2 \langle \lambda \rangle \frac{\langle m_\nu \rangle}{m_e} \cos \psi_1 + C_3 \langle \eta \rangle \frac{\langle m_\nu \rangle}{m_e} \cos \psi_2 \\ &+ C_4 \langle \lambda \rangle^2 + C_5 \langle \eta \rangle^2 + C_6 \langle \lambda \rangle \langle \eta \rangle \cos(\psi_1 - \psi_2) \ . \qquad (2.18) \end{aligned}$$

Here ψ_1 and ψ_2 are the phase angles between the generally complex numbers m_ν, λ and η. (However, when CP invariance is assumed $\psi_{1,2}$ are either 0 or π.) The phase space integrals *and* the nuclear matrix elements are combined in the factors C_i. Assuming that we can calculate them, equation (2.18) represents an ellipsoid which restricts the allowed range of the unknown parameters $\langle m_\nu \rangle$, $\langle \lambda \rangle$ and $\langle \eta \rangle$ for a given value (or limit) of the 0ν double beta decay lifetime.

The neutrino propagator is defined in order to evaluate the nuclear matrix elements. Assuming that $\langle m_\nu \rangle^2$ is the only relevant quantity, one can perform the

integration over the four-momentum of the exchanged particle and obtain the "neutrino potential", which for $m_\nu < 10$ MeV has the form

$$H(r, \Delta E) \; = \; \frac{2R}{\pi r} \int_0^\infty dq \frac{\sin(qr)}{q + \Delta E} \; , \qquad (2.19)$$

where $\Delta E = \langle E_N \rangle - 1/2(M_i + M_f)$ is the average excitation energy of the intermediate odd-odd nucleus and the factor R (the nuclear radius) has been added to make the neutrino potential dimensionless.

When the 0ν decay is mediated by the right-handed weak current interaction the evaluation of the decay rate becomes more complicated, since many more terms must be included (see [49, 93, 189]). If the four-momentum of the virtual neutrino is $q_\mu \equiv \omega, \vec{q}$, the neutrino propagator contains

$$\omega\gamma_0 - \vec{q} \cdot \vec{\gamma} + m_j \; .$$

The part of the propagator proportional to m_j is responsible for the neutrino potential equation(2.19). The part containing $\vec{q}$ leads to a new potential related to the derivative of $H(r, \Delta E)$, and the part with ω leads to yet another potential, which is a combination of $H(r, \Delta E)$ and its derivative.

Similarly, there are now also more nuclear matrix elements, which contain in addition the nucleon momenta (i.e., the gradient operators), and depend on the nucleon spins and radii in a more complicated way (e.g., they contain tensor operators). The outgoing electrons are no longer just in the $s_{1/2}$ states, because for some of the operators one of the electrons will be in the $p_{1/2}$ state. The recoil matrix element, which originates from the recoil term in the nuclear vector current is numerically relatively large [189], resulting in more sensitivity to the parameter $\langle \eta \rangle$. The current best limits on $\langle \eta \rangle$ and $\langle \lambda \rangle$ are listed in [29].

2.2.1   The $0\nu\beta\beta$–decay and effective neutrino mass

Here only the simplest case of the left-handed $V - A$ weak currents and light massive Majorana neutrinos is considered. This is the case of current interest provided the neutrino mass revealed in the oscillation experiments is of Majorana character. The more general expressions can be found e.g. in the reviews [49]. (For recent formulation of the general problem, see [138].)

The differential decay rate of the $0\nu\beta\beta$ process is [49]

$$d\Gamma_{0\nu} = 2\pi \sum_{spin} |R_{0\nu}|^2 \delta(\epsilon_1 + \epsilon_2 + E_f - M_i) \frac{d\vec{p}_1}{(2\pi)^3} \frac{d\vec{p}_2}{(2\pi)^3} \; , \qquad (2.20)$$

where $\epsilon_{1(2)}$ and $\vec{p}_{1(2)}$ are total energies and momenta of the electrons and $E_f(M_i)$ is the energy of the final (mass of the initial) nuclear state. The quantity $R_{0\nu}$ is

the reaction amplitude to be evaluated in the second order pertubation theory with respect to the weak interactions. The lepton part of $R_{0\nu}$, involving the emission and reabsorption of the Majorana neutrino of mass m_j, is

$$-i \int \frac{d^4 q}{(2\pi)^4} e^{-iq(x-y)} \bar{e}(x) \gamma_\rho P_L \frac{q^\mu \gamma_\mu + m_j}{q^2 - m_j^2} P_L \gamma_\sigma e^c(y) \ , \qquad (2.21)$$

where $P_L = (1 - \gamma_5)/2$, $\bar{e}(x), e^c(y)$ are the electron creation operators, and q is the momentum transfer four-vector. Since γ_μ anticommute with γ_5, this amplitude is proportional to m_j and the term with $q^\mu \gamma_\mu$ vanishes. After integrating over the energy of the virtual neutrino dq^0, the denominator $q^2 - m_j^2$ is replaced by its residue ω_j / π, where $\omega_j = \sqrt{\vec{q}^{\,2} + m_j^2}$. The amplitude is therefore proportional to $m_j / \omega_j \ll 1$ for light neutrinos. The remaining integration over the virtual neutrino momentum $\vec{q}$ leads to the appearance of the neutrino potentials

$$H_k(r, A_k) = \frac{2R_N}{\pi r} \int_0^\infty dq \frac{q \sin(qr)}{\omega(\omega + A_k)} \ , \ A_{1(2)} = E_m - (M_i + M_f)/2 \pm (\epsilon_1 - \epsilon_2)/2 \ , \ (2.22)$$

where 1 and 2 label the emitted electrons, E_m is the excitation energy of the intermediate nucleus, M_f is the mass of the final nucleus, and r is the distance between the two neutrons that are changed into protons. The factor R_N, the nuclear radius, is introduced in order to make the potential H dimensionless. In the case of the $0\nu\beta\beta$ decay one can use the closure approximation, replacing E_m by an appropriate mean value. (This is justified because we expect that the momentum of the virtual neutrino is determined by the uncertainty relation $q \sim 1/r \sim 100$ MeV, thus the variation of E_m from state to state can be neglected.) The contributions of the two electrons are then added coherently, and thus the neutrino potential to use is

$$H(r) = [H_1(r, A_1) + H_2(r, A_2)]/2 \approx H(r, \bar{A}) \ , \qquad (2.23)$$

where $\bar{A} = \bar{E}_m - (M_i + M_f)/2$ and $\bar{E}_m$ is the average energy of the intermediate nucleus. The potential $H(r)$ only very weakly depends on m_j as long as the neutrino mass is less than ~ 10 MeV. For the ground state to ground state, i.e., $0_i^+ \rightarrow 0_f^+$ transitions, it is enough to consider s-wave outgoing electrons, and the nonrelativistic approximation for the nucleons. The nuclear part of the amplitude then turns into a sum of the Gamow-Teller and Fermi nuclear matrix elements, where the superscript 0ν is used to signify the presence of the neutrino potential $H(r)$:

$$|M_{0\nu}| \equiv M_{GT}^{0\nu} - \frac{g_V^2}{g_A^2} M_F^{0\nu} = \langle f | \sum_{lk} H(r_{lk}, \bar{A}) \tau_l^+ \tau_k^+ \left(\vec{\sigma}_l \cdot \vec{\sigma}_k - \frac{g_V^2}{g_A^2} \right) | i \rangle \ . \qquad (2.24)$$

The summation is over all nucleons, $|f\rangle$ ($|i\rangle$) are the final (initial) nuclear states, and $g_V (g_A)$ are the vector (axial vector) coupling constants. Such an expression is now analogous to the allowed approximation of the ordinary beta decay.

Thus, in the approximations described above, which are quite accurate, the transition amplitude for a Majorana neutrino of mass m_j is simply a product of m_j and the above combination of the nuclear matrix elements. However, since in each of the two vertices an electron is emitted, the mixing amplitude U_{ej} apears in each of them, and the physical reaction amplitude contains the factor U_{ej}^2 (not $|U_{ej}|^2$) and is proportional to the factor

$$\langle m_\nu \rangle = \left| \sum_j m_j U_{ej}^2 \right| \ , \tag{2.25}$$

where the sum is only over light neutrinos with $m_j < 10$ MeV (for heavier ones one cannot neglect the mass in the neutrino propagator, Equation 2.21). The quantity m_ν is the effective neutrino mass. Since U_{ej}^2 and not $|U_{ej}|^2$ appear in m_ν, its value depends on the Majorana phases discussed above. To obtain the decay rate, the reaction amplitude has to be squared, and multiplied by the corresponding phase space integral, which in this case, see Equation 2.20, is simply the two-electron phase space integral proportional to

$$G^{0\nu} \sim \int F(Z, \epsilon_1) F(Z, \epsilon_2) p_1 p_2 \epsilon_1 \epsilon_2 \delta(E_0 - \epsilon_1 - \epsilon_2) d\epsilon_1 d\epsilon_2 \ , \tag{2.26}$$

where E_0 is the available energy (the sum electron kinetic energy peak is at $Q = E_0 - 2m_e$). $F(Z, \epsilon)$ is the usual Fermi function that describes the Coulomb effect on the outgoing electron.

Summarizing, if the $0\nu\beta\beta$ decay is mediated by the exchange of a light massive Majorana neutrino (the assumption that we wish to test), the half-life is

$$[T_{1/2}^{0\nu}(0^+ \rightarrow 0^+)]^{-1} \ = \ G^{0\nu}(E_0, Z) \left| M_{GT}^{0\nu} - \frac{g_V^2}{g_A^2} M_F^{0\nu} \right|^2 \langle m_\nu \rangle^2 \ , \tag{2.27}$$

where $G^{0\nu}$ is the exactly calculable phase space integral, is the effective neutrino mass and $M_{GT}^{0\nu}$, $M_F^{0\nu}$ are the nuclear matrix elements, defined in Equation 2.24. The way these nuclear matrix elements are evaluated, and the associated uncertainty, is discussed in the next Section. (As explained earlier, the neutrino mass appears in the amplitude in the combination $m_j/\omega_j \ll 1$; the denominator ω_j has been absorbed in the neutrino potential $H(r)$.) Thus, if an upper limit on $0\nu\beta\beta$ rate is experimentally established, and the nuclear matrix elements are known, one can deduce the corresponding upper limit on m_ν. On the other hand, if $0\nu\beta\beta$ is observed, one can deduce the appropriate value of m_ν. That is a justified procedure, however, only if the exchange of the light Majorana neutrino, discussed above, is indeed the mechanism responsible for the decay. There is no way to decide on the mechanism when only the decay rate is known. However, a general theorem [163] states that once $0\nu\beta\beta$ has been observed, in gauge theories the Majorana neutrino mass necessarily

arises. But the magnitude of the corresponding neutrino mass is difficult to estimate if the exchange of a virtual light Majorana neutrino is not the dominant mechanism of the $\beta\beta$ decay.

2.2.2 Neutrino oscillations and the $0\nu\beta\beta$–decay

Let us assume that there are N massive Majorana neutrinos $\nu_i, i = 1, \dots, N$. In that case the weak eigenstate neutrinos ν_e, ν_μ and ν_τ can be expressed as superpositions of ν_i using the $3 \times N$ mixing matrix $U_{\ell i}$. In particular, electron neutrinos are then superpositions,

$$\nu_e = \sum_i^N U_{ei}\nu_i \ , \tag{2.28}$$

and the rate of the $0\nu\beta\beta$ decay is proportional to (see Equation 2.27)

$$\langle m_\nu \rangle^2 = \left| \sum_i^N U_{ei}^2 m_i \right|^2 = \left| \sum_i^N |U_{ei}|^2 e^{\alpha_i} m_i \right|^2 \ , \quad (\text{all} \ \ m_i \geq 0) \ . \tag{2.29}$$

This quantity depends, on the $N - 1$ Majorana phases $\alpha_i/2$ of the matrix U which are irrelevant in neutrino oscillation experiments that do not change the total lepton number. If CP is conserved, $\alpha_i = k\pi$, but generally any values of α_i are possible. Thus, m_ν could be complex and cancellations in the sum are possible. (For example, a Dirac neutrino corresponds to a pair of degenerate Majorana neutrinos with $e^{\alpha_i} = \pm 1$ whose contribution to m_ν exactly cancel.)

While the quantity m_ν depends on the unknown phases α_i, the upper and lower limits of m_ν , $\langle m_\nu \rangle_{max}$ and $\langle m_\nu \rangle_{min}$, depend only on the absolute values of the mixing angles,

$$\langle m_\nu \rangle_{max} = \sum_i |U_{ei}|^2 m_i \ , \ \ \langle m_\nu \rangle_{min} = \max[(2|U_{ei}|^2 m_i - \langle m_\nu \rangle_{max}), 0] \ . \tag{2.30}$$

Thus, if the search for $0\nu\beta\beta$ is successful and the value of m_ν is determined, and at the same time the mixing angles $|U_{ei}|^2$ and the mass square differences Δm_{ij}^2 are known from oscillation experiments, a **range** of absolute values of the neutrino masses can be deduced. This is illustrated in Figure 2.1 for supposing that $N = 3$, that the Large Mixing Angle (LMA) solution of the solar neutrinos is correct, and that the atmospheric neutrino problem requires maximum mixing of the μ and τ neutrinos. There are two consider two possibilities, the normal and inverted hierarchies (see the inserts in Figure 2.1) because given the information, we cannot distinguish between them. (Note that the uncertainty in the mixing parameters is not included in Figure 2.1.)
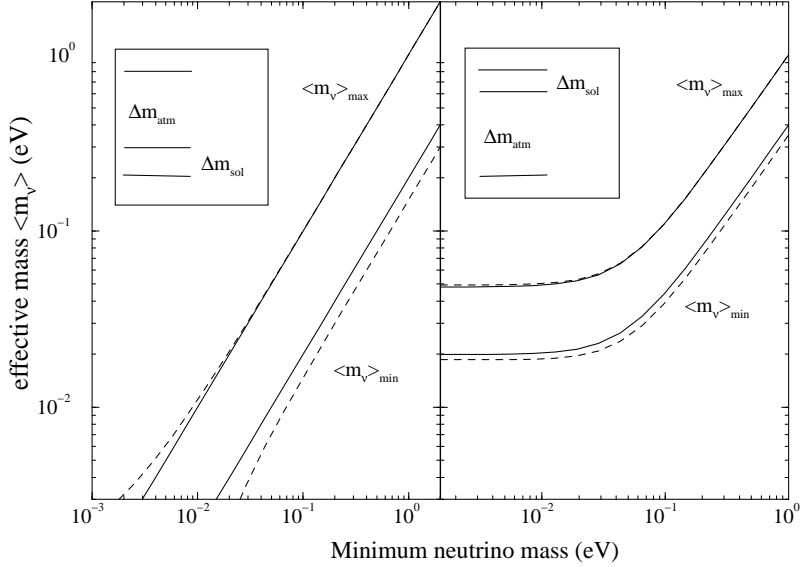
Figure 2.1: Effective mass m_ν as a function of the smallest neutrino mass m_{min}. The left panel is for the normal mass hierarchy, as indicated in the insert (not to scale), and the right panel is for the inverted hierarchy. Both panels are evaluated for the LMA solar solution with $\Delta m^2_{atm} = 2.4 \times 10^{-3}$ eV^2, $\Delta m^2_{sol} = 4.5 \times 10^{-5}$ eV^2, and $|U_{e2}|^2 = 0.3$. The full lines show $m_{\nu max}$ and $m_{\nu min}$, defined in Equation 2.30, for $U_{e3} = 0$ and the dashed lines use the maximum value $|U_{e3}|^2 = 0.025$ allowed by the CHOOZ and PALO VERDE reactor experiments [?, ?].

Naturally, if another constraint exists, for example a successful determination of the neutrino mass square $\sum_i |U_{ei}|^2 m_i^2$ in the tritium β decay experiments, one can use the knowledge of m_ν to determine or constrain the phases α_i.

Altogether, one cannot predict, in general, what the value of m_ν ought to be using the present knowledge. On the other hand, as shown in Figure 2.1 for the currently most likely oscillation scenario, one can show that certain classes of solutions, such as the inverted hierarchy, or the normal hierarchy with the smallest neutrino mass $\gg \sqrt{\Delta m^2_{sol}}$ (degenerate neutrino spectrum) lead to potentially observable $2\nu\beta\beta$ decay.

2.3   Nuclear structure aspects

The rate of the 2ν $\beta\beta$ decay is simply

$$1/T^{2\nu}_{1/2} = G_{2\nu}(E_0, Z)|M_{2\nu}|^2 \ , \tag{2.31}$$

while for the $0\nu\beta\beta$–decay (assuming that it is mediated by a light Majorana neutrino and that there are no right-handed weak interactions), and for the decay with Majoron emission, it is given by

$$
\begin{aligned}
1/T_{1/2}^{0\nu} &= G_{0\nu}(E_0, Z)|M_{0\nu}|^2\langle m_\nu\rangle^2 \ , \\
1/T_{1/2}^{0\nu,\chi} &= G_{0\nu,\chi}(E_0, Z)|M_{0\nu,\chi}|^2\langle g_{\nu,\chi}\rangle^2 \ .
\end{aligned}
\tag{2.32}
$$

Here the phase space functions $G(E_0, Z)$ are accurately calculable, and the nuclear matrix elements M are the topic of this section. Obviously, the accuracy with which the fundamental particle physics parameters $\langle m_\nu\rangle$ and $\langle g_{\nu,\chi}\rangle$ can be determined is limited by our ability to evaluate these nuclear matrix elements.

In that context there are three distinct set of problems:

- 2ν decay: the physics of the Gamow-Teller amplitudes

- 0ν decay with the exchange of light massive Majorana neutrinos: no selection rules on multipoles, role of nucleon correlations, sensitivity to nuclear models.

- 0ν decay with the exchange of heavy neutrinos: physics of the nucleon-nucleon states at short distances.

2.3.1   The $2\nu\beta\beta$–decay

Since the energies involved are modest, the allowed approximation should be applicable, and the rate is governed by the double Gamow-Teller matrix element

$$
M_{GT}^{2\nu} = \sum_m \frac{\langle f||\sigma\tau_+||m\rangle \times \langle m||\sigma\tau_+||i\rangle}{E_m - (M_i + M_f)/2} \ ,
\tag{2.33}
$$

where i, f are the ground states in the initial and final nuclei, and m are the intermediate 1^+ (virtual) states in the odd-odd nucleus. The first factor in the numerator above represents the β^+ (or (n, p)) amplitude for the final nucleus, while the second one represents the β^- (or (p, n)) amplitude for the initial nucleus. Thus, in order to correctly evaluate the 2ν decay rate, one has to know, at least in principle, *all* GT amplitudes for both β^- and β^+ processes, including their signs. The difficulty is that the 2ν matrix element exhausts a very small fraction $(10^{-5} - 10^{-7})$ of the double GT sum rule [62], and hence it is sensitive to details of nuclear structure.

Various approaches used in the evaluation of the 2ν decay rate have been reviewed recently in Ref. [62, 182]. The Quasiparticle Random Phase Approximation (QRPA) has been the most popular theoretical tool in the recent past. Its main ingredients, the repulsive particle-hole spin-isospin interaction, and the attractive particle-particle interaction, clearly play a decisive role in the concentration of the

β^- strength in the giant GT resonance, and the relative suppression of the β^+ strength and its concentration at low excitation energies. Together, these two ingredients are able to explain the suppression of the 2ν matrix element when expressed in terms of the corresponding sum rule.

Yet, the QRPA is often criticized. Two "undesirable", and to some extent unrelated, features are usually quoted. One is the extreme sensitivity of the decay rate to the strength of the particle-particle force (often denoted as g_{pp}). This decreases the predictive power of the method. The other one is the fact that for a realistic value of g_{pp} the QRPA solutions are close to their critical value (so called collapse). This indicates a phase transition, i.e., a rearrangement of the nuclear ground state. QRPA is meant to describe small deviations from the unperturbed ground state, and thus is not fully applicable near the point of collapse. Numerous approaches have been made to extend the range of validity of QRPA, see e.g. [182, 62]. Altogether, QRPA and its various extensions, with their ability to adjust at least one free parameter, are typically able to explain the observed 2ν decay rates.

At the same time, detailed calculations show that the sum over the excited states in equation(2.33) converges quite rapidly [60]. In fact, a few low lying states usually exhaust the whole matrix element. Thus, it is not really necessary to describe all GT amplitudes; it is enough to describe correctly the β^+ and β^- amplitudes of the low-lying states, and include everything else in the overall renormalization (quenching) of the GT strength.

Nuclear shell model methods are presently capable of handling much larger configuration spaces than even a few years ago. Thus, for many nuclei the evaluation of the 2ν rates within the $0\hbar\omega$ shell model space is feasible. (Heavy nuclei with permanent deformation, like ^{150}Nd and ^{238}U remain, however, beyond reach of the shell model techniques.) Using the shell model avoids, naturally, the above difficulties of QRPA. At the same time, the shell model can describe, using the same method and the same residual interaction, a wealth of spectroscopic data, allowing much better tests of its predictive power.

2.3.2 The light neutrino mechanism of the $0\nu\beta\beta$–decay

If one assumes that the 0ν decay is caused by the exchange of a virtual light Majorana neutrino between the two nucleons, then several new features arise: a) the exchanged neutrino has a momentum $q \sim 1/r_{nn} \simeq 50 - 100$ MeV (r_{nn} is the distance between the decaying nucleons). Hence, the dependence on the energy in the intermediate state is weak and the closure approximation is applicable and one does not have to sum explicitly over the nuclear intermediate states. Also, b) since $qR > 1$ (R is the nuclear radius), the expansion in multipoles is not convergent, unlike in the 2ν decay. In fact, all possible multipoles contribute by a comparable amount. Finally, c) the neutrino propagator results in a neutrino potential of a relatively long

range (see equation (15)).

Thus, in order to evaluate the rate of the 0ν decay, is necessary to estimate only the matrix element connecting the ground states 0^+ of the initial and final nuclei. QRPA and the shell model are the appropriate methods. Both calculations show that the features enumerated above are indeed present. In addition, the QRPA typically shows less extreme dependence on the particle-particle coupling constant g_{pp} than for the 2ν decay, since the contribution of the 1^+ multipole is relatively small. The calculations also suggest that for quantitatively correct results one has to treat the short range nucleon-nucleon repulsion carefully, despite the long range of the neutrino potential.

Does that mean that the calculated matrix elements are insensitive to nuclear structure? An answer to that question has obviously great importance, since unlike the 2ν decay, we cannot directly test whether the calculation is correct or not.
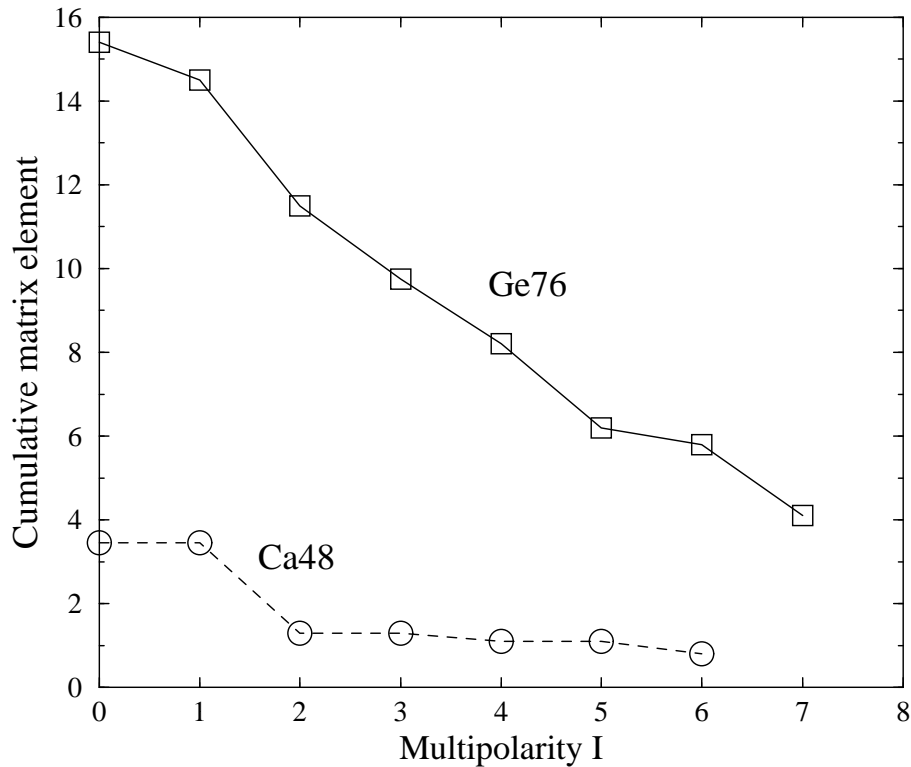

Figure 2.2: The cumulative contribution, i.e., the summed contribution of all natural parity multipoles up to I of the exchanged nn and pp pair, to the 0ν nuclear matrix element combination $M_{GT}^{0\nu} - M_F^{0\nu}$. The full line is for ^{76}Ge and the dashed line for ^{48}Ca.

For simplicity, let us assume that the 0ν $\beta\beta$ decay is mediated only by the

exchange of a light Majorana neutrino. The relevant nuclear matrix element is then the combination $M_{GT}^{0\nu} - M_F^{0\nu}$, where the GT and F operators change two neutrons into two protons, and contain the corresponding operator plus the neutrino potential. One can express these matrix elements either in terms of the proton particle - neutron hole multipoles (i.e., the usual beta decay operators) or in terms of the multipole coupling of the exchanged pair, nn and pp.

When using the decomposition in the proton particle - neutron hole multipoles, one finds that all possible multipoles (given the one-nucleon states near the Fermi level) contribute, and the contributions have typically equal signs. Hence, there does not seem to be much cancellation.

However, perhaps more physical is the decomposition into the exchanged pair multipoles. There one finds, first of all, that only natural parity multipoles ($\pi = (-1)^I$) contribute noticeably. And there is a rather severe cancellation. The biggest contribution comes from the 0^+ multipole, i.e., the pairing part. All other multipoles, related to higher seniority states, contribute with an opposite sign. The final matrix element is then a difference of the pairing and higher multipole (or broken pair $\equiv$ higher seniority) parts, and is considerably smaller than either of them. This is illustrated in Fig. 2.2 where the cumulative effect is shown, i.e., the quantity $M(I) = \sum_J^I [M_{GT}^{0\nu}(J) - M_F^{0\nu}(J)]$ is displayed for ^{76}Ge (from [130]) and ^{48}Ca (from [32]). Thus, the final result depends sensitively on both the correct description of the pairing and on the admixtures of higher seniority configurations in the corresponding initial and final nuclei. It appears, moreover, that the final result might depend on the size of the single particle space included. That important question requires further study.

Since there is no objective way to judge which calculation is correct, one often uses the spread between the calculated values as a measure of the theoretical uncertainty. In Fig. 2.3 are chosen two representative QRPA sets of results, the highly truncated "classical" shell model result of Haxton and Stephenson, and the result of more recent shell model calculation which is convergent for the set of single particle states chosen (essentially $0\hbar\omega$ space).

For the most important case of ^{76}Ge the calculated rates differ by a factor of 6-7. Since the effective neutrino mass $\langle m_\nu \rangle$ is inversely proportional to the square root of the lifetime, the experimental limit of 1.6×10^{25} y translates into limits of about 1 eV using the NME of [55, 33], and about 0.4 eV with the NME of [93, 130]. On the other hand, if one would accept the more stringent limit of 5.7×10^{25} [16], even the more pessimistic matrix elements restrict $\langle m_\nu \rangle < 0.5$ eV. Needless to say, a more objective measure of the theoretical uncertainty would be highly desirable.

In Tables 1.2 and 1.3 are listed the deduced limits on the fundamental parameters, the effective neutrino Majorana mass $\langle m_\nu \rangle$, and the Majoron coupling constant $\langle g_{\nu,\chi} \rangle$. The references to the source of the corresponding nuclear matrix elements, used to translate the experimental half-life limit into the listed limits on $\langle m_\nu \rangle$ and
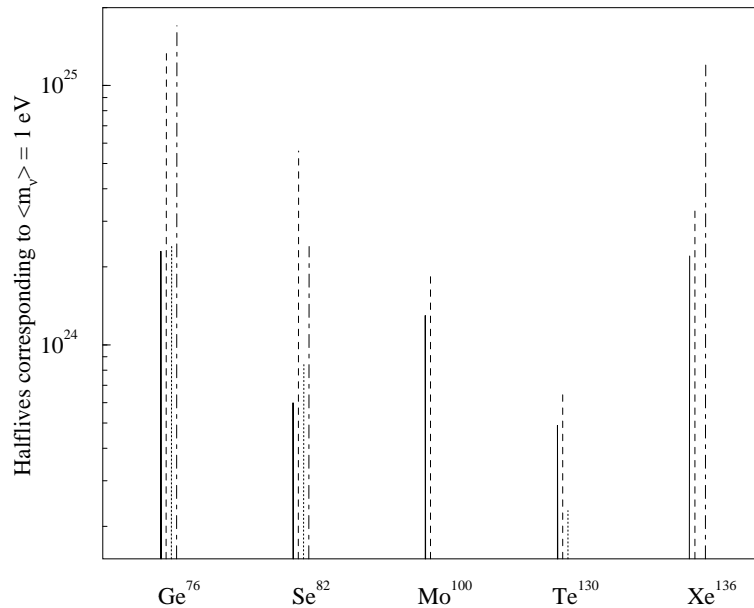
Figure 2.3: Half-lives (in years) calculated for $\langle m_\nu \rangle = 1$ eV by various representative methods and different authors for the most popular double-beta decay candidate nuclei. Solid lines are QRPA from [130], dashed lines are QRPA from [55] (recalculated for $g_A = 1.25$ and $\alpha' = -390$ MeV fm^3), dotted lines are shell model [93], and dot-and-dashed lines are shell model [33].

$\langle g_{\nu,\chi} \rangle$ are also given. When using the tables one has to keep in mind the uncertainties illustrated in Fig. 2.3.

2.3.3   The heavy neutrino mechanism of the $0\nu\beta\beta$–decay

The neutrinoless $\beta\beta$ decay can be also mediated by the exchange of a heavy neutrino. The decay rate is then inversely proportional to the square of the effective neutrino mass [197]. In this context it is particularly interesting to consider the left-right symmetric model proposed by Mohapatra [124]. In it, one can find a relation between the mass of the heavy neutrino M_N and the mass of the right-handed vector boson W_R. Thus, the limit on the $\beta\beta$ rate provides, within that specific model, a stringent lower limit on the mass of W_R.

The process then involves the emission of the heavy W_R^- by the first neutron and its virtual decay into an electron and the heavy Majorana neutrino, $W_R^- \rightarrow e^- + \nu_N$. This is followed by the transition $\nu_N \rightarrow e^- + W_R^+$ and the absorption of the W_R^+ on the second neutron, changing it into the second proton. Since all exchanged particles between the two neutrons are very heavy, the corresponding "neutrino potential" is of essentially zero range. Hence, when calculating the nuclear matrix element, one
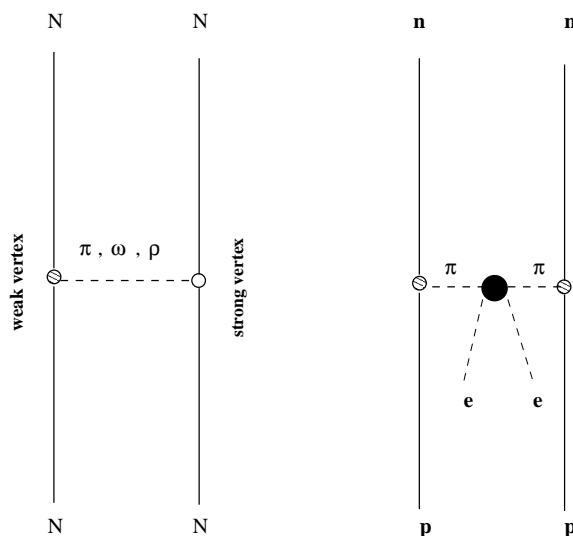
Figure 2.4: The Feynman graph description of the parity-violating nucleon-nucleon force (left graph) and of the $\beta\beta$ decay with the exchange of a heavy neutrino mediated by the pion exchange. The short range lepton number violating amplitude is symbolically described by the filled blob in the right graph.

has to take into account carefully the short range nucleon-nucleon repulsion.

As long as we treat the nucleus as an ensemble of nucleons only, the only way to have nonvanishing nuclear matrix elements for the above process is to treat the nucleons as finite size particles. In fact, that is the standard way to approach the problem [197]; the nucleon size is described by a dipole form factor with the cut-off parameter $\Lambda \simeq 0.85$ GeV. Using such a treatment of the nucleon size, and the half-life limit for the ^{76}Ge 0ν decay listed in Table 1.2, one obtains a very interesting limit on the mass of the vector boson W_R [98]

$$m_{W_R} \geq 1.6 \text{ TeV .} \tag{2.34}$$

However, another way of treating the problem is possible, and already mentioned in [197]. The analogous situation is treated in the description of the parity-violating nucleon-nucleon force [2]. There, instead of the weak (i.e., very short range) interaction of two nucleons, one assumes that a meson (π, ω, ρ) is emitted by one nucleon and absorbed by another one. One of the vertices is the parity-violating one, and the other one is the usual parity-conserving strong one. The corresponding range is then just the meson exchange range, easily treated. The situation is schematically depicted in the left-hand panel of Fig. 2.3.3. The analogy for $\beta\beta$ decay is shown in the right-hand graph. It involves two pions, and the "elementary" lepton number violating $\beta\beta$ decay then involves a transformation of two pions into two electrons.

Again, the range is just the pion exchange range. It would be interesting to see
if a detailed treatment of this graph would lead to more or less stringent limit on
the mass of the W_R than the treatment with form factors. The relation to the
claim in [166] that an analogous graph contributing to the lepton number violating
muon capture identically vanishes should be further investigated; in fact that claim
is probably not valid.

Chapter 3

Many-body approaches for β and $\beta\beta$–decay matrix elements

The complexity of the calculation of the double beta decay matrix elements lies in the fact that it is a second order process, i.e., in addition to the initial and final nuclear states the knowledge of the complete set of the states of the intermediate nucleus is required. In order to solve this problem different models as well as different nuclear structure scenarios were applied [52, 62, 182]. Since the nuclei undergoing double beta decay are open shell nuclei, the proton-neutron Quasiparticle Random Phase Approximation (pn-QRPA) method has been mostly employed in the evaluation of the double beta decay matrix elements [62, 182]. In addition, this approach has succeeded in reproducing the experimentally observed suppression of the $2\nu\beta\beta$-decay transitions. However, a strong sensitivity of the computed matrix elements to an increase of the strength of the particle-particle residual interaction in the 1^+ channel leads to a problem of fixing this parameter [62]. Thus various refinements of the original pn-QRPA have been proposed. One of them is to take into account the nuclear deformation parameter in order to calculate the ground state properties of the nuclei, the pairing correlations and the transition probabilities in the neutral or charge-exchange channel. Another interesting effect of deformation might occur in the double beta decay matrix elements. The deformed QRPA formalism [112, 157], allows an unified description of the $2\nu\beta\beta$-decay in spherical and deformed nuclei.

The deformation degrees of freedom of nuclei undergoing the $2\nu\beta\beta$-decay were first considered within the Nilsson model with pairing [206]. Bogdan, Faessler, Petrovici and Holan calculated the $0\nu\beta\beta$-decay in the pairing model including deformation and rotation [24]. The first QRPA calculation of the $2\nu\beta\beta$-decay matrix elements in a deformed Nilsson-BCS basis were presented in Ref. [90]. The authors did not take into account the particle-particle interaction of the nuclear Hamiltonian and assumed the initial and final nuclei to be equally deformed. The effects of the nuclear deformation were considered also within the $SU(3)$ scheme [100] which has been found successful in describing the heavy rotational nuclei. The $SU(3)$ scheme is a tractable shell model theory for deformed nuclei which requires a severe truncation of the single particle basis. This approach was used for calculation of the double beta decay half-life of different heavy nuclear systems [101] and the predictions were found to be in good agreement with available experimental data for ^{150}Nd and ^{238}U [193]. The effect of the deformation of the nuclear shape on the two-neutrino double beta decay matrix element has been discussed in details within a method developed by Raduta, Faessler and Delion [145]. The authors used the angular momentum projected single particle basis having the energies close to those of Nilsson levels. The Gamow-Teller states were generated with the help of the spherical proton-neutron QRPA with a good angular momentum quantum number within the considered basis. The results were presented for the $2\nu\beta\beta$-decay of ^{82}Se. It was shown that the deformation affects significantly the $2\nu\beta\beta$-decay matrix element. The deformation effect on the double Gamow-Teller matrix element of ^{100}Mo were investigated in the Hartree–Fock–Bogoliubov (HFB) framework in Ref. [45]. It was noticed that there

is a necessity of an appropriate amount of deformation in the HFB intrinsic state to reproduce the experimental $2\nu\beta\beta$-decay half-life. The deformed pn–QRPA approach has been successful in the description of the single β-decay transitions of medium and heavy nuclei a long time ago. In first applications only the particle-hole terms of the Gamow-Teller force were taken into account [112, 157]. It was supposed that the particle-particle terms have minor effect on the Gamow-Teller strength function. However, from the spherical QRPA calculations it is known that the particle-particle force plays an important role for describing the β^+- and $\beta\beta$-processes [38, 130, 203]. Recently, the importance of the particle-particle interaction has been confirmed also in the deformed QRPA treatment of the Gamow-Teller strength distributions [157]. A strong sensitivity of the single β-decay characteristics to the nuclear shape, RPA ground state correlations and pairing correlations was found.

3.1   Deformed single-particle mean field

In the present work, two different assumptions for the deformed mean field are considered, a deformed Woods-Saxon potential and a self–consistent mean field obtained from a Hartree-Fock procedure with Skyrme forces. In the first approach a deformed WS potential with axial symmetry is used to generate single particle energies and wave functions. The parameters of this potential are taken from the work of Tanaka *et al.* [186]. This parametrization was proposed originally for spherical nuclei ranging from ^{16}O to ^{208}Pb but the derived isospin dependence of the parameters allows an extension to deformed nuclei as well. Previous QRPA calculations have shown that this parametrization provides realistic levels also for deformed nuclei and good results on $M1$ excitations were obtained [155] for nuclei in various mass regions as well. The quadrupole deformation (β_2) of the WS potential is usually determined by fitting the microscopically calculated ground state quadrupole moment to the corresponding experimental value. The hexadecapole deformation (β_4) is expected to be small for these nuclei and we assume it is equal to zero.

The force Sk3 [17] and the force SG2 [78] that has been successfully tested against spin and isospin excitations in spherical [78] and deformed nuclei [156, 157] are considered. For the solution of the HF equations one follows the McMaster procedure that is based on the formalism developed in Ref. [196] as described in Ref. [195]. Time reversal and axial symmetry are also assumed here [1].

In both schemes, WS and HF, the single-particle wave functions are expanded in terms of the eigenstates of an axially symmetric harmonic oscillator in cylindrical coordinates, which are written in terms of Laguerre and Hermite polynomials. The single-particle states $|i\rangle$ and their time reversed $|\bar{i}\rangle$ are characterized by the eigenvalues Ω of J_z, parity π_i, and energy ϵ_i

---

[1]See Appendix B for more detailed calculations

$$|i\rangle = \sum_N \frac{(-1)^N + \pi_i}{2} \sum_{n_r, n_z, \Lambda \geq 0, \Sigma} C^i_{N n_r n_z \Lambda \Sigma} |N n_r n_z \Lambda \Sigma\rangle \qquad (3.1)$$

with $\Omega_i = \Lambda + \Sigma \geq \frac{1}{2}$, and

$$|\bar{i}\rangle = \sum_N \frac{(-1)^N + \pi_i}{2} \sum_{n_r, n_z, \Lambda \geq 0, \Sigma} C^i_{N n_r n_z \Lambda \Sigma} (-1)^{\frac{1}{2} - \Sigma} |N n_r n_z - \Lambda - \Sigma\rangle, \qquad (3.2)$$

with $\Omega_{\bar{i}} = -\Omega_i = -\Lambda - \Sigma \leq -\frac{1}{2}$. For each N the sum over $n_r, n_z, \Lambda \geq 0$ is extended to the quantum numbers satisfying $2n_r + n_z + \Lambda = N$.

3.2   Deformed quasiparticle mean field

In order to define the proton–neutron gap, the $T = 0$ and $T = 1$ coupling, general notions concerning the origin of the pairing gap have to be introduced. This section is reserved to the theoretical considerations concerning this topic and it has a very general character. The model space is defined by a finite, M-dimensional, set of orthonormal single nucleon wave functions $|i>, |k>, ...M$ being discrete eigenstates of a spherically symmetric one body potential, e.g. the harmonic oscillator. The creation and annihilation operators will be denoted by $c_i^\dagger, c_k^\dagger ...M$ and $c_i, c_k ...M$ respectively. They fulfill the usual anti-commutation relations for Fermion operators. The corresponding particle vacuum $|0>$ is defined by $c_i|0>= 0$ for all $i = 1, ..., M$.

Each of the states:

$$|i> = c_i^\dagger|0> = |n_i, l_i, j_i; m_i, \tau_i>, \qquad (3.3)$$

is characterized by a set of quantum numbers: the orbital angular momentum l_i is coupled with the nucleon spin $s = 1/2$ to the angular momentum j_i, the different magnetic substates which are denoted by $m_i = -j_i, ...j_i$; the isospin projection τ_i distinguishes a neutron$(\tau_i = 1/2)$ from a proton $(\tau_i = -1/2)$ state. Under time reversal the states (equation 3.3) transform as

$$\hat{\tau}|i> = \hat{K} e^{-i\pi\hat{s}_y}|i> = (-)^{j_i + l_i - m_i}|\underline{i}; -m_i, \tau_i>, \qquad (3.4)$$

where $\hat{s}_y$ denotes the y component of the spin operator and $\hat{K}$ stands for a complex conjugation. Similarly for each state (equation 3.3), its charge conjugate partner can be introduced by:

$$\hat{c}|i> = \hat{K}_c e^{-i\pi\hat{t}_y}|i> = (-)^{1/2 - \tau_i}|\underline{i}; m_i - \tau_i>. \qquad (3.5)$$

The effective many body Hamiltonian appropriate for this model space is represented as a sum of one and two body terms

$$\hat{H} = \sum_{ik} t(ik)c_i^\dagger c_k + 1/4 \sum_{ikrs} v(ikrs)c_i^\dagger c_k^\dagger c_s c_r. \tag{3.6}$$

In order to guarantee the real energy eigenvalues for the discrete nuclear excitation, the Hamiltonian $\hat{H}$, has, obviously, to be hermitian. It is a scalar in normal space and commutes with the square j^2 of the total angular momentum operator and its 3-components $\hat{J}_z$. In addition $\hat{H}$ conserves the total number of nucleons as well as the charge of the considered system. If the weak interactions are neglected, the total parity is conserved. The following relations are fulfilled by the matrix elements of the hamiltonian. Here,

$$t(ik) = <i|\hat{T}|k> = \delta(\tau_i, \tau_k)\delta(l_i, l_k)\delta(j_i, j_k)\delta(m_i, m_k)t(ik), \tag{3.7}$$

are the matrix elements of the one body part $\mathcal{T}$ (usually the kinetic energy operator) and

$$\begin{aligned}
v(ikrs) &= <ik|\hat{V}|rs - sr> \\
&\delta(\tau_i + \tau_k, \tau_r + \tau_s)\delta((-)^{l_i+l_k}, (-)^{l_r+l_s})\delta(m_i + m_k, m_r + m_s) \\
&\delta(Min[j_i + j_k, j_r + j_s] \geq Max[|j_i - j_k|, |j_r - j_s|])v(ikrs),
\end{aligned} \tag{3.8}$$

are the antisymmetrized matrix elements of the effective two body interaction $\hat{V}$. The matrix elements

$$t(ik) = t(ki) = t(ik)^* = t(\overline{ik}), \tag{3.9}$$

as well as

$$v(ikrs) = -v(kirs) = -v(iksr) = v(kisr) = v(rsik) = v(ikrs)^* = v(\overline{ikrs}), \tag{3.10}$$

are real numbers and time-reversal invariant.

3.2.1   The HFB transformation

The most general quasiparticle creation operator resulting from a linear transformation of the creation and annihilation operators of the chosen single particle basis states, has the form:

$$a_\alpha^\dagger = \sum_{i=1}^{M}(A_{i\alpha}c_i^\dagger + B_{i\alpha}c_i), \tag{3.11}$$

where $\alpha = 1, M$. The matrix notation of the previous equation is:

$$\begin{pmatrix} a^\dagger \\ a \end{pmatrix} = \begin{pmatrix} A^T & B^T \\ B^+ & A^+ \end{pmatrix} \begin{pmatrix} c^\dagger \\ c \end{pmatrix} = F \begin{pmatrix} c^\dagger \\ c \end{pmatrix} \tag{3.12}$$

with F being a unitary matrix (in order to fulfill the Fermion anti-commutation relation). The last equation defines a general HFB transformation. The corresponding vacuum $a_\alpha|F>=0$ for all $\alpha=1...M$ can be uniquely represented by:

$$|F> = \left(\prod_{\alpha=1}^{M} a_\alpha\right)|0>.\tag{3.13}$$

The vacuum properties are completely characterized by the density matrix

$$\rho_{sk} =<F|c_k^\dagger c_s|F> = (B^* B^T)_{sk}, \quad k,s=1,...,M,\tag{3.14}$$

and the pairing tensor

$$\kappa_{sk} =<F|c_s c_r|F> = (B^* A^T)_{rs}; \quad r,s=1,...,M,\tag{3.15}$$

where ρ is hermitian and positive definite ($\rho=\rho^+ \geq 0$) and κ is antisymmetric ($\kappa = -\kappa^T$). In this representation the pairing gap has the following form:

$$\Delta(i\overline{k}) : = \Delta(\underline{i}m\tau_i, \underline{k}\overline{m}\tau_k) = -\frac{1}{2}\sum_{r,s}v(i\overline{k},r\overline{s})\kappa_{r\overline{s}}$$

$$-\frac{1}{2}\sum_{m'}\sum_{\underline{r}\tau_r,\underline{s}\tau_s}v(\underline{i}m\tau_i,k\overline{m}\tau_k;rm'\tau_r,s\overline{m'}\tau_s)<c_{\overline{s}}c_r>.\tag{3.16}$$

Assuming time-reversal and axial symmetry for the HFB transformation F and also taking into account the symmetry relationship for the pairing tensor, the pairing gap can be written as:

$$\Delta(i\overline{k}) : = \Delta(\underline{i}m\tau_i, \overline{\underline{k}m\tau_k}) = -\frac{1}{2}\sum_{m'>0}\sum_{\underline{r}\tau_r\leq\underline{s}\tau_s}\frac{1}{1+\delta(\underline{r},\underline{s})\delta(\tau_r,\tau_s)}$$

$$v(i\overline{k};r\overline{s})\kappa_{r\overline{s}} + v(i\overline{k};\overline{r}s)\kappa_{\overline{r}s} + v(i\overline{k};s\overline{r})\kappa_{s\overline{r}} + v(i\overline{k},\overline{s}r)\kappa_{\overline{s}r}$$

$$= -\frac{1}{2}\sum_{m'>0}\sum_{\underline{r}\tau_r\leq\underline{s}\tau_s}\frac{1}{1+\delta(\underline{r},\underline{s})\delta(\tau_r,\tau_s)}$$

$$\{[v(i\overline{k};r\overline{s}) - v(i\overline{k};\overline{r}s)]Re\kappa_{r\overline{s}} + [v(i\overline{k};r\overline{s}) - v(i\overline{k};\overline{r}s)]iIm\kappa_{r\overline{s}}$$

$$+[v(i\overline{k};r\overline{s}) - v(i\overline{k};\overline{r}s)]Re\kappa_{\overline{s}r} + [v(i\overline{k};r\overline{s}) - v(i\overline{k};\overline{r}s)]iIm\kappa_{r\overline{s}}\}$$

$$= -\frac{1}{2}\sum_{m'>0}\sum_{\underline{r}\tau_r\leq\underline{s}\tau_s}\frac{1}{1+\delta(\underline{r},\underline{s})\delta(\tau_r\tau_s)}$$

$$\{[v(i\overline{k};r\overline{s}) - v(i\overline{k};\overline{r}s)]Re\kappa_{r\overline{s}} + [v(i\overline{k};r\overline{s}) - v(i\overline{k};\overline{r}s)]iIm\kappa_{r\overline{s}}\}\tag{3.17}$$

Coupling the two body matrix elements to angular momentum I and isospin T one obtains the proton-proton, neutron-neutron and proton-neutron contribution.

$$\Delta_m^{\tau\tau}(i\overline{k}): \ = \ \Delta(im_\tau; \overline{km\tau}) = -2\sum_{\underline{r}\leq\underline{s}}^{\tau}\sqrt{\frac{1+\delta(\underline{i},\underline{k})}{1+\delta(\underline{r},\underline{s})}}\sum_I v_{\tau\tau}^{I1}(\underline{ik};\underline{s})(-1)^{j_k+l_k-m}(j_i j_k I|m-m0)$$

$$\{\sum_{m'>0}(-1)^{j_s+l_s-m'}(j_r j_s I|m'-m'0)[\frac{1}{2}[1+(-1)^{l_r+l_s+I}]Re\kappa_{rs}^{\tau\tau}(m')+$$

$$\frac{1}{2}[1-(-1)^{l_r+l_s+I}]iIm\kappa_{rs}^{\tau\tau}(m')]\}, \tag{3.18}$$

and

$$\Delta_m^{\tau-\tau}(i\overline{k}): \ = \ \Delta(im_\tau; \overline{km-\tau}) = \sum_{\underline{r}}^{\tau}\sum_{\underline{s}}^{-\tau}\sqrt{(1+\delta(\underline{i},\underline{k}))(1+\delta(\underline{r},\underline{s}))}$$

$$\sum_{IT}v_{\tau-\tau}^{IT}(\underline{ik};\underline{s})(-1)^{j_k+l_k-m}(j_i j_k I|m-m0)$$

$$\{\sum_{m'>0}(-1)^{j_s+l_s-m'}(j_r j_s I|m'-m'0)[\frac{1}{2}[1+(-1)^{l_r+l_s+I}]Re\kappa_{rs}^{\tau-\tau}(m')+$$

$$\frac{1}{2}[1-(-1)^{l_r+l_s+I}]iIm\kappa_{rs}^{\tau-\tau}(m')]\}. \tag{3.19}$$

Equation (3.18) describes the pairing between two like nucleons and contains just $T = 1$ components. Equation (3.19) gives the part of the pairing potential resulting from proton-neutron pairing. Here obviously $T = 1$ as well as $T = 0$ components do occur. It is immediately seen from these two equations that the coupling of the nucleon pairs to natural parity states gives rise to the real part of the pairing potential while unnatural parity pairing is responsible for the imaginary parts. The above equations are easy to interpret for a single j-shell. Then the like nucleon pairing as well as the $T = 1$ component are purely real, while the $T = 0$ components of the proton-neutron pairing potential are purely imaginary.

3.2.2 Pairing hamiltonian

The ground state of even-even nuclei is determined by the deformed pairing Hamiltonian, which includes monopole ($K = 0$) proton, neutron and proton-neutron pairing interactions:

$$H \ = \ \sum_s(\epsilon_{ps}^0 - \lambda_p)\sum_\sigma c_{ps\sigma}^\dagger c_{ps\sigma} + \sum_s(\epsilon_{ns}^0 - \lambda_n)\sum_\sigma c_{ns\sigma}^\dagger c_{ns\sigma}$$

$$-G_{pp}^{T=1}\sum_{s,s'}S_{spp}^{T=1\dagger}S_{s'pp}^{T=1} - G_{nn}^{T=1}\sum_{s,s'}S_{snn}^{T=1\dagger}S_{s'nn}^{T=1}$$

$$-G_{pn}^{T=1}\sum_{s,s'}S_{spn}^{T=1\dagger}S_{s'pn}^{T=1} - G_{pn}^{T=0}\sum_{s,s'}S_{spn}^{T=0\dagger}S_{s'pn}^{T=0}, \tag{3.20}$$

where the ϵ^0_{ps} and ϵ^0_{ns} are the unrenormalized proton and neutron single particle energies, respectively. λ_p (λ_n) is the proton (neutron) Fermi energy and $S^T_{s\tau\tau'}{}^\dagger$ creates isovector (T=1) or isoscalar (T=0) pairs in time reversed orbits

$$
\begin{aligned}
S^{T=1}_{spp}{}^\dagger &= \sum_\sigma c^\dagger_{ps\sigma} c^\dagger_{ps\tilde\sigma}, \quad S^{T=1}_{snn}{}^\dagger = \sum_\sigma c^\dagger_{ns\sigma} c^\dagger_{ns\tilde\sigma}, \\
S^{T=1}_{spn}{}^\dagger &= \sum_\sigma \frac{1}{\sqrt{2}}(c^\dagger_{ps\sigma} c^\dagger_{ns\tilde\sigma} + c^\dagger_{ns\sigma} c^\dagger_{ps\tilde\sigma}), \\
S^{T=0}_{spn}{}^\dagger &= \sum_\sigma \frac{1}{\sqrt{2}}(c^\dagger_{ps\sigma} c^\dagger_{ns\tilde\sigma} - c^\dagger_{ns\sigma} c^\dagger_{ps\tilde\sigma}).
\end{aligned}
\tag{3.21}
$$

Here, $c^\dagger_{\tau s\sigma}$ and $c_{\tau s\sigma}$ stand for the creation and annihilation operators of a particle ($\tau = p$ and $\tau = n$ denote proton and neutron, respectively) in the axially–symmetric harmonic oscillator potential. These states are completely determined by a principal set of quantum numbers $s = (N, n_z, \Lambda, \Omega)$. σ is the sign of the angular momentum projection Ω ($\sigma = \pm 1$). The intrinsic states are twofold degenerate. The states with Ω and $-\Omega$ have the same energy as a consequence of the time reversal invariance. $\sim$ indicates time reversed states.

The Hamiltonian in equation (3.20) is invariant under hermitian and time reversal operations. The four coupling strengths $G^{T=1}_{pp}$, $G^{T=1}_{nn}$, $G^{T=1}_{pn}$ and $G^{T=0}_{pn}$ are real and characterize the associated isovector (pp, nn and pn) and isoscalar (pn) monopole (K=0) pairing interactions. The isospin symmetry of the Hamiltonian in equation (3.20) is restored for $\epsilon^0_{ps} = \epsilon^0_{ns}$ and $G^{T=1}_{pp} = G^{T=1}_{nn} = G^{T=1}_{pn} = G^{T=0}_{pn}$. For the particular case, $G^{T=1}_{pn} = G^{T=0}_{pn}$

$$
H = \sum_{s\sigma\tau}(\epsilon^0_{\tau s} - \lambda_\tau)c^\dagger_{\tau s\sigma} c_{\tau s\sigma} - \sum_{\tau\tau'} G_{\tau\tau'} \sum_{s\sigma s'\sigma'} c^\dagger_{\tau s\sigma} c^\dagger_{\tau' s\tilde\sigma} c_{\tau' s'\tilde\sigma'} c_{\tau s'\sigma'}.
\tag{3.22}
$$

It is assumed that $G_{\tau\tau'} = G_{\tau'\tau}$. In this limit one can not distinguish between T=0 and T=1 pairing. A similar Hamiltonian was discussed in Ref. [39], where the representation of the single particle states with good angular momentum quantum number was considered.

3.2.3 Generalized BCS transformation

If the proton-proton, neutron-neutron and proton-neutron pairing correlations are considered for axially-symmetric nuclei, the particle ($c^\dagger_{\tau s\sigma}$ and $c_{\tau s\sigma}$, $\tau = p, n$) and the quasiparticle ($a^\dagger_{\rho s\sigma}$ and $a_{\rho s\sigma}$, $\rho = 1, 2$) creation and annihilation operators for the deformed shell model states are related each to other by the generalized BCS

transformation [82]:

$$
\begin{pmatrix}
c^+_{ps\sigma} \\
c^+_{ns\sigma} \\
c_{ps\tilde{\sigma}} \\
c_{ns\tilde{\sigma}}
\end{pmatrix}
=
\begin{pmatrix}
u_{s1p} & u_{s2p} & -v_{s1p} & -v_{s2p} \\
u_{s1n} & u_{s2n} & -v_{s1n} & -v_{s2n} \\
v_{s1p} & v_{s2p} & u_{s1p} & u_{s2p} \\
v_{s1n} & v_{s2n} & u_{s1n} & u_{s2n}
\end{pmatrix}
\begin{pmatrix}
a^+_{1s\sigma} \\
a^+_{2s\sigma} \\
a_{1s\tilde{\sigma}} \\
a_{2s\tilde{\sigma}}
\end{pmatrix},
\tag{3.23}
$$

where the occupation amplitudes u_{s1p}, v_{s1p}, u_{s2n}, v_{s2n} are real and u_{s1n}, v_{s1n}, u_{s2p}, v_{s2p} are complex [81]. In the case when only the T=1 proton-neutron pairing is considered all amplitudes are real [35, 81]. In the limit in which there is no proton-neutron pairing $u_{s2p} = v_{s2p} = u_{s1n} = v_{s1n} = 0$. Then the isospin generalized BCS transformation in equation (3.23) reduces to two conventional BCS two–dimensional transformations, first for protons ($u_{s1p} = u_{sp}$, $v_{s1p} = v_{sp}$) and second for neutrons ($u_{s2n} = u_{sn}$, $v_{s2n} = v_{sn}$).

The diagonalization of the Hamiltonian (3.20) is equivalent to the matrix diagonalization [82]

$$
\begin{pmatrix}
\epsilon_{ps} - \lambda_p & 0 & \Delta_{pp} & \Delta_{pn} \\
0 & \epsilon_{ns} - \lambda_n & \Delta^*_{pn} & \Delta_{nn} \\
\Delta_{pp} & \Delta_{pn} & -(\epsilon_{ps} - \lambda_p) & 0 \\
\Delta^*_{pn} & \Delta_{nn} & 0 & -(\epsilon_{ns} - \lambda_n)
\end{pmatrix}
\begin{pmatrix}
u_{s\rho p} \\
u_{s\rho n} \\
v_{s\rho p} \\
v_{s\rho n}
\end{pmatrix}
= E_{s\rho}
\begin{pmatrix}
u_{s\rho p} \\
u_{s\rho n} \\
v_{s\rho p} \\
v_{s\rho n}
\end{pmatrix}
\tag{3.24}
$$

that yields the quasiparticle energies $E_{s\rho}$ and the occupation amplitudes. Here, $\epsilon_{\tau s}$ ($\tau = p, n$) are the renormalized single particle energies which include terms describing the coupling of the nuclear average field with the characteristics of the pairing interactions [178]. The proton (Δ_{pp}), neutron (Δ_{nn}) and proton–neutron (Δ_{pn}) pairing gaps are given as

$$
\begin{aligned}
\Delta_{\tau\tau} &= G^{T=1}_{\tau\tau} \sum_{s,\rho} v_{s\rho\tau} u^*_{s\rho\tau} = G^{T=1}_{\tau\tau} \sum_{s,\rho} v^*_{s\rho\tau} u_{s\rho\tau} \quad (\tau = p, n), \\
\Delta_{pn} &= \Delta^{T=1}_{pn} + i\Delta^{T=0}_{pn}
\end{aligned}
\tag{3.25}
$$

with

$$
\begin{aligned}
\Delta^{T=1}_{pn} &= G^{T=1}_{pn} \, Re\{ \sum_{s,\rho} v_{s\rho p} u^*_{s\rho n} \}, \\
\Delta^{T=0}_{pn} &= G^{T=0}_{pn} \, Im\{ \sum_{s,\rho} v_{s\rho p} u^*_{s\rho n} \}.
\end{aligned}
\tag{3.26}
$$

The real and imaginary parts of the proton–neutron pairing gap Δ_{pn} are associated with T=1 and T=0 pairing modes, respectively. This phenomenon was first pointed out by Goodman [40, 82], permitting almost all subsequent treatments of pn pairing. For $G^{T=0}_{pn}$ equal to zero the occupation amplitudes of the isospin generalized BCS

transformations are real. The Langrange multipliers λ_p and λ_n entering (3.24) are adjusted so that the number-conservation relations

$$Z = 2 \sum_{s\rho} v_{s\rho p} v_{s\rho p}^*, \quad N = 2 \sum_{s\rho} v_{s\rho n} v_{s\rho n}^*, \tag{3.27}$$

are satisfied.

The ground state energy can be written as

$$H_{g.s.} = H_0 + H_{pair.}, \tag{3.28}$$

where H_0 is the BCS expectation value of the single-particle Hamiltonian

$$H_0 = 2 \sum_{\tau s} \epsilon_{\tau s} \sum_\rho v_{s\rho\tau} v_{s\rho\tau}^* \tag{3.29}$$

and $H_{pair.}$ represents the pairing energy

$$H_{pair} = -\frac{\Delta_{pp}^2}{G_{pp}^{T=1}} - \frac{\Delta_{nn}^2}{G_{nn}^{T=1}} - \frac{(\Delta_{pn}^{T=1})^2}{G_{pn}^{T=1}} - \frac{(\Delta_{pn}^{T=0})^2}{G_{pn}^{T=0}}. \tag{3.30}$$

The proton-proton, neutron-neutron and proton-neutron (T=0 and T=1) pairing modes contribute coherently to the ground state energy $H_{g.s.}$.

In Ref. [56] it has been suggested that the effect of different pairing modes can be quantified by measuring pair numbers in the nuclear wave function [48]. For that purpose the operators

$$\begin{aligned}
\mathcal{N}_{pp} &= \sum_{s,s'} S_{spp}^{T=1\dagger} S_{s'pp}^{T=1}, \quad \mathcal{N}_{nn} = \sum_{s,s'} S_{snn}^{T=1\dagger} S_{s'nn}^{T=1}, \\
\mathcal{N}_{pn}^{T=1} &= \sum_{s,s'} S_{spn}^{T=1\dagger} S_{s'pn}^{T=1}, \quad \mathcal{N}_{pn}^{T=0} = \sum_{s,s'} S_{spn}^{T=0\dagger} S_{s'pn}^{T=0},
\end{aligned} \tag{3.31}$$

which are rough measures of the numbers pp, nn, pn (T=1) and pn (T=0) pairs, respectively, are defined. The BCS ground state expectation values of these operators are related with the corresponding pairing gaps. After subtracting the mean field values we find

$$\begin{aligned}
< \mathcal{N}_{pp} > &\approx \frac{\Delta_{pp}^2}{(G_{pp}^{T=1})^2}, \quad < \mathcal{N}_{nn} >\approx \frac{\Delta_{nn}^2}{(G_{nn}^{T=1})^2}, \\
< \mathcal{N}_{pn}^{T=1} > &\approx \frac{(\Delta_{pn}^{T=1})^2}{(G_{pn}^{T=1})^2}, \quad < \mathcal{N}_{pn}^{T=0} >\approx \frac{(\Delta_{pn}^{T=0})^2}{(G_{pn}^{T=0})^2}.
\end{aligned} \tag{3.32}$$

The number of these pairs can not be observed directly.

3.2.4   Empirical pairing gaps

The magnitudes of proton, neutron and proton–neutron pairing gaps can be determined only indirectly from the experimental data. Usually they are deduced from systematic studies of experimental odd-even mass differences:

$$
\begin{aligned}
M(Z,N)_{even-even} &= \mathcal{M}(Z,N) \\
M(Z,N)_{odd-proton} &= \mathcal{M}(Z,N) + \Delta_p^{emp.} \\
M(Z,N)_{odd-neutron} &= \mathcal{M}(Z,N) + \Delta_n^{emp.} \\
M(Z,N)_{odd-odd} &= \mathcal{M}(Z,N) + \Delta_p^{emp.} + \Delta_n^{emp.} - \delta_{pn}^{emp.}.
\end{aligned}
\tag{3.33}
$$

Here, $M(Z,N)$ are the experimental nuclear masses and $\mathcal{M}(Z,N)$ denotes a smooth mass surface formed by a set of even–even nuclei, i.e. for these nuclei the measured mass is identical to the smooth mass. The mass of an odd–proton (odd–neutron) nucleus is given by addition of the proton pairing gap $\Delta_p^{emp.}$ (neutron pairing gap $\Delta_n^{emp.}$) to $\mathcal{M}(Z,N)$. The mass of an odd-odd nucleus is the sum of the smooth mass $\mathcal{M}(Z,N)$ and the sum of the proton and neutron pairing gaps minus the attractive residual proton–neutron interaction energy $\delta_{pn}^{emp.}$.

Using the Taylor series expansion of the $\mathcal{M}(Z,N)$, the quantities $\Delta_p^{emp.}$, $\Delta_n^{emp.}$ and $\delta_{pn}^{emp.}$ for even mass nuclei can be expressed as

$$
\begin{aligned}
\Delta_p^{emp.} &= -\frac{1}{8}[M(Z+2,N) - 4M(Z+1,N) + 6M(Z,N) \\
&\quad -4M(Z-1,N) + M(Z-2,N)], \\
\Delta_n^{emp.} &= -\frac{1}{8}[M(Z,N+2) - 4M(Z,N+1) + 6M(Z,N) \\
&\quad -4M(Z,N-1) + M(Z,N-2)], \\
\delta_{pn}^{emp.} &= \frac{1}{4}\{2[M(Z,N+1) + M(Z,N-1) \\
&\quad +M(Z-1,N) + M(Z+1,N)] - 4M(Z,N)] \\
&\quad -[M(Z+1,N+1) + M(Z-1,N+1) \\
&\quad +M(Z+1,N-1) + M(Z-1,N-1)]\}.
\end{aligned}
$$

$$\tag{3.34}$$

The first systematic studies of nuclear masses have shown that the average pairing gaps ($\overline{\Delta}_{\tau\tau}$, $\tau = p,\ n$) decrease slowly with $A^{1/2}$ (traditional model) [26]. Vogel *et al.* found evidence for a dependence of the average pairing gaps upon the relative neutron excess $(N-Z)/A$ [201]. The parameterizations of the average pairing gaps and the average proton-neutron residual interaction within these two models are as follows:

$$
\overline{\Delta}_\tau = 12\ MeV/A^{1/2}, \quad \overline{\delta}_{pn} = 20\ MeV/A \quad (traditional\ model)
$$

$$\overline{\Delta}_\tau \quad = \quad (7.2 - 44\frac{(N-Z)^2}{A^2})\ MeV/A^{1/3}, \quad \overline{\delta}_{pn} = 31\ MeV/A \quad (Vogel\ et.al) \quad (3.35)$$

Recently, Madland and Nix [118] presented a model for calculation of these average quantities by fixing a larger set of parameters.

Table 3.1: The empirical [see equation (3.34)] and average [see equation (3.35)] pairing gaps and proton–neutron residual energy for Ge isotopes with A=64-76.

	Empirical values			Average values			
				Traditional m.		Vogel et al.	
Nucleus	$\Delta_p^{emp.}$	$\Delta_n^{emp.}$	$\delta_{pn}^{emp.}$	$\overline{\Delta}_{p,n}$	$\overline{\delta}_{pn}$	$\overline{\Delta}_{p,n}$	$\overline{\delta}_{pn}$
	[MeV]	[MeV]	[MeV]	[MeV]	[MeV]	[MeV]	[MeV]
^{64}Ge	1.807	2.141	1.498	1.500	0.313	1.800	0.484
^{66}Ge	1.586	1.859	0.816	1.477	0.303	1.770	0.470
^{68}Ge	1.609	1.882	0.630	1.455	0.294	1.727	0.455
^{70}Ge	1.551	1.866	0.594	1.434	0.285	1.668	0.443
^{72}Ge	1.614	1.836	0.583	1.414	0.278	1.600	0.430
^{74}Ge	1.621	1.715	0.424	1.350	0.270	1.523	0.419
^{76}Ge	1.561	1.535	0.388	1.376	0.263	1.441	0.408

In Table 3.1, the experimental pairing gaps and proton–neutron excitation energies for Ge isotopes with A=64–76 are compared with the averaged ones. A better agreement between empirical and average values is achieved for the model developed by Vogel et al. [201]. The differences between empirical and average values are small especially for isotopes close to the valley of β stability. It is worthwhile to notice that the values of proton–neutron interaction energies are not negligible in comparison with the values of pairing gaps even for isotopes with large neutron excess. This fact is clearly illustrated in Fig. 3.1. Thus the proton–neutron pairing interaction is expected to play a significant role in the construction of the quasiparticle mean field even for these nuclei. It is supposed that the origin of this phenomenon is associated with the effect of nuclear deformation, which is changing the distribution of proton and neutron single particle levels inside the nucleus.

For performing a realistic calculation within the deformed BCS approach it is necessary to fix the parameters of the nuclear Hamiltonian in equation (3.20). Following the procedure of Ref. [35] this is done in two steps:

i) The proton (neutron) pairing interaction strength $G_{pp}^{T=1}$ ($G_{nn}^{T=1}$) is adjusted by requiring that the lowest proton (neutron) quasiparticle energy to be equal to the empirical proton (neutron) pairing gap $\Delta_p^{emp.}$ ($\Delta_n^{emp.}$).
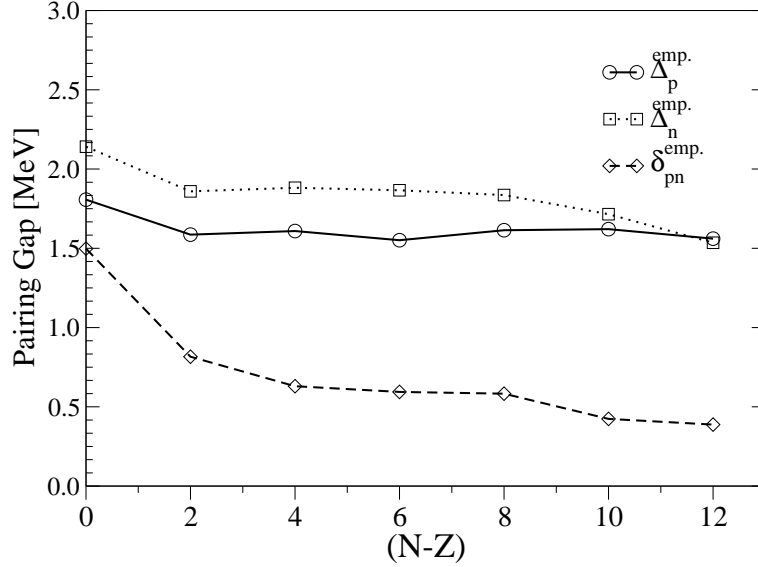
Figure 3.1: The experimental proton ($\Delta_p^{emp.}$) and neutron ($\Delta_n^{emp.}$) pairing gaps and proton–neutron interaction energy ($\delta_{pn}^{emp.}$) for even–even Ge isotopes with A=64–76 [see equation (3.34)] .

ii) With already fixed $G_{pp}^{T=1}$ and $G_{nn}^{T=1}$ the proton–neutron pairing interaction strengths $G_{pn}^{T=1}$ and $G_{pn}^{T=0}$ are adjusted to the empirical proton–neutron interaction energy $\delta_{pn}^{emp.}$ using the formula

$$\delta_{pn}^{theor.} = -[(H_{g.s.}^{(12)} + E_1 + E_2) - (H_{g.s.}^{(pn)} + E_p + E_n)]. \tag{3.36}$$

Here, $H_{g.s.}^{(12)}$ ($H_{g.s.}^{(pn)}$) is the total deformed BCS ground state energy with (without) proton-neutron pairing and $E_1 + E_2$ ($E_p + E_n$) is the sum of the lowest two quasiparticle energies with (without) proton–neutron pairing gap Δ_{pn}. The calculation of the ground state energies of odd-odd nuclei within macroscopic pairing models is based on the assumption that there is one unpaired proton and neutron close to the Fermi surface [125, 127, 201]. The resulting expectation value of an attractive short-range residual interaction between them, which can be approximated by a delta force, is considered to be the origin of the proton-neutron interaction energy. Unfortunately, this simplified approach can not be exploited in a microscopic treatment of nuclear properties of open shell nuclei, as the construction of the many-body wave function is required. In the deformed BCS approach the ground state of the odd-odd nucleus is described as the lowest two quasiparticle excitation of the even-even nucleus. This procedure of fixing the pairing strengths was exploited already in Refs. [35, 126]. However, some questions arise about the ambiguity of equating the microscopic pairing gap expressions, used to determine the strengths of the pairing matrix elements. Thus, one has to study the importance of the proton-neutron pairing effect

for $N > Z$ nuclei also by assuming a different scenario, namely the commonly used pairing strengths,

$$G_{pp}^{T=1} = G_{nn}^{T=1} = 16/A \ MeV, \quad G_{pn}^{T=0} = 20/A \ MeV, \tag{3.37}$$

which decrease with increasing neutron excess.

3.3   Deformed QRPA

The theoretical approach, used in this work to derive the single and double beta transition probabilities, is based on the deformed proton-neutron Quasiparticle Random Phase Approximation [2] with a separable proton-neutron residual interaction, which is relevant for the allowed Gamow-Teller transitions [112, 157].

3.3.1   Residual interaction for charge-exchange channel

The total nuclear Hamiltonian takes the form

$$H = H_0 + H_{int}. \tag{3.38}$$

H_0 denotes the Hamiltonian for the quasiparticle mean field described by a deformed axially-symmetric Woods-Saxon potential [186]

$$H_0 = \sum_{\tau\rho} E_\tau a_{\tau\rho_\tau}^\dagger a_{\tau\rho_\tau}(\tau = p, n), \tag{3.39}$$

where E_τ are the quasiparticle energies. $a_{\tau\rho_\tau}^\dagger$ $(a_{\tau\rho_\tau})$ is the quasiparticle creation (annihilation) operator. The p (n) index denotes proton (neutron) quasiparticle states with projection Ω_p (Ω_n) of the full angular momentum on the nuclear symmetry axis and parity π_p (π_n). The index ρ $(\rho = \pm 1)$ represents the sign of the angular momentum projection Ω. The intrinsic states are twofold degenerate. The states with Ω_τ and $-\Omega_\tau$ have the same energy as a consequence of the time reversal invariance. Ω_τ is taken to be positive for states and negative for time reversed states.

The method includes pairing between like nucleons in the BCS approximation with fixed gap parameters for protons, Δ_p, and neutrons, Δ_n.

The residual interaction part H_{int} of nuclear Hamiltonian in equation (3.38) contains two terms associated with particle–hole (ph) and particle–particle (pp) interaction:

$$\begin{aligned} H_{int} &= \chi \sum_{K=0,\pm 1} (-1)^K (\beta_{1K}^- \beta_{1-K}^+ + \beta_{1-K}^+ \beta_{1K}^-) \\ &\quad -\kappa \sum_K (-1)^K (P_{1K}^- P_{1-K}^+ + P_{1-K}^+ P_{1K}^-). \end{aligned} \tag{3.40}$$

---

[2]See Appendix C and D

The operators β^- and P^- are particle-hole (ph) and particle-particle (pp) components of the spin-isospin $\tau^+\sigma$, namely,

$$\beta_K^- = \sum_{p\rho_p n\rho_n} <p\rho_p|\tau^+\sigma_K|n\rho_n> c_{p\rho_p}^\dagger c_{n\rho_n}, \quad \beta_K^+ = (\beta_K^-)^\dagger,$$

$$P_K^- = \sum_{p\rho_p n\rho_n} <p\rho_p|\tau^+\sigma_K|n\rho_n> c_{p\rho_p}^\dagger \tilde{c}_{n\rho_n}^\dagger, \quad P_K^+ = (P_K^-)^\dagger. \tag{3.41}$$

The ph and pp forces in equation (3.25) are defined to be repulsive and attractive ($\chi, \kappa \geq 0$), respectively, reflecting the general feature of the nucleon-nucleon interaction in the $J^\pi = 1^+$ channel. The explicit form of the matrix element $<p\rho_p|\tau^+\sigma_K|n\rho_n>$ is presented in Appendix F.

After neglecting the scattering terms $a_{p\rho_p}^\dagger a_{n\rho_n}$ and $a_{n\rho_n}^\dagger a_{p\rho_p}$ the quasiparticle representation of H_{int} takes the form

$$
\begin{aligned}
H_{int} = &\ \chi \sum_{K=0,\pm1} \sum_{ij} [(\sigma_K(i)\overline{\sigma}_K(j) + \overline{\sigma}_K(i)\sigma_K(j))(A^\dagger(i,K)A^\dagger(\bar{j},K) + A(\bar{j},K)A(i,K)) \\
&+ (\sigma_K(i)\sigma_K(j) + \overline{\sigma}_K(i)\overline{\sigma}_K(j))(A^\dagger(i,K)A(j,K) + A(j,K)A^\dagger(i,K))] \\
&- \kappa \sum_{K=0,\pm1} \sum_{ij} [-(\pi_K(i)\overline{\pi}_K(j) + \overline{\pi}_K(i)\pi_K(j))(A^\dagger(i,K)A^\dagger(\bar{j},K) + A(\bar{j},K)A(i,K)) \\
&+ (\pi_K(i)\pi_K(j) + \overline{\pi}_K(i)\overline{\pi}_K(j))(A^\dagger(i,K)A(j,K) + A(j,K)A^\dagger(i,K))], \tag{3.42}
\end{aligned}
$$

with

$$
\begin{aligned}
\sigma_K(i) &= <p\rho_p|\tau^+\sigma_K|n\rho_n> u_p v_n, \quad \overline{\sigma}_K(i) = <p\rho_p|\tau^+\sigma_K|n\rho_n> v_p u_n, \\
\pi_K(i) &= <p\rho_p|\tau^+\sigma_K|n\rho_n> u_p u_n, \quad \overline{\pi}_K(i) = <p\rho_p|\tau^+\sigma_K|n\rho_n> v_p v_n. \tag{3.43}
\end{aligned}
$$

$A_i^\dagger$ and A_i are the two-quasiparticle creation and annihilation operators

$$A^\dagger(i,K) = a_{p\rho_p}^\dagger a_{n\rho_n}^\dagger, \quad A^\dagger(\bar{i},K) = \tilde{a}_{p\rho_p}^\dagger \tilde{a}_{n\rho_n}^\dagger, \quad A(i,K) = (A^\dagger(i,K))^\dagger. \tag{3.44}$$

The quasiparticle pairs i and $\bar{i}$ are defined by the selection rules $\Omega_p - \Omega_n = K$ and $\Omega_n - \Omega_p = K$, respectively, and $\pi_p \pi_n = 1$.

3.3.2 Phonon operator

The above considered model Hamiltonian includes terms with $K = 0, \pm1$ and describes $J^\pi K = 1^+1, 1^+0$ excitations. In the laboratory frame the proton-neutron QRPA phonon wave functions for Gamow-Teller excitations in even-even nuclei have the form

$$
\begin{aligned}
|1M(K), m> &= \sqrt{\frac{3}{16\pi^2}}[\mathcal{D}_{MK}^1(\phi,\theta,\psi)Q_K^{m\dagger} + \\
&\quad (-1)^{1+K}\mathcal{D}_{M-K}^1(\phi,\theta,\psi)Q_{-K}^{m\,\dagger}]|rpa> \quad (K = \pm1), \\
|1M(K), m> &= \sqrt{\frac{3}{8\pi^2}}\mathcal{D}_{MK}^1(\phi,\theta,\psi)Q_K^{m\dagger}|rpa> \quad (K = 0), \tag{3.45}
\end{aligned}
$$

where $|rpa>$ denotes the QRPA ground state. The intrinsic states are generated by the phonon creation operator

$$Q_K^{m\dagger} = \sum_i [X_{i,K}^m A^\dagger(i, K) - Y_{i,K}^m A(\bar{i}, K)]. \tag{3.46}$$

In the case $K = \pm 1$ ($K = 0$) the sum in equation (3.46) includes all bound and quasibound two-quasiparticle spin–projection–flip (non–spin–projection–flip) configurations. The $K = -1$ and $K = 1$ modes are related to each other through time reversal and are degenerate.

3.3.3   Secular equation

The excitation energy ω_k and the amplitudes $X_{i,K}^m$ and $Y_{i,K}^m$ of the phonon $Q_K^{m\dagger}$ are obtained by solving the RPA matrix equation

$$\begin{pmatrix} \mathcal{A}(K) & \mathcal{B}(K) \\ \mathcal{B}(K) & \mathcal{A}(K) \end{pmatrix} \begin{pmatrix} X_K^m \\ Y_K^m \end{pmatrix} = \omega_K^m \begin{pmatrix} 1 & 0 \\ 0 & -1 \end{pmatrix} \begin{pmatrix} X_K^m \\ Y_K^m \end{pmatrix}, \tag{3.47}$$

where

$$\begin{aligned} \mathcal{A}_{ij}(K) &= \mathcal{E}_i \delta_{ij} + 2\chi[\sigma_K(i)\sigma_K(j) + \bar{\sigma}_K(i)\bar{\sigma}_K(j)] - 2\kappa[\pi_K(i)\pi_K(j) + \bar{\pi}_K(i)\bar{\pi}_K(j)], \\ \mathcal{B}_{ij}(K) &= 2\chi[\sigma_K(i)\bar{\sigma}_K(j) + \bar{\sigma}_K(i)\sigma_K(j)] + 2\kappa[\pi_K(i)\bar{\pi}_K(j) + \bar{\pi}_K(i)\pi_K(j)] \end{aligned} \tag{3.48}$$

with $\mathcal{E}_i = E_p + E_n$ the two-quasiparticle excitation energy.

An advantage of using the separable forces is that the RPA matrix equation reduces to a homogeneous system of only four equations for the four unknown norms N_σ, $N_{\bar{\sigma}}$, N_π and $N_{\bar{\pi}}$, which is much easier to solve in comparison with the full diagonalization of RPA matrix of large dimension. The corresponding secular equation is given by

$$\begin{vmatrix} 1 + \chi(-P_{\sigma\sigma}^K + R_{\bar{\sigma}\bar{\sigma}}^K) & \chi(-P_{\sigma\bar{\sigma}}^K + R_{\bar{\sigma}\sigma}^K) & \kappa(P_{\sigma\pi}^K + R_{\bar{\sigma}\bar{\pi}}^K) & \kappa(P_{\sigma\bar{\pi}}^K + R_{\bar{\sigma}\pi}^K) \\ \chi(-P_{\bar{\sigma}\sigma}^K + R_{\sigma\bar{\sigma}}^K) & 1 + \chi(-P_{\bar{\sigma}\bar{\sigma}}^K + R_{\sigma\sigma}^K) & \kappa(P_{\bar{\sigma}\pi}^K + R_{\sigma\bar{\pi}}^K) & \kappa(P_{\bar{\sigma}\bar{\pi}}^K + R_{\sigma\pi}^K) \\ \chi(-P_{\pi\sigma}^K - R_{\bar{\pi}\bar{\sigma}}^K) & \chi(-P_{\pi\bar{\sigma}}^K - R_{\bar{\pi}\sigma}^K) & 1 + \kappa(P_{\pi\pi}^K - R_{\bar{\pi}\bar{\pi}}^K) & \kappa(P_{\pi\bar{\pi}}^K - R_{\bar{\pi}\pi}^K) \\ \chi(-P_{\bar{\pi}\sigma}^K - R_{\pi\bar{\sigma}}^K) & \chi(-P_{\bar{\pi}\bar{\sigma}}^K - R_{\pi\sigma}^K) & \kappa(P_{\bar{\pi}\pi}^K - R_{\pi\bar{\pi}}^K) & 1 + \kappa(P_{\bar{\pi}\bar{\pi}}^K - R_{\pi\pi}^K) \end{vmatrix} = 0, \tag{3.49}$$

with

$$P_{\alpha\acute{\alpha}}^K = 2\sum_i \frac{\alpha(i)\acute{\alpha}(i)}{\omega_K^m - \mathcal{E}_i}, \qquad R_{\alpha\acute{\alpha}}^K = 2\sum_i \frac{\alpha(i)\acute{\alpha}(i)}{\omega_K^m + \mathcal{E}_i}, \qquad (\alpha, \acute{\alpha} = \sigma, \bar{\sigma}, \pi, \bar{\pi}). \tag{3.50}$$

The forward and backward amplitudes are written as

$$\begin{aligned} X_{iK}^m &= \frac{2N_\sigma}{\omega_K^m - \mathcal{E}_i} [\; \chi(\sigma_K(i) + \bar{\sigma}_K(i)\frac{N_{\bar{\sigma}}}{N_\sigma}) - \kappa(\pi_K(i)\frac{N_\pi}{N_\sigma} + \bar{\pi}_K(i)\frac{N_{\bar{\sigma}}}{N_\sigma}) \;], \\ Y_{iK}^m &= \frac{-2N_\sigma}{\omega_K^m + \mathcal{E}_i} [\; \chi(\bar{\sigma}_K(i) + \sigma_K(i)\frac{N_{\bar{\sigma}}}{N_\sigma}) + \kappa(\bar{\pi}_K(i)\frac{N_\pi}{N_\sigma} + \pi_K(i)\frac{N_{\bar{\sigma}}}{N_\sigma}) \;], \end{aligned} \tag{3.51}$$

where for the norms N_σ, $N_{\bar{\sigma}}$, N_π and $N_{\bar{\pi}}$ one gets

$$
\begin{aligned}
N_\sigma &= \sum_j [\sigma_K(i) X^m_{jK} + \bar{\sigma}_K(i) Y^m_{jK}], & N_{\bar{\sigma}} &= \sum_j [\bar{\sigma}_K(i) X^m_{jK} + \sigma_K(i) Y^m_{jK}], \\
N_\pi &= \sum_j [\pi_K(i) X^m_{jK} - \bar{\pi}_K(i) Y^m_{jK}], & N_{\bar{\pi}} &= \sum_j [\bar{\pi}_K(i) X^m_{jK} - \pi_K(i) Y^m_{jK}].
\end{aligned}
\tag{3.52}
$$

The normalization factor N_σ is determined from the condition

$$
< rpa|[Q^m_K, Q^{m\dagger}_K]|rpa> = \sum_i (X^m_{iK} X^m_{iK} - Y^m_{iK} Y^m_{iK}) = 1.
\tag{3.53}
$$

The QRPA equations are calculated separately for different values of K and the solutions for $K = +1$ and $K = -1$ coincide each to other due to the assumed axial symmetry.

3.4 Single and double beta transition in deformed nuclei

3.4.1 Single beta transitions

The β^- and β^+ transition amplitudes from an 0^+ even-even initial nuclear state to an one-phonon state in the odd-odd final nucleus are expressed by

$$
\begin{aligned}
< 1M(K), m|\hat{\beta}^-_M|0^+_{g.s.}> &= \sum_i [\sigma(i) X^m_{iK} + \bar{\sigma}(i) Y^m_{iK}], \\
< 1M(K), m|\hat{\beta}^+_M|0^+_{g.s.}> &= \sum_i [\bar{\sigma}(i) X^m_{iK} + \sigma(i) Y^m_{iK}].
\end{aligned}
\tag{3.54}
$$

Here, $|0^+_{g.s.}>$ denotes the correlated RPA ground state in the laboratory frame. The $\hat{\beta}^\pm$ transition operators in equation (3.54) are related to the intrinsic $\beta^\pm$ operators in equation (3.40) as follows:

$$
\hat{\beta}^\pm_M = \sum_\mu \mathcal{D}^1_{M\mu}(\phi, \theta, \psi)\beta^\pm_\mu.
\tag{3.55}
$$

The β strength function is given by

$$
\begin{aligned}
B^-_{GT}(\omega) &= \sum_{K=0,\pm 1} \sum_m |< 1(K), m \parallel \hat{\beta}^- \parallel 0^+_{g.s.}>|^2 \delta(\omega - \omega_K), \\
B^+_{GT}(\omega) &= \sum_{K=0,\pm 1} \sum_m |< 1(K), m \parallel \hat{\beta}^+ \parallel 0^+_{g.s.}>|^2 \delta(\omega - \omega_K).
\end{aligned}
\tag{3.56}
$$

From the $\beta^{\pm}$ amplitudes one obtains, straightforwardly, the total $\beta^{\pm}$ strengths:

$$
\begin{aligned}
S_{GT}^{-} &= \sum_{K=0,\pm 1} \sum_{m} | < 1(K), m \parallel \hat{\beta}^{-} \parallel 0_{g.s.}^{+} > |^{2}, \\
S_{GT}^{+} &= \sum_{K=0,\pm 1} \sum_{m} | < 1(K), m \parallel \hat{\beta}^{+} \parallel 0_{g.s.}^{+} > |^{2}
\end{aligned}
\tag{3.57}
$$

3.4.2   Ikeda sum rule (ISR)

The Ikeda sum rule is given by

$$
\begin{aligned}
S_{GT}^{-} - S_{GT}^{+} &= \sum_{K=0,\pm 1} [(\sigma_K(i))^2 - (\bar{\sigma}_K(i))^2] \\
&= \sum_{K=0,\pm 1} \sum_{p\rho_p n\rho_n} | < p\rho_p|\tau^{+}\sigma_K|n\rho_n > |^{2}(v_n^2 - v_p^2) = 3(N - Z)
\end{aligned}
\tag{3.58}
$$

The factor 3 comes from the sum over K, i.e., the contribution from each component K is equal to (N-Z). In deriving the above expression the closure condition for QRPA states and the assumed completeness relation for single particle states

$$
\sum_{\tau\rho_{\tau}} |\tau\rho_{\tau} > < \tau\rho_{\tau}| = 1
\tag{3.59}
$$

has been used. If a truncated single particle basis is considered instead of the full single particle basis of the Woods-Saxon potential, the condition in equation (3.59) is violated and in consequence the Ikeda sum rule as well.

3.4.3 $2\nu\beta\beta$ -matrix elements

The inverse half-life of the $2\nu\beta\beta$-decay can be expressed as a product of an accurately known phase-space factor $G^{2\nu}$ and the Gamow-Teller transition matrix element $M_{GT}^{2\nu}$ in second order:

$$
[T_{1/2}^{2\nu}(0_{g.s.}^{+} \to 0_{g.s.}^{+})]^{-1} = G^{2\nu} (g_A)^4 |M_{GT}^{2\nu}|^2.
\tag{3.60}
$$

The contribution from the two successive Fermi transitions is safely neglected as they come from isospin mixing effects [93]. Within the deformed QRPA approach the double Gamow-Teller matrix element $M_{GT}^{2\nu}$ for ground state to ground state $2\nu\beta\beta$-decay transitions takes the form

$$
\begin{aligned}
M_{GT}^{2\nu} &= \sum_{m_i m_f} \sum_{K=0,\pm 1} \frac{< 0_f^{+} \parallel \beta^{-} \parallel 1(K), m_f > \mathcal{O} < 1(K), m_i \parallel \beta^{-} \parallel 0_i^{+} >}{(\omega_K^{m_f} + \omega_K^{m_i})/2}, \\
\mathcal{O} &= < 1(K), m_f|1(K), m_i > .
\end{aligned}
\tag{3.61}
$$

The sum extends over all 1^{+} states of the intermediate nucleus. The index i (f) indicates that the quasiparticles and the excited states of the nucleus are defined

with respect to the initial (final) nuclear ground state $|0_i^+ > (|0_f^+ >)$. The overlap
is necessary since these intermediate states are not orthogonal to each other. The
two sets of intermediate nuclear states generated from the initial and final ground
states are not identical within the considered approximation scheme. Therefore the
overlap factor of these states is introduced in the theory as follows [170, 171]:

$$< 1(K), m_f | 1(K), m_i > = \sum_{j_i j_f} [X_{j_f K}^{m_i} X_{j_i K}^{m_f} - Y_{j_f K}^{m_i} Y_{j_i K}^{m_f}] < j_f | j_i >, \qquad (3.62)$$

with

$$< j_f | j_i > = < p_f \rho_{p_f} | p_i \rho_{p_i} >< n_f \rho_{n_f} | n_i \rho_{n_i} >< BCS(^{76}Se) | BCS(^{76}Ge) > . \quad (3.63)$$

The overlap factor of the single particle wave functions of the initial and final nucleus
is given explicitly in the Appendix F and the overlap factor of the initial and final
BCS vacuum is given by [90]

$$< BCS(^{76}Se) | BCS(^{76}Ge) > \;\; = \;\; \Pi_p (u_p^{(f)} u_p^{(i)} + v_p^{(f)} v_p^{(i)})$$
$$\Pi_n (u_n^{(f)} u_n^{(i)} + v_n^{(f)} v_n^{(i)}). \qquad (3.64)$$

Here, p (n) denotes a pair of the proton (neutron) single particle states of the initial
and final nucleus with maximal overlap. For spherical nuclei this factor is given in
[104]. In the spherical limit the value of the BCS overlap factor is about 0.8 and it
was commonly neglected in the double beta decay calculations [38, 89, 130, 184].

The overlap matrix elements between the intermediate states generated from
initial and final nuclei with different K, are very small due to the different struc-
ture of the corresponding RPA configurations. They have been neglected in this
calculations. Thus the spin–projection–flip ($K = \pm 1$) and non–spin–projection–flip
($K = 0$) excitations contribute coherently to the $2\nu\beta\beta$-decay matrix element $M_{GT}^{2\nu}$.

3.5   The fully-renormalized QRPA (FR-QRPA)

Unfortunately the limitations of the QRPA formalism (for both spherical and de-
formed nuclei) cannot be overcame in the previous described formalism. The collapse
due to the overestimated ground state correlations is present (in the next chapter
the numerical calculations will show this fact), Ikeda sum rule is not totaly ful-
filled and implicit the $2\nu\beta\beta$ matrix elements cannot be rigourously evaluated. The
main questions, what mechanism can avoid the collapse of QRPA, still doesn't have
an answer. But one step further is done by formulating another QRPA extension,
namely FR-QRPA and to present the differences between this present method and
the previous QRPA extensions.

Renormalized QRPA (RQRPA) was formulated in Refs. [95] to restore (Pauli Exclusion Principle) PEP in an approximate way. The method uses a self-consistent iteration of the QRPA equation, taking into account quasiparticle occupation numbers in the QRPA ground state. This assumption leads to a modification of the commutation relations for the bifermionic operators as compared to the ordinary quasiboson approximation (QBA). At the same time so-called scattering terms (describing transitions of the quasiparticles) are neglected in the Hamiltonian and in the phonon operators. The RQRPA does not collapse for physical values of the particle-particle interaction strength and it is extensively used to calculate the intensities of the double beta decay [62, 65, 146, 168, 172, 173, 190, 191]. Moreover, RQRPA provides better agreement with the exact solution of the many-body problem within schematic models, even beyond the critical point of the standard QRPA (see, e.g. [174] and references therein).

The self-consistent RQRPA (SCQRPA) is a more complex version of RQRPA to describe the strongly correlated Fermi systems. In the SCQRPA, at the same time, the quasiparticle mean field is changed by minimizing the energy and fixing the number of particles in the correlated ground state of the RQRPA instead of the uncorrelated one of BCS as is done in the other versions of the RQRPA. In this way SCQRPA partially overcomes the inconsistency between RQRPA and the BCS approach and is closer to a fully variational theory. Nevertheless, the main drawback of the modern versions of RQRPA is the violation of the model-independent Ikeda sum rule (ISR) [23, 180, 191]. A modification of the phonon operator by including scattering terms is needed in order to restore the ISR within RQRPA.

The fully-renormalized QRPA (FR-QRPA) was formulated in Ref. [149] for even-even nuclei in such a way that it complies the restrictions imposed by the commutativity of the phonon creation operator with the total particle number operator. It was shown analytically that the Ikeda sum rule is fulfilled within the FR-QRPA [149]. Also FR-QRPA is free from the spurious low-energy solutions which would be generated by the scattering terms considered as additional degrees of freedom.

3.5.1 The FR-QRPA matrices

Within RPA an excited nuclear state, with angular momentum J and projection M, is created by applying the phonon operator $Q^{\dagger}_{JM}$ to the vacuum state $|0^{+}_{RPA}\rangle$ of the initial, even-even, nucleus: with the same nucleon number A:

$$|JM\rangle = Q^{\dagger}_{JM}|0^{+}_{RPA}\rangle \qquad \text{with} \qquad Q_{JM}|0^{+}_{RPA}\rangle = 0. \qquad (3.65)$$

As was shown in Ref. [149], the most appropriate way is to write down the phonon structure in terms of the particle creation and annihilation operators. That allows to fulfill the important principle of the commutativity of $Q^{\dagger}_{JM}$ with the total particle

number operator $\hat{A} = \hat{N} + \hat{Z}$. The phonon operator has the following structure:

$$Q^\dagger_{JM} = \sum_{\tau\tau'} \left[x_{(\tau\tau',J)} C^\dagger(\tau\tau', JM) - y_{(\tau\tau',J)} \tilde{C}(\tau\tau', JM) \right], \tag{3.66}$$

with $C^\dagger(\tau\tau', JM) = \left[c^\dagger_\tau \tilde{c}_{\tau'} \right]_{JM}$ and $\tilde{C}(\tau\tau', JM) = (-)^{J-M} C(\tau\tau', J - M)$, where $c^\dagger_{\tau m_\tau}$ $(c_{\tau m_\tau})$ denotes the particle creation (annihilation) operator.

Going into the quasiparticle representation, the quasiparticle creation and annihilation operators $a^\dagger_{\tau m_\tau}$ and $a_{\tau m_\tau}$ can be defined by the Bogolyubov transformation

$$\begin{pmatrix} a^+_{\tau m_\tau} \\ \tilde{a}_{\tau m_\tau} \end{pmatrix} = \begin{pmatrix} u_\tau & v_\tau \\ -v_\tau & u_\tau \end{pmatrix} \begin{pmatrix} c^+_{\tau m_\tau} \\ \tilde{c}_{\tau m_\tau} \end{pmatrix}, \tag{3.67}$$

that leads to the following expression for the phonon operator $Q^\dagger_{JM}$:

$$Q^\dagger_{JM} = \sum_{\tau\tau'} \left[X_{(\tau\tau',J)} \bar{A}^\dagger(\tau\tau', JM) - Y_{(\tau\tau',J)} \tilde{\bar{A}}(\tau\tau', JM) \right], \tag{3.68}$$

$$\bar{A}^\dagger = A^\dagger + \left(u_{\tau'} v_{\tau'} B^\dagger - u_\tau v_\tau \tilde{B} \right) / (v^2_{\tau'} - v^2_\tau),$$
$$A^\dagger(\tau\tau', JM) = \left[a^\dagger_\tau a^\dagger_{\tau'} \right]_{JM} \; ; \quad B^\dagger(\tau\tau', JM) = \left[a^\dagger_\tau \tilde{a}_{\tau'} \right]_{JM},$$

where $X = u_\tau v_{\tau'} x - v_\tau u_{\tau'} y$, $Y = u_\tau v_{\tau'} y - v_\tau u_{\tau'} x$. The bifermionic operators $\bar{A}^\dagger, \bar{A}$ being the basic building blocks of the FR-QRPA automatically contain the quasiparticle scattering terms which, however, are not associated with any additional degrees of freedom. That means that there are no spurious low-lying solutions in the present theoretical scheme which would be generated by the scattering terms considered as independent degrees of freedom.

From this point one can follow the usual way to formulate the RQRPA [95], substituting A by $\bar{A}$ everywhere. The forward- and backward-going free variational amplitudes X and Y satisfy the equation:

$$\begin{pmatrix} \mathcal{A} & \mathcal{B} \\ \mathcal{B} & \mathcal{A} \end{pmatrix} \begin{pmatrix} X^m \\ Y^m \end{pmatrix} = \mathcal{E}_m \begin{pmatrix} \mathcal{U} & 0 \\ 0 & -\mathcal{U} \end{pmatrix} \begin{pmatrix} X^m \\ Y^m \end{pmatrix}, \tag{3.69}$$

where m marks different roots of the QRPA equations for a given J^π,

$$\mathcal{A} = \langle 0^+_{RPA} | \left[\bar{A}, \left[H_F, \bar{A}^\dagger \right] \right] | 0^+_{RPA} \rangle,$$
$$\mathcal{B} = -\langle 0^+_{RPA} | \left[\bar{A}, \left[H_F, \bar{A} \right] \right] | 0^+_{RPA} \rangle, \tag{3.70}$$

and the renormalization matrix $\mathcal{U}_{\tau\tau'}$ is

$$\mathcal{U}_{\tau\tau'} = \langle 0^+_{RPA} | \left[\bar{A}(\tau\tau', JM), \bar{A}^\dagger(\sigma\sigma', JM) \right] | 0^+_{RPA} \rangle = \delta_{\tau\sigma} \delta_{\tau'\sigma'} \mathcal{D}_{\tau\tau'}. \tag{3.71}$$

3.5.2   The FR-QRPA equations

A rather simple, but realistic, Hamiltonian H consisting of the quasiparticle mean field H_0 and the residual separable particle–hole (ph) and particle–particle (pp) interactions is used,

$$H = H_0 + H_{int}^{ph} + H_{int}^{pp}, \qquad (3.72)$$

$$H_0 = \sum_{\tau=p,n} E_\tau a_\tau^\dagger a_\tau, \qquad (3.73)$$

$$H_{int}^{ph} = \chi \sum_M (-1)^M (\beta_{1M}^- \beta_{1-M}^+ + \beta_{1-M}^+ \beta_{1M}^-), \qquad (3.74)$$

$$H_{int}^{pp} = -\kappa \sum_M (-1)^M (P_{1M}^- P_{1-M}^+ + P_{1-M}^+ P_{1M}^-), \qquad (3.75)$$

with $\beta_{1M}^- = -\hat{J}^{-1} \sum_{pn} \langle p\|\sigma\|n\rangle \left[c_p^\dagger \tilde{c}_n\right]_{1M}$, $P_{1M}^- = \hat{J}^{-1} \sum_{pn} \langle p\|\sigma\|n\rangle \left[c_p^\dagger c_n^\dagger\right]_{1M}$

Taking into account the exact (fermionic) expressions for the commutators in the equations (3.70), (3.71), one gets the following expressions for the FR-QRPA matrices $\mathcal{A}$ and $\mathcal{B}$:

$$
\begin{aligned}
\mathcal{A} = {} & \left[(E_\tau + E_{\tau'})\mathcal{D}_{\tau\tau'} - 2(E_\tau - E_{\tau'})(u_\tau^2 v_\tau^2 + u_{\tau'}^2 v_{\tau'}^2)\mathcal{R}_{\tau\tau'}\right]\delta_{\tau\sigma}\delta_{\tau'\sigma'} \\
& + 2\chi(u_\tau v_{\tau'} u_\sigma v_{\sigma'} + v_\tau u_{\tau'} v_\sigma u_{\sigma'})\mathcal{D}_{\tau\tau'}\mathcal{D}_{\sigma\sigma'} \\
& - 2\kappa(u_\tau u_{\tau'} u_\sigma u_{\sigma'}\bar{\bar{\mathcal{D}}}_{\tau\tau'}\bar{\bar{\mathcal{D}}}_{\sigma\sigma'} - v_\tau v_{\tau'} v_\sigma v_{\sigma'}\bar{\mathcal{D}}_{\tau\tau'}\bar{\mathcal{D}}_{\sigma\sigma'}),
\end{aligned} \qquad (3.76)
$$

$$
\begin{aligned}
\mathcal{B} = {} & 2(E_\tau - E_{\tau'})u_\tau v_\tau u_{\tau'} v_{\tau'}\mathcal{R}_{\tau\tau'}\delta_{\tau\sigma}\delta_{\tau'\sigma'} \\
& + 2\chi(u_\tau v_{\tau'} v_\sigma u_{\sigma'} + v_\tau u_{\tau'} v_\sigma u_{\sigma'})\mathcal{D}_{\tau\tau'}\mathcal{D}_{\sigma\sigma'} \\
& + 2\kappa(u_\tau u_{\tau'} v_\sigma v_{\sigma'}\bar{\bar{\mathcal{D}}}_{\tau\tau'}\bar{\mathcal{D}}_{\sigma\sigma'} + v_\tau v_{\tau'} u_\sigma u_{\sigma'}\bar{\mathcal{D}}_{\tau\tau'}\bar{\bar{\mathcal{D}}}_{\sigma\sigma'}).
\end{aligned} \qquad (3.77)
$$

The renormalization matrices $\mathcal{D}, \bar{\mathcal{D}}, \bar{\bar{\mathcal{D}}}$ entering the equations (3.71), (3.76), (3.77) can be represented in terms of the relative quasiparticle occupation numbers $\mathcal{N}_\tau$ for the level τ in the RQRPA vacuum:

$$
\begin{aligned}
\mathcal{D}_{\tau\tau'} &= 1 - \mathcal{N}_{\tau'} - \mathcal{N}_\tau + \left(1 - v_\tau^2 - v_{\tau'}^2\right)\mathcal{R}_{\tau\tau'}, \qquad (3.78) \\
\bar{\mathcal{D}}_{\tau\tau'} &= 1 - \mathcal{N}_{\tau'} - \mathcal{N}_\tau - \left(u_\tau^2 + u_{\tau'}^2\right)\mathcal{R}_{\tau\tau'}, \\
\bar{\bar{\mathcal{D}}}_{\tau\tau'} &= 1 - \mathcal{N}_{\tau'} - \mathcal{N}_\tau + \left(v_\tau^2 + v_{\tau'}^2\right)\mathcal{R}_{\tau\tau'},
\end{aligned}
$$

with $\mathcal{R}_{\tau\tau'} = \frac{\mathcal{N}_\tau - \mathcal{N}_{\tau'}}{v_{\tau'}^2 - v_\tau^2}$. In turn, the quasiparticle occupation numbers

$$\mathcal{N}_\tau = \hat{j}_\tau^{-2}\langle 0_{RPA}^+|\sum_{m_\tau} a_{\tau m_\tau}^\dagger a_{\tau m_\tau}|0_{RPA}^+\rangle \qquad (3.79)$$

can be calculated in terms of the backgoing amplitudes Y of the RQRPA solution
(3.69) [95]:

$$
\begin{aligned}
\mathcal{N}_\tau &= \hat{j}_\tau^{-2} \sum_{\tau'} \left(\sum_{J,m} (2J+1)|Y_{\tau\tau',J}^m|^2 \right) \mathcal{D}_{\tau\tau'}, \\
\mathcal{N}_{\tau'} &= \hat{j}_{\tau'}^{-2} \sum_{\tau} \left(\sum_{J,m} (2J+1)|Y_{\tau\tau',J}^m|^2 \right) \mathcal{D}_{\tau\tau'},
\end{aligned}
\tag{3.80}
$$

where $\hat{j} \equiv \sqrt{2j+1}$. Along with the modified FR-QRPA equations for the chemical
potential

$$
\begin{aligned}
\langle 0_{RPA}^+ | \hat{N} | 0_{RPA}^+ \rangle &= \sum_n \hat{j}_n^2 \left(v_n^2 + (u_n^2 - v_n^2)\mathcal{N}_n \right) = N, \\
\langle 0_{RPA}^+ | \hat{Z} | 0_{RPA}^+ \rangle &= \sum_p \hat{j}_p^2 \left(v_p^2 + (u_p^2 - v_p^2)\mathcal{N}_p \right) = Z,
\end{aligned}
\tag{3.81}
$$

a rather complicated set of equations (3.69)-(3.81) has to be solved.

It is noteworthy that the renormalization matrices (3.78) become the same,
$\bar{\bar{\mathcal{D}}}_{\tau\tau'} = \bar{\mathcal{D}}_{\tau\tau'} = \mathcal{D}_{\tau\tau'}$, in the limit $\mathcal{R}_{\tau\tau'} = 0$ and coincide with the renormalization
matrix of the usual RQRPA (see,e.g., [191]). Thus, one can argue that the standard versions of RQRPA neglect effectively the differences between the quasiparticle
occupation numbers whereas FR-QRPA takes the differences into account.

From now on one follows the usual way of solving RQPA equations [95]. It is
useful to introduce the notation:

$$
\bar{X} = \mathcal{U}^{1/2} X, \qquad \bar{Y} = \mathcal{U}^{1/2} Y,
\tag{3.82}
$$

$$
\bar{\mathcal{A}} = \mathcal{U}^{-1/2} \mathcal{A} \mathcal{U}^{-1/2}, \qquad \bar{\mathcal{B}} = \mathcal{U}^{-1/2} \mathcal{B} \mathcal{U}^{-1/2}.
\tag{3.83}
$$

Then the amplitudes $\bar{X}$ and $\bar{Y}$ satisfy the equation of usual QRPA:

$$
\begin{pmatrix} \bar{\mathcal{A}} & \bar{\mathcal{B}} \\ \bar{\mathcal{B}} & \bar{\mathcal{A}} \end{pmatrix} \begin{pmatrix} \bar{X}^m \\ \bar{Y}^m \end{pmatrix} = \mathcal{E}_m \begin{pmatrix} 1 & 0 \\ 0 & -1 \end{pmatrix} \begin{pmatrix} \bar{X}^m \\ \bar{Y}^m \end{pmatrix}.
\tag{3.84}
$$

Solving the FR-QRPA equations, one gets the fully renormalized amplitudes $\bar{X}$, $\bar{Y}$
with the usual normalization and closure relations:

$$
\begin{aligned}
\sum_{\tau\tau'} \bar{X}_{(\tau\tau',J)}^m \bar{X}_{(\tau\tau',J)}^k - \bar{Y}_{(\tau\tau',J)}^m \bar{Y}_{(\tau\tau',J)}^k &= \delta_{km}, \\
\sum_m \bar{X}_{(\tau\tau',J)}^m \bar{X}_{(\tau_1\tau_2',J)}^m - \bar{Y}_{(\tau\tau',J)}^m \bar{Y}_{(\tau_1\tau_2',J)}^m &= \delta_{\tau\tau_1} \delta_{\tau'\tau_2'}, \\
\sum_m \bar{X}_{(\tau\tau',J)}^m \bar{Y}_{(\tau_1\tau_2',J)}^m - \bar{Y}_{(\tau\tau',J)}^m \bar{X}_{(\tau_1\tau_2',J)}^m &= 0.
\end{aligned}
\tag{3.85}
$$

It was shown analytically that the Ikeda sum rule is fulfilled within the FR-QRPA [149], in contrast to the earlier versions of the RQRPA [95]. The Ikeda sum rule states that the difference between the total Gamow-Teller strengths $S^{(-)}$ and $S^{(+)}$ in the β^- and β^+ channels, respectively, is $3(N-Z)$ [103]:

$$ISR = S^{(-)} - S^{(+)} = 3(N-Z), \tag{3.86}$$

$$S^{(-)} = \sum_{Mm} \left| \langle 1^+ M, m | \beta^-_{1M} | 0^+_{RPA} \rangle \right|^2, \qquad S^{(+)} = \sum_{Mm'} \left| \langle 1^+ M, m' | \beta^+_{JM} | 0^+_{RPA} \rangle \right|^2. \tag{3.87}$$

With the use of the closure conditions (3.85), the expressions for $\mathcal{D}_{pn}$ (3.78) and the chemical potentials (3.81), one can show [149] that

$$ISR = \sum_{pn} |\langle p \| q_J \| n \rangle|^2 \, (v_n^2 - v_p^2) \mathcal{D}_{pn} = 3(N-Z). \tag{3.88}$$

The inverse half-life of the $2\nu\beta\beta$-decay can be expressed as a product of an accurately known phase-space factor $G^{2\nu}$ and the second order Gamow-Teller transition matrix element $M^{2\nu}_{GT}$:

$$[T^{2\nu}_{1/2}(0^+_{g.s.} \to 0^+_{g.s.})]^{-1} = G^{2\nu} \, (g_A)^4 \, |M^{2\nu}_{GT}|^2. \tag{3.89}$$

The contribution from the two successive Fermi transitions is safely neglected as they arise from isospin mixing effect [93]. The double Gamow-Teller matrix element $M^{2\nu}_{GT}$ for ground state to ground state $2\nu\beta\beta$-decay transitions acquires the form

$$M^{2\nu}_{GT} = \sum_{m_i m_f} \frac{\langle 0^+_f \| \beta^- \| 1^+_{m_f} \rangle \langle 1^+_{m_f} | 1^+_{m_i} \rangle \langle 1^+_{m_i} \| \beta^- \| 0^+_i \rangle}{(\omega^{m_f} + \omega^{m_i})/2}. \tag{3.90}$$

The sum extends over all 1^+ states of the intermediate nucleus. The index $i(f)$ indicates that the quasiparticles and the excited states of the nucleus are defined with respect to the initial (final) nuclear ground state $|0^+_i\rangle$ ($|0^+_f\rangle$).

The overlap is necessary since these intermediate states are not orthogonal to each other. The two sets of intermediate nuclear states generated from the initial and final ground states are not identical within the considered approximation scheme. Therefore the overlap factor of these states is introduced in the theory as follows:

$$\langle 1^+_{m_f} | 1^+_{m_i} \rangle = \sum_{\tau\tau'} [X_{\tau\tau'}(1^+ m_i) X_{\tau\tau'}(1^+ m_f) - Y_{\tau\tau'}(1^+ m_i) Y_{\tau\tau'}(1^+ m_f)]. \tag{3.91}$$

Chapter 4

CALCULATIONS AND RESULTS

4.1   The proton-neutron pairing for N>Z nuclei

The starting point of the numerical calculations is the eigenstates of a deformed axially-symmetric Woods-Saxon potential with the parameterization of Ref. [186] [1], i.e., spherical symmetry is broken already from the beginning. For the description of the ground states of the Ge isotopes, the values of the quadrupole (β_2) and the hexadecapole (β_4) nuclear deformation parameters are from Ref. [113], which are in good agreement with the predictions of the macroscopic-microscopic model of Möller, Nix, Myers and Swiatecki [126]. In the BCS calculation the single particle states are identified with the asymptotic quantum numbers $(N, n_z, \Lambda, \Omega)$. The intrinsic states are twofold degenerate. The states with Ω and $-\Omega$ have the same energy as consequence of the time reversal invariance. A truncated model space with $N \leq 5$ is considered in this case. The coupling of nucleon states in time-reversed components of the same orbitals are taken into account.
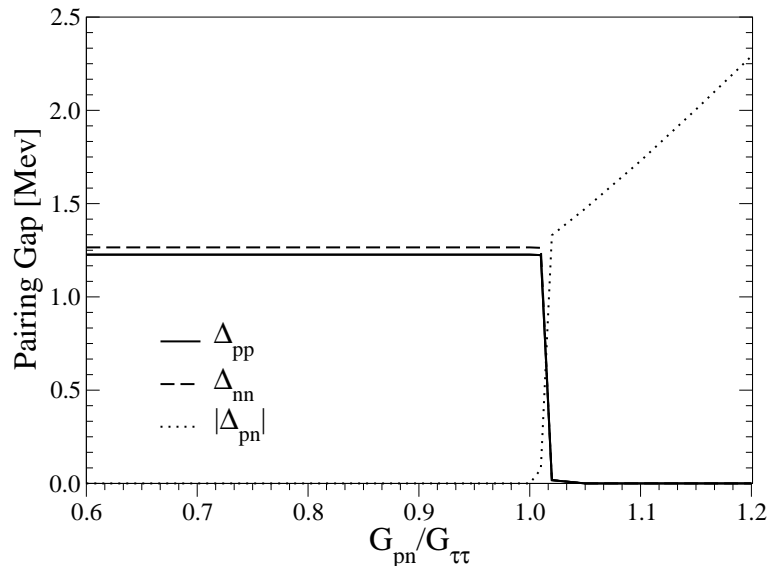

Figure 4.1: The proton (Δ_{pp}), neutron (Δ_{nn}) and proton–neutron (Δ_{pn}) pairing gaps as a function of the ratio $G_{pn}/G_{\tau\tau}$ for the $^{64}_{32}Ge$. $G_{\tau\tau}$ represents the proton and neutron pairing strengths ($G_{\tau\tau} = G_{pp}^{T=1} = G_{nn}^{T=1}$). G_{pn} stands for the larger of T=0 ($G_{pn}^{T=0}$) and T=1 ($G_{pn}^{T=1}$) proton-neutron pairing strengths. $G_{\tau\tau}$ were taken to be 0.250 MeV.

The calculation of the gap parameters is performed within the generalized BCS formalism associated with the nuclear Hamiltonian in equation (3.20). The solutions obtained can be classified as follows:

---

[1]See also Appendix B

i) The BCS solution without pn-pairing. In this case Δ_{pp} and Δ_{nn} are real and $\Delta_{pn}=0$.

ii) The BCS solution with T=1 pn-pairing. It corresponds to the case the Δ_{pp}, Δ_{nn} and Δ_{pn} are real ($\Delta_{pn}^{T=0}=0$), i.e., all the occupation amplitudes are real.

iii) The BCS solution with T=0 pn-pairing, which is characterized by real Δ_{pp} and Δ_{nn} and purely imaginary Δ_{pn} ($\Delta_{pn}^{T=1}=0$). In this case the occupation amplitudes associated with pn-pairing (u_{s1n}, v_{s1n}, u_{s2p} and v_{s2p}) are imaginary.

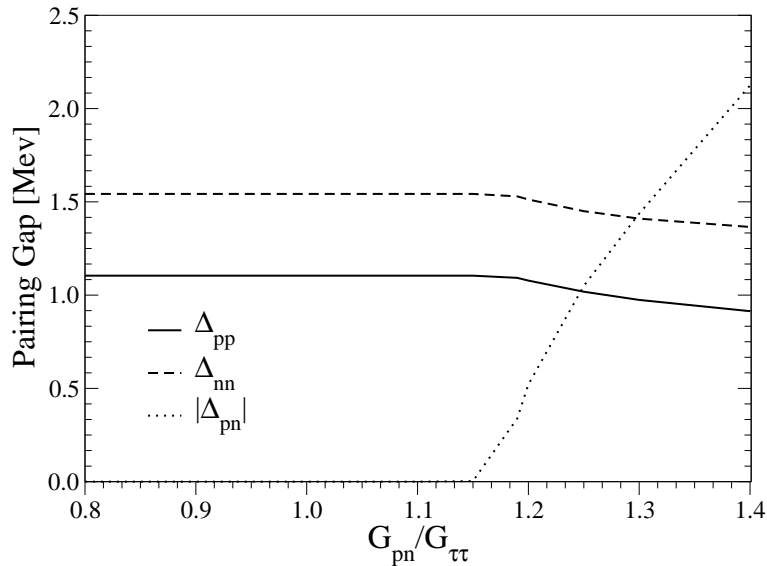No coexistence of $T = 0$ and $T = 1$ proton–neutron pairing modes was found. There

Figure 4.2: The proton (Δ_p), neutron (Δ_n) and proton–neutron (Δ_{pn}) pairing gaps as a function of the ratio $G_{pn}/G_{\tau\tau}$ for the $^{70}_{32}Ge$. Conventions are the same as in Fig. 4.1 and $G_{\tau\tau}$ were equal to $0.229\ MeV$.

is a very simple competition between the two kinds of pn-pairing. For $G_{pn}^{T=1} > G_{pn}^{T=0}$ and $G_{pn}^{T=1} < G_{pn}^{T=0}$ scenarios ii) and iii) are realized, respectively. In a particular case $G_{pn}^{T=1} = G_{pn}^{T=0}$ both T=0 and T=1 pairing modes are indistinguishable. The absolute values of the occupation amplitudes associated with the solutions ii) and iii) are equal one to another if the T=1 pn–pairing strength used in generating solution ii) is equal to the T=0 pn–pairing strength considered in the calculation of iii) solution (proton and neutron pairing strengths are the same). In the case of $N = Z$ (^{64}Ge), for sufficiently large pn-pairing strength, $G_{pn}^{T=0}$ or $G_{pn}^{T=1}$, a BCS solution without like–particle pairing modes can be observed.

In Figs. 4.1 and 4.2 the BCS gap parameters are plotted as a function of the ratio $G_{pn}/G_{\tau\tau}$ for ^{64}Ge and ^{70}Ge, respectively. The G_{pn} stands for the larger of the T=1

$(G_{pn}^{T=1})$ and T=0 $(G_{pn}^{T=0})$ proton–neutron pairing strengths and $G_{\tau\tau} = G_{pp}^{T=1} = G_{nn}^{T=1}$. There is no coexistence of $T = 0$ and $T = 1$ proton–neutron pairing modes and the absolute value of the pn-pairing gap Δ_{pn} is the same in the case of $T = 1$ $(G_{pn} = G_{pn}^{T=1} > G_{pn}^{T=0})$ and $T = 0$ $(G_{pn} = G_{pn}^{T=0} > G_{pn}^{T=1})$ pairing solutions. In the case of ^{64}Ge (^{70}Ge), the $G_{\tau\tau}$ was assumed to be 0.250 MeV (0.229 MeV). Below some critical value of the ratio $G_{pn}/G_{\tau\tau}$ there are only proton and neutron pairing modes. For ^{64}Ge there is only a narrow region above this critical point in which like–particle and proton–neutron pairs coexist. With an additional increase of the ratio $G_{pn}/G_{\tau\tau}$, the system prefers to form only proton–neutron pairs. For nuclei with non-zero neutron excess ($N \neq Z$), like ^{70}Ge, there is a different situation. In Fig. 4.2 there is a less sharp phase transition to the proton-neutron pairing mode in comparison with that in Fig. 4.1. In addition, the proton-neutron pairing mode does exist only in coexistence with the like particle pairing modes.

The binding energy gains between a system with no proton-neutron interaction and a system where the proton–neutron pairs do exist. The ground state energy decreases monotonically with increasing $G_{pn}^{T=0,1}$. Although the energy gain due to the pairing correlations is rather modest, it is expected that the pn correlations influence many properties of the atomic nuclei. In order to perform corresponding studies the problem of fixing the pairing strength parameters has to be understood.
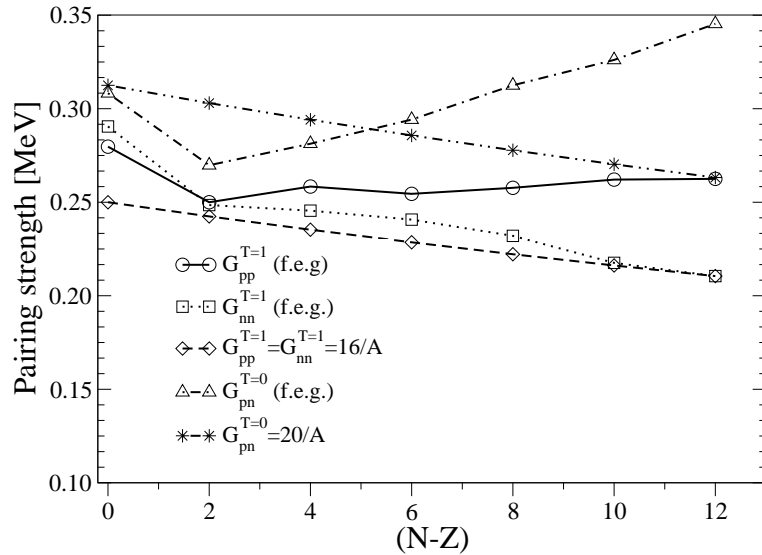

Figure 4.3: The proton $(G_{pp}^{T=1})$, neutron $(G_{nn}^{T=1})$ and proton–neutron $(G_{pn}^{T=0})$ pairing strengths as function of the neutron excess $N - Z$. For the curves f.e.g. (fitted to the experimental gaps) the strength is adjusted to the experimental pairing gap $(\Delta_p^{emp.}$ or $\Delta_n^{emp.})$ or proton–neutron interaction energy $(\delta_{pn}^{emp.})$.

There is very little known about the T=0 and T=1 strengths of the pn-pairing. The T=0, ^3S pairing force is expected to be stronger in than the T=1, ^1S pairing forces. A strong evidence of this is that the deuteron and many other even-even N=Z nuclei prefer this type of coupling due to the strong tensor force contribution. This fact favors solution iii) over ii). In Fig. 4.3 the values of the pairing strength, adjusted to the experimental pairing gaps and proton-neutron interaction energy, are presented. By comparing the $G_{pp}^{T=1}$ and $G_{nn}^{T=1}$ strengths one can see that the isospin invariance is significantly violated especially for isotopes with large neutron excess (N-Z). The T=0 proton–neutron force $G_{pn}^{T=0}$ is larger than the T=1 pp and nn ($G_{pp}^{T=1}$ and $G_{nn}^{T=1}$) forces for all considered Ge isotopes. The N=Z ^{64}Ge seems to be a special case. For other Ge isotopes $G_{pp}^{T=1}$ is more or less stable with respect to the N-Z difference and $G_{nn}^{T=1}$ slightly decreases with increasing N-Z. The T=0 pn-force offers different behavior, namely, $G_{pn}^{T=0}$ is growing significantly with increasing neutron excess N-Z. The largest differences among $G_{pn}^{T=0}$, $G_{pp}^{T=1}$ and $G_{pp}^{T=1}$ forces are visible for the maximal value of $N - Z = 12$. For Ge isotopes with $N - Z < 0$ and $N - Z > 12$ the pairing strengths can not be fixed following the procedure presented in the previous section due to the lack of experimental information on nuclear masses and/or proton and neutron separation energies.

It is interesting to compare the behavior of the adjusted pairing strengths with the commonly used prescriptions

$$G_{pp}^{T=1} = G_{nn}^{T=1} = 16/A, \qquad G_{pn}^{T=0} = 20/A. \tag{4.1}$$

From the Fig. 4.3 it is evident that these expressions do not work well for Ge isotopes, probably due to the absent of (N-Z) degree of freedom.

It is an open issue whether the value of the pairing strength $G_{pn}^{T=0}$ depends on the deformation of the considered isotope. In Fig. 4.4 this point is analyzed for ^{64}Ge, ^{68}Ge and ^{76}Ge assuming different deformations. The $G_{pn}^{T=0}$ is displayed as a function of the deformation parameter β_2 within the range $-0.4 \le \beta_2 \le 0.4$. The T=0 pairing strength ($G_{pn}^{T=0}$) is sensitive to the change of the quadrupole parameter β_2 especially if the shape of the considered nucleus is oblate. From the considered Ge isotopes ^{68}Ge exhibits the strongest sensitivity of $G_{pn}^{T=0}$ to β_2 parameter.

In Fig. 4.5 the competition among pp, nn and pn pairs in the ground state of even-even Ge isotopes is studied, as a function of $N - Z$. The displayed quantities $< \mathcal{N}_{pp} >$, $< \mathcal{N}_{nn} >$ and $< \mathcal{N}_{pn}^{T=0} >$ correspond roughly to the number of pp, nn and T=0 pn pairs [see equation (3.32)], respectively. These quantities, as it was already stressed above, are closely related to the different contributions to the total pairing energy (3.30). The number of pairs were measured both for the system with only like–particle pairs [phase i] and for the system where like–particle and proton–neutron pairs coexist [phase iii]. In Fig 4.5 a) the results obtained with the pairing strengths adjusted to the experimental pairing gaps ($\Delta_p^{emp.}$ and $\Delta_n^{emp.}$)
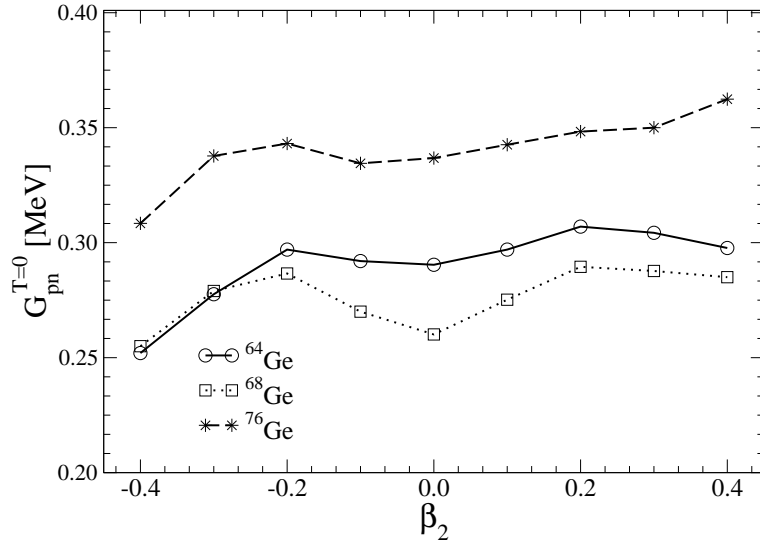
Figure 4.4: The T=0 proton–neutron pairing strength $G_{pn}^{T=0}$ as function of the deformation parameter β_2 for ^{64}Ge, ^{68}Ge and ^{76}Ge.

and proton–neutron interaction energy $(\delta_{pn}^{emp.})$ are presented. In phase i) there is a rough constancy of the number of pp-pairs for Ge isotopes and that the number of nn-pairs is slightly larger and exhibits some fluctuations. There is a different behavior if the system of nucleons prefers the phase iii). The $< \mathcal{N}_{pp} >$ and $< \mathcal{N}_{nn} >$ are equal to zero for ^{64}Ge and grow up to maximum values about 7.6 and 4.8, respectively, for ^{74}Ge. The behavior of $< \mathcal{N}_{pn}^{T=0} >$ is different. The effect of the proton-neutron pairing decreases with increasing N-Z. For large N-Z the value of $< \mathcal{N}_{pn}^{T=0} >$ is significantly smaller as $< \mathcal{N}_{pp} >$ and $< \mathcal{N}_{nn} >$, but not negligible. If pairing strengths given in (3.37) are used in the BCS calculation, the effect of proton-neutron pairing disappears at $N - Z \geq 8$ in real nuclei as it is shown in Fig. 4.5 b). Then, for these isotopes one fails to explain the non-zero value of the proton-neutron interaction energy $\delta_{pn}^{emp.}$ (see Table 3.1). The values of $\delta_{pn}^{emp.}$ for all $^{70,72,74,76}Ge$ isotopes are of the same order. Thus, it is expected that the role of the pn-pairing for all these isotopes is of comparable importance and not negligible.

From the above discussion it follows that the T=0 proton–neutron pairing correlations should be considered also for medium-heavy nuclei with large neutron excess. Usually, the correlations between protons and neutrons in medium and heavy nuclei were neglected on the ground that two Fermi levels are apart. Here, it is shown that the proton-neutron pairing effect is not negligible for such nuclear systems. The competition between the different kinds of pairs can affect measurable properties of nuclei, in particular β^+ strengths. The previous β- and $\beta\beta$-decay studies [35] performed within the spherical QRPA with T=1 proton-neutron pairing support this
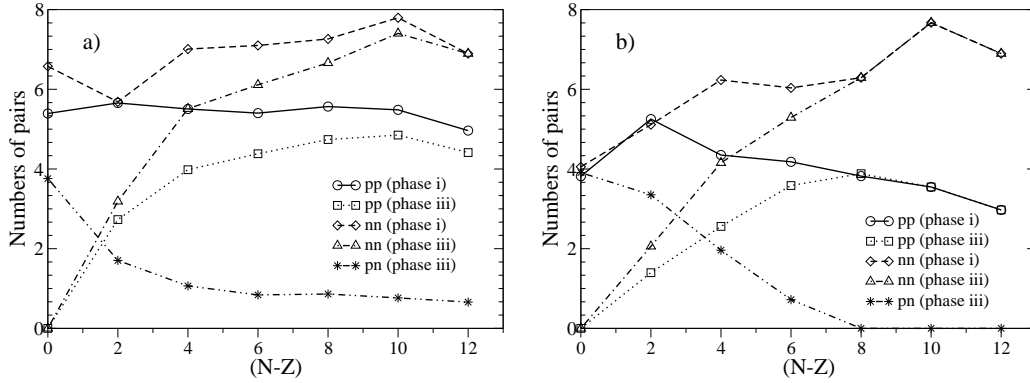
Figure 4.5: The quantities $< \mathcal{N}_{pp} >$, $< \mathcal{N}_{nn} >$ and $< \mathcal{N}_{pn}^{T=0} >$ [representing number of pp,nn and pn pairs; see Eqs. (3.32) for definition] for Ge isotopes, as a function of $N - Z$. The results are presented for a pure like particle pairing phase (phase i) and for a phase where like-particle and T=0 proton-neutron pairs coexist (phase iii). The figure a) refers to the calculation with pairing strengths adjusted to experimental pairing gaps and proton-neutron interaction energy. The figure b) refers to the calculation with pairing strengths is taken from equation (3.37).

conclusion as well.

4.2   Ground state properties of the double beta decay emitters

In this section the results for the bulk properties of the nuclei studied in the WS and HF descriptions, are presented. First, the energy surfaces are analyzed as a function of deformation (Fig. 4.6). In the case of WS, this is simply done by varying the quadrupole deformation of the potential β_2, which is an input parameter. In the case of HF, this is achieved by minimizing the HF energy while keeping the nuclear deformation fixed [71]. The HF calculations predict the existence of two energy minima close in energy, giving rise to shape isomers, while the WS potential shows a single energy minimum, which is in agreement with the absolute prolate minimum in the case of ^{76}Ge and close to the prolate HF solution in the case of ^{76}Se. In Table 7.5.1[2] the experimental and the microscopically calculated charge root mean square radii r_c with the forces Sk3 and SG2 are given. Both, oblate-prolate, results are quoted when the energies for the two shapes are very close are quoted. The values obtained for the charge radii are in good agreement with the experimental values
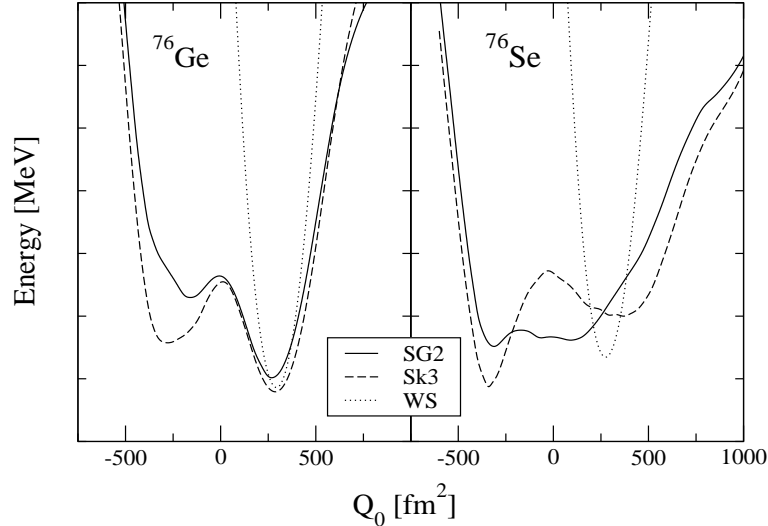
---

[2]See Appendix E

Figure 4.6: Total energy as a function of the mass quadrupole moment obtained from deformed Hartree-Fock calculations with the Skyrme forces SG2 (solid line) and Sk3 (dashed lines), and from deformed Woods-Saxon potentials (dotted line). The origin of the energy axis is different in each case but the distance between ticks corresponds always to 1 MeV.

from Ref. [205]. They are also in good agreement with the results obtained from relativistic mean field. calculations [113].

In Table 7.5.2[3] the theoretical and experimental quadrupole deformations are shown. Experimental values have been extracted from the measured quadrupole moments with two different methods. In the first one the quadrupole deformation is obtained analytically, using the empirical intrinsic moments derived from the laboratory moments of Ref. [147] assuming a well defined deformation. In the second case the quadrupole deformations are taken from Ref. [148], where they were derived from experimental values of $B(E2)$ strengths. With this approach the sign cannot be extracted. The theoretical values have been derived microscopically from the forces Sk3 and SG2, using the intrinsic quadrupole moments obtained as ground state expectations of the Q_{20} operator and the microscopic charge radii. For WS calculations using the mean square radii r_c and quadrupole moments Q_p one gets the quadrupole deformations β ($\beta = \sqrt{\frac{\pi}{5}}\frac{Q_p}{Zr_c^2}$).
There is still another important experimental information relevant for the purpose of this work. Since the final goal is to establish the ingredients to perform reliable calculations of the double beta decay, the $Q_{\beta\beta}$ energy of the decay is of relevance. The energy released in a double beta process in a transition from ground-state to

---

[3]See Appendix E

ground-state is given by

$$
\begin{aligned}
Q_{\beta\beta} &= [M_{\text{parent}} - M_{\text{daughter}} - 2m_e] \\
&= [2(m_n - m_p - m_e) + BE(Z, N) - BE(Z + 2, N - 2)] , \quad (4.2)
\end{aligned}
$$

in terms of the nuclear masses M's, or similarly, in terms of the binding energies BE's of parent (Z, N) and daughter $(Z + 2, N - 2)$ nuclei. In Table 4.1 the ex-

Table 4.1: Differences of binding energies ($\delta = BE_i - BE_f$) (MeV) in double beta partner nuclei. Experimental $Q_{\beta\beta}$ (MeV) values are within parenthesis. In the last column we show the deformations that reproduce the experimental $Q_{\beta\beta}$. Only those marked with an asterisk are considered in GT calculations.

Double beta transition	δ_{exp} ($Q_{\beta\beta}$)	δ_{Sk3}	β_{new}
^{48}Ca $\rightarrow$ ^{48}Ti	2.708 (4.272)	1.38	^{48}Ca : 0.0 $\rightarrow$ 0.087
^{76}Ge $\rightarrow$ ^{76}Se	0.474 (2.039)	-0.21	^{76}Ge : 0.161 $\rightarrow$ 0.107 (*)
^{82}Se $\rightarrow$ ^{82}Kr	1.430 (2.995)	1.01	^{82}Se : 0.126 $\rightarrow$ 0.130
^{96}Zr $\rightarrow$ ^{96}Mo	1.786 (3.350)	4.03	^{96}Mo : 0.147 $\rightarrow$ 0.027 (*)
^{100}Mo $\rightarrow$ ^{100}Ru	1.470 (3.034)	2.01	^{100}Ru : 0.175 $\rightarrow$ 0.147 (*)
^{116}Cd $\rightarrow$ ^{116}Sn	1.240 (2.805)	0.31	^{116}Cd : 0.206 $\rightarrow$ 0.149 (*)
^{128}Te $\rightarrow$ ^{128}Xe	-0.698 (0.867)	-1.67	^{128}Te : -0.088 $\rightarrow$ -0.005
^{130}Te $\rightarrow$ ^{130}Xe	0.964 (2.529)	-0.37	^{130}Te : -0.076 $\rightarrow$ 0.128
^{136}Xe $\rightarrow$ ^{136}Ba	0.903 (2.468)	-0.77	^{136}Xe : 0.001 $\rightarrow$ 0.102
^{150}Nd $\rightarrow$ ^{150}Sm	1.803 (3.367)	2.03	^{150}Sm : 0.207 $\rightarrow$ 0.201

perimental values of $Q_{\beta\beta}$ are shown as well as and the corresponding experimental difference of nuclear binding energies between parent and daughter nuclei. They are compared with the values calculated with the force Sk3. The agreement with experiment is reasonable taking into account that we are dealing with differences of energies ranging from 400 MeV in A=48 systems to 1200 MeV in A=150. From Table 4.1 it can be seen that to match the experimental energies, one needs to slightly increase the energy difference in A=48,76,82,116,128,130,136 and to decrease it in A=96,100,150. In view of these results, and taking into account that, at the same time, one has to consider the selfconsistent deformation, the deformation that reproduces the $Q_{\beta\beta}$ value and the various values of the experimental deformation, the $\beta-$values are adopted to yield the best global agreement. These are the $\beta-$ values given for force Sk3 in Table 7.5.2, except for the cases ^{76}Ge, ^{96}Mo, ^{100}Ru and ^{116}Cd. For the except cases, modified values are given in Table 4.1: 0.107, 0.027, 0.147 and 0.149, respectively.

For the calculation using Woods-Saxon potential, the values from both Refs. [147] and [148] are taken. For each nucleus, the two references give two different

values of the β−parameter. In the next section the GT distributions obtained with the two values are discussed.

Summarizing , the choice of deformation is still a very difficult task. First, because the experimental values are rather different, the uncertainties involved depending on the method. Second because the model has to be selfconsistent.

It has to be kept in mind, the Gammov-Teller strength is different for HF and WS for the same deformation. An explicit presentation of this difference is given in Table 7.5.2[4]

4.3   Gamow-Teller strength for double beta emitters

This Section is reserved to discuss the Gamow-Teller strength distributions obtained from different choices of the deformed mean fields and residual interactions.

As a general rule, the following figures show the GT strength distributions plotted versus the excitation energy of the daughter nucleus. The distributions of the GT strength have been folded with Breit-Wigner functions of 1 MeV width and the comparison among the various calculations is facilitated, so that the original discrete spectrum is transformed into a continuous profile. These distributions are given in units of $g_A^2/4\pi$ and one should keep in mind that a quenching of the g_A factor, typically $g_{A,\text{eff}} = (0.7 - 0.8)\ g_{A,\text{free}}$, is expected because of the observed quenching in charge exchange reactions. In Fig. 4.7 the dependence of the GT strength distributions on the deformed quasiparticle mean field of ^{76}Ge and ^{76}Se is shown. To make the comparison meaningful the results are obtained at the two-quasiparticle level without including the spin-isospin residual interactions. In figure the $B(GT_-)$ and $B(GT_+)$ strength distributions are plotted in the upper and lower panels, respectively.

It has to be noticed that the relevant strength distributions for the double β-decay of ^{76}Ge are the $B(GT_-)$ distribution of the parent (^{76}Ge) nucleus and the $B(GT_+)$ distribution of the daughter (^{76}Se) nucleus, but for completeness both distributions for each nucleus are shown in Fig. 4.7. Solid lines correspond to the results obtained with the Skyrme force SG2 within a HF scheme, dashed lines correspond to the results obtained with the WS potential. Pairing correlations are included in both cases in a similar way, using the gap parameters for neutrons and protons mentioned earlier. Then, the only source of discrepancy between HF and WS comes from the different single particle wave functions and energies.

In general, one can observe that WS and HF produce a similar structure of three
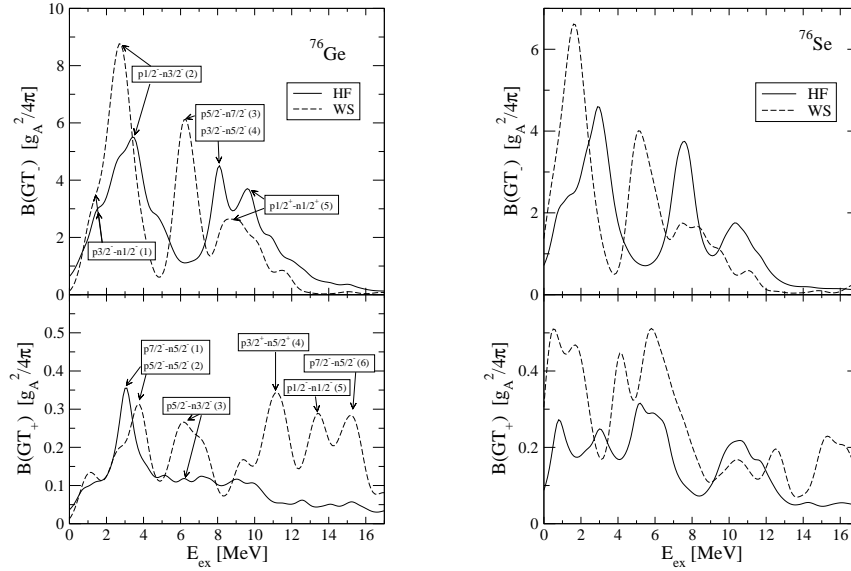
---

[4]See Appendix E

Figure 4.7: Gamow-Teller $B(GT_-)$ and $B(GT_+)$ strength distributions $[g_A^2/4\pi]$ in ^{76}Ge and $^Se76$ plotted as a function of the excitation energy of the daughter nucleus. We compare results of HF(SG2)+BCS (solid line) and WS+BCS (dashed line) approximations for the prolate minima.

peaks in the $B(GT_-)$ profiles of ^{76}Ge and ^{76}Se, although the WS results are somewhat displaced to lower energies with respect to the HF peaks. The strengths contained in the peaks are also comparable. In the case of the $B(GT_+)$ distributions, there is a different scale, which is about one order of magnitude lower than the $B(GT_-)$ scale. This is a consequence of the Pauli blocking. While the occupation amplitudes u and v (see equation3.43) favor M_- strengths, they are very small factors in M_+ strengths when connecting similar proton and neutron states. As seen in Fig. 4.7, the difference between total $B(GT_-)$ and $B(GT_+)$ strengths (the ISR is exhausted in this nuclei up to $95\div$), is a large number $3(N-Z) = 36$ in ^{76}Ge and $3(N-Z) = 24$ in ^{76}Se.

The profiles of the $B(GT_+)$ distributions with WS and HF present some discrepancies that are amplified by the different scale. It is remarkable the large strength produced by WS in the region of high excitation energies in ^{76}Ge. This aspect is discussed later in terms of the single particle wave functions.

In order to clarify the origin of the various peaks in the strength distributions, in Fig. 4.8 labels are added to show some of the leading transitions generating the strength. The labels stand for $pK^\pi - nK'^\pi$ of the orbitals connected by the spin operator and a number that identifies the transition. In both cases, $B(GT_-)$ and $B(GT_+)$, the same type of transitions are connected by the GT operator but the occupation probabilities, weighting the matrix elements, enhance or reduce them

accordingly. Basically, the structure of the profiles in both WS and HF are generated by the same type of GT transitions.
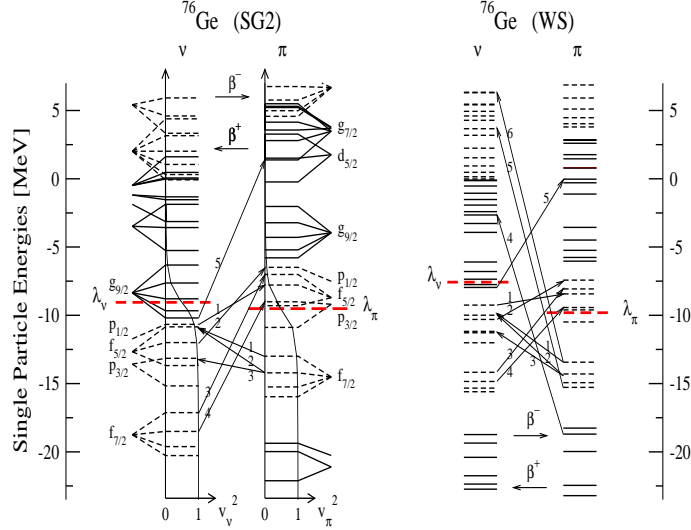

Figure 4.8: Hartree-Fock and Woods-Saxon single particle energies for protons and neutrons in ^{76}Ge.

This can be further illustrated by looking at Fig. 4.8, where the single particle energies for protons and neutrons obtained in HF(SG2) and WS in ^{76}Ge are shown. In the left part of the figure are plotted the occupation probabilities v_ν^2 and v_π^2 and the Fermi energies λ_ν and λ_π corresponding to the HF. Here ν stands for neutrons and π for protons. For completeness the spherical levels are labelled by their ℓ_j values. Indicated by arrows are the most relevant Gamow-Teller transitions in the β^- and β^+ directions and are labelled by the same numbers used to identify the peaks in Fig. 4.7. To be more precise, one can see the correspondence between these labels and the transitions connecting the proton and neutron states Table 4.2.

Now, looking at Fig. 4.7, one can understand that the two first peaks in $B(GT_-)$ are generated mainly by transitions between neutrons and protons dominated by contributions within the $N = 3$ shell and that the third peak is generated by transitions between neutrons and protons with main contributions coming from the $N = 4$ shell. The different energies of the peaks are due to the different concentration of energy levels in HF and WS.

In the case of $B(GT_+)$, the strength below 8 MeV is mainly generated by transitions within the $N = 3$ shells. Beyond 8 MeV the strength, which is negligible in HF, is generated by transitions between the proton shell $N = 2$ and the neutron shell $N = 4$ as well as between the proton shell $N = 3$ and the neutron shell $N = 5$, always understood as the main components of the wave functions. Then, very deep

Table 4.2: Correspondence of the labels used in Fig. 4.8 with the asymptotic quantum numbers notation $[Nn_z\Lambda]K^\pi$.

	β^-	β^+
(1)	$\nu[301]1/2^- \to \pi[301]3/2^-$	$\pi[303]7/2^- \to \nu[303]5/2^-$
(2)	$\nu[301]3/2^- \to \pi[301]1/2^-$	$\pi[312]5/2^- \to \nu[303]5/2^-$
(3)	$\nu[303]7/2^- \to \pi[303]5/2^-$	$\pi[312]5/2^- \to \nu[312]3/2^-$
(4)	$\nu[312]5/2^- \to \pi[312]3/2^-$	$\pi[202]3/2^+ \to \nu[413]5/2^+$
(5)	$\nu[420]1/2^+ \to \pi[440]1/2^+$	$\pi[330]1/2^- \to \nu[530]1/2^-$
(6)		$\pi[303]7/2^- \to \nu[523]5/2^-$

inside protons ($v_p = 1$) are connected with very unoccupied neutron states ($u_n = 1$), giving rise to maximum occupation factors. The different behavior in this high energy region between HF and WS is therefore, due to the structure of the deformed orbitals.

To illustrate the role of the different single particle wave functions in the development of the peak structure, the case of the last peak observed in the $B(GT_+)$ distribution of the WS potential is considered in detail. As one can see it is mainly due to a transition between the proton state [303] in the $N = 3$ shell with $K^\pi = 7/2^-$ and the neutron state [523] in the $N = 5$ shell with $K^\pi = 5/2^-$. The structure of the single particle wave functions, according to the expansion in equation (3.1), of these two states can be seen in Table 4.3. With these coefficients one can construct the matrix elements in equation (3.59). The resulting strength is almost two orders of magnitude, which explains the huge discrepancy observed between WS and HF in the higher energy domain. Nevertheless, these discrepancies are smaller in the case of the $B(GT_+)$ of ^{76}Se, which is the relevant branch for the double β-decay of the parent nucleus ^{76}Ge.

The role of the residual interactions in the GT strengths was already studied in Ref. [157], where it was shown that the repulsive particle-hole (ph) force introduces two types of effects: A shift of the GT strength to higher excitation energies with the corresponding displacement of the position of the GT resonance and a reduction of the total GT strength. The residual particle-particle force (pp), being an attractive force, shifts the strength to lower excitation energies, reducing the total GT strength as well. Also shown in Ref. [157] was the effect of the BCS correlations on the GT strength distribution. The main effect of pairing correlations is to create new transitions that are forbidden otherwise. The main effect of increasing the Fermi diffuseness is to smooth out the profile of the GT strength distribution, increasing the strength at high energies and decreasing the strength at low energies. The role of deformation was also studied in Ref. [157], showing that the GT strength distribu-

Table 4.3: Main coefficients C_α^i in the expansion of equation (3.1) for the proton state [303] with $K^\pi = 7/2^-$ and the neutron state [523] with $K^\pi = 5/2^-$. This is the main contribution to the peak at 15 MeV in the $B(GT_+)$ strength distribution of ^{76}Ge with the Woods-Saxon potential. The basis states are labelled by $|Nn_z\Lambda\rangle$ quantum numbers. The table contains also the contributions from these basis states to the spin matrix elements.

		$|303\rangle$	$|503\rangle$	$|523\rangle$	$|703\rangle$	$|723\rangle$	$|903\rangle$
$7/2^-$ proton	HF(SG2)	-0.9742	0.2204	-0.0061	0.0219	-0.0272	0.0122
	WS	0.9876	-0.1400	0.0563	-0.0233	0.0107	-0.0295
$5/2^-$ neutron	HF(SG2)	0.1369	0.5933	-0.5031	-0.3928	0.2349	0.2385
	WS	-0.2397	-0.5173	0.5049	0.3794	-0.2596	-0.2056
contr. to $\Sigma_K^{\nu\pi}$	HF(SG2)	-0.1333	0.1308	0.0031	-0.0107	-0.0064	0.0029
	WS	-0.2367	0.0724	0.0284	-0.0088	-0.0028	0.0061

tions in deformed nuclear shapes are much more fragmented than the corresponding spherical ones. This is expected because deformation breaks down the degeneracy of the spherical shells. It was also shown that the crossing of deformed energy levels depending on the magnitude of the quadrupole deformation as well as on the oblate or prolate character, may lead to sizable differences between the GT strength distributions corresponding to different shapes. In Fig. 4.9 the dependence of the

Figure 4.9: Gamow-Teller strength distributions $[g_A^2/4\pi]$ in ^{150}Nd and ^{150}Sm for various values of the coupling strength χ_{GT}^{ph} [MeV].

GT strength distributions on the coupling strength of the particle-hole residual interaction χ_{GT}^{ph} is plotted for a fixed value of the particle-particle coupling constant $\kappa_{GT}^{pp} = 0$. The results correspond to the force Sk3 in the A=150 case. In the left

panel, the $B(GT_-)$ strength distribution of the parent nucleus ^{150}Nd is shown and in the right panel the $B(GT_+)$ the strength distribution of the daughter nucleus ^{150}Sm is presented. The pairing gap parameters are given in Table 7.5.1 and the deformations are given in Table 7.5.2. It can be seen in Fig. 4.9 how the most important effect of χ_{GT}^{ph} on the $B(GT_-)$ strength distribution is a shift of the strength toward higher excitation energies. This displacement of the GT strength is accompanied by a reduction of the strength. This reduction can be more clearly seen in the $B(GT_+)$ strength distribution because its scale is about one order of magnitude smaller, as is expected from the Ikeda sum rule $\sum[B(GT_-) - B(GT_+)] = 3(N - Z) = 90, 78$ for Nd and Sm, respectively. Therefore, the coupling constant χ_{GT}^{ph} plays an important role to reproduce the position of the GT_- resonance. On the other hand, the sensitivity
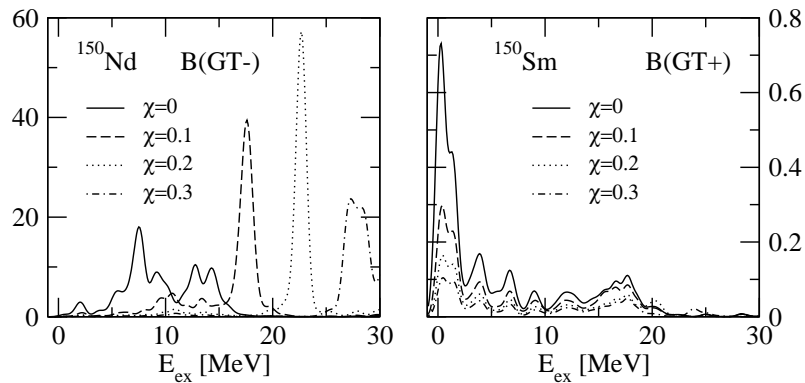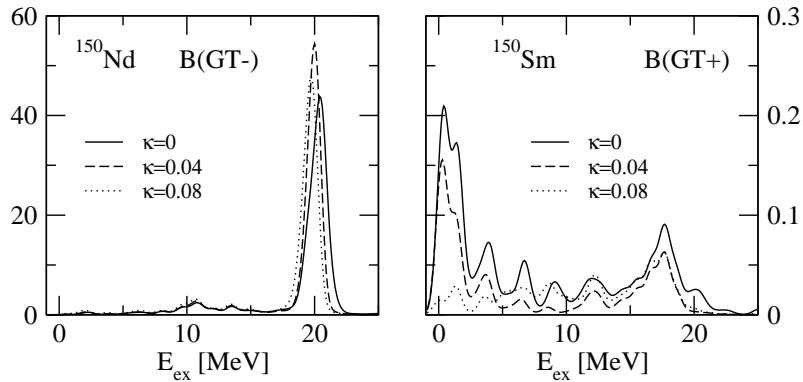

Figure 4.10: Gamow-Teller strength distributions $[g_A^2/4\pi]$ in ^{150}Nd and ^{150}Sm for various values of the coupling strength κ_{GT}^{pp} [MeV].

of the GT strength distribution on the particle-particle coupling constant κ_{GT}^{pp} is not so important. This is shown in Fig. 4.10 where the GT strength distributions for a fixed value of $\chi_{GT}^{ph} = 0.156$ MeV [102] and for several values of κ_{GT}^{pp} are plotted. The position of the resonance does not change appreciably. Therefore, other methods, such as fitting the half-lives of unstable nuclei in the same mass region, have to be used to phenomenologically determined their values. Fig. 4.11 shows the dependence on the deformation for fixed values of the residual interaction constants $\chi_{GT}^{ph} = 0.207$ MeV and $\kappa_{GT}^{pp} = 0.023$ MeV for two examples with A=100. The results correspond to values of the deformation parameter $\beta = -0.2$, 0 and 0.2. The role of the deformation was also studied in Ref. [157]. The results here confirm the general conclusion drawn in this work. The GT strength distributions from different deformed nuclear shapes can differ from the corresponding spherical ones because of the larger fragmentation produced by the breaking of degeneracy of the spherical shells. It was also shown that the crossing of deformed energy levels, depending on the magnitude of the quadrupole deformation as well as on the oblate or prolate
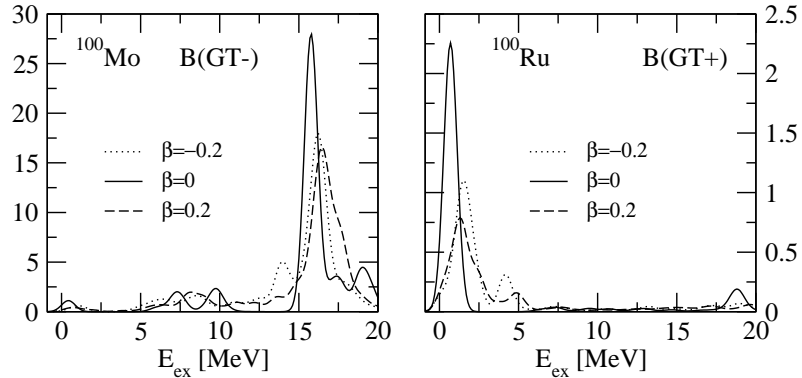
Figure 4.11: Gamow-Teller strength distributions $[g_A^2/4\pi]$ in ^{100}Mo and ^{100}Ru for various values of the quadrupole deformation parameter β.

character, may lead to sizeable differences between the GT strength distributions corresponding to different shapes.

For each of pair of beta decay partners, the calculated $B(GT_-)$ and $B(GT_+)$ strength distributions are shown in Figs. 4.12, 4.13. The $B(GT_-)$ distribution of the parent nucleus is always is shown in the top panel whereas the $B(GT_+)$ distribution of the daughter nucleus is found in the lower panel for each pair. Also, the experimental data, whenever they are available, are included. In each figure the left panels correspond to HF+BCS+QRPA calculations with the force Sk3 and the right panels to WS+BCS+QRPA calculations.

The 2qp results for HF+BCS calculations where the residual interaction is not considered are plotted with dotted lines. This serves as a reference and can be used to see the necessity of the residual force to be into agreement with experiment. Dashed lines correspond to the use of the residual interactions given by the parametrization of Ref. [102]. Finally, solid lines are the results obtained with $\chi_{GT}^{ph} = 0.1$ MeV and $\kappa_{GT}^{pp} = 0.03$ MeV, which produce a good fit to all the measured GT resonances of the double beta emitters. The small value of the χ_{GT}^{ph} coupling constant needed to reproduce the experimental GT resonances within a selfconsistent approach with Skyrme forces is in agreement with a similar value reported in Refs. [158] it reflects the fact that one needs less residual interaction when using realistic effective density-dependent forces instead of using phenomenological potentials to generate the single-particle energies and wave functions.
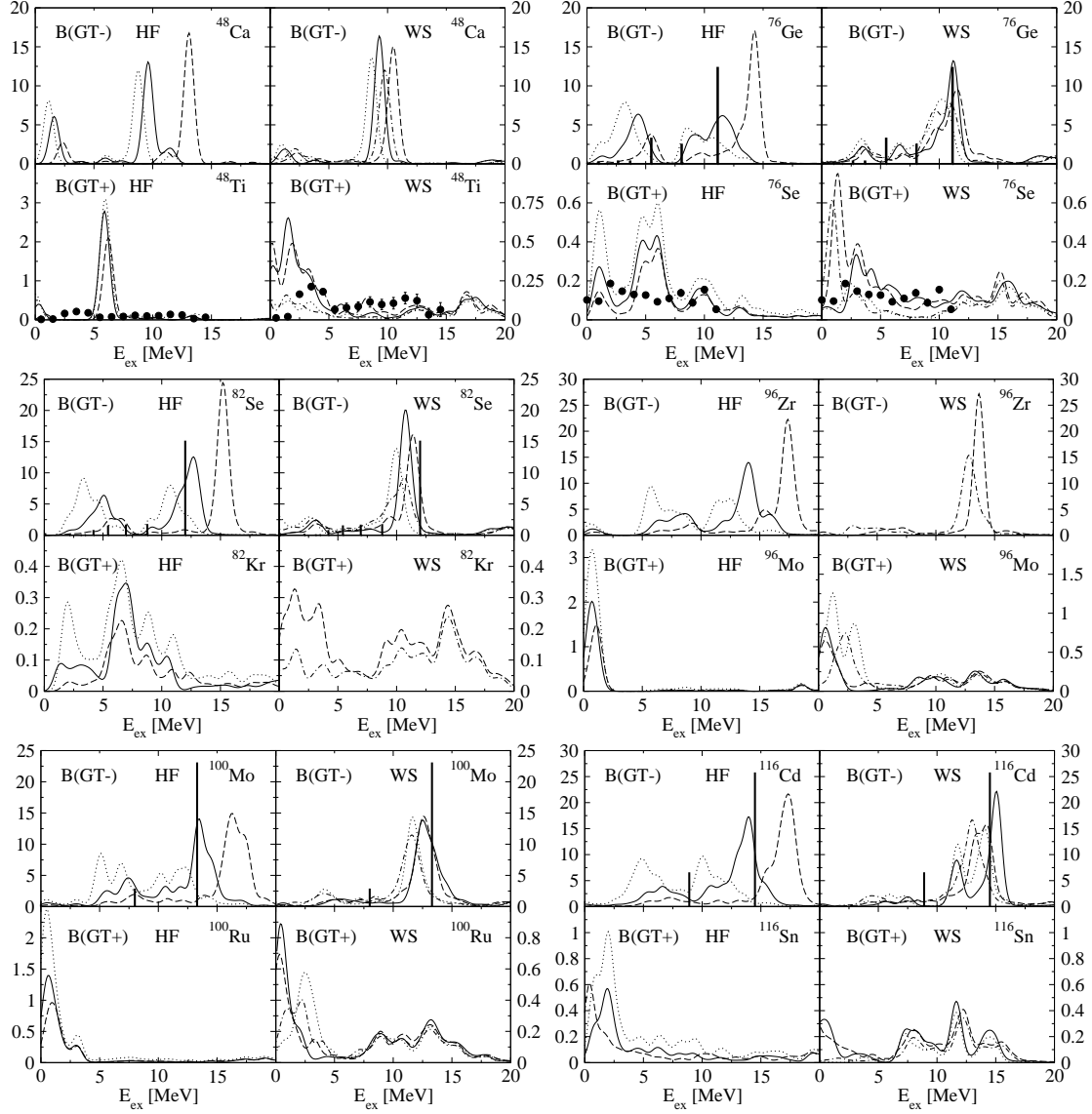
Figure 4.12: Gamow-Teller $B(GT_-)$ and $B(GT_+)$ strength distributions $[g_A^2/4\pi]$ $2\nu\beta\beta$ plotted as function of the excitation energies of the corresponding daughter nuclei. Left panels show results from HF(Sk3) calculations a) without residual interaction (dotted lines); b) with residual interaction from Ref. [102] (dashed lines); and c) with $\chi_{GT}^{ph} = 0.10$ MeV; $\kappa_{GT}^{pp} = 0.03$ MeV (solid lines). Right panels show results using WS potentials with χ_{GT}^{ph} from Ref.[102] and with two different values for the quadrupole deformation β and residual interaction κ_{GT}^{pp}: i) Solid lines are obtained using β from [147] and κ_{GT}^{pp} from [102]; ii) dashed lines are for β from [148] and κ_{GT}^{pp} from [102]; iii) dotted lines are for β from [147] and the κ_{GT}^{pp} from set 2 in Table 4.4; iv) dash-dotted lines are for β from [148] and the same κ_{GT}^{pp} as in the previous case. Experimental data are from Ref.[5] for Ti, for ^{76}Se from [96]. Vertical lines in ^{76}Ge and ^{82}Se are experimental data from [117]. Vertical lines in ^{100}Mo and ^{116}Cd are experimental data from [4]
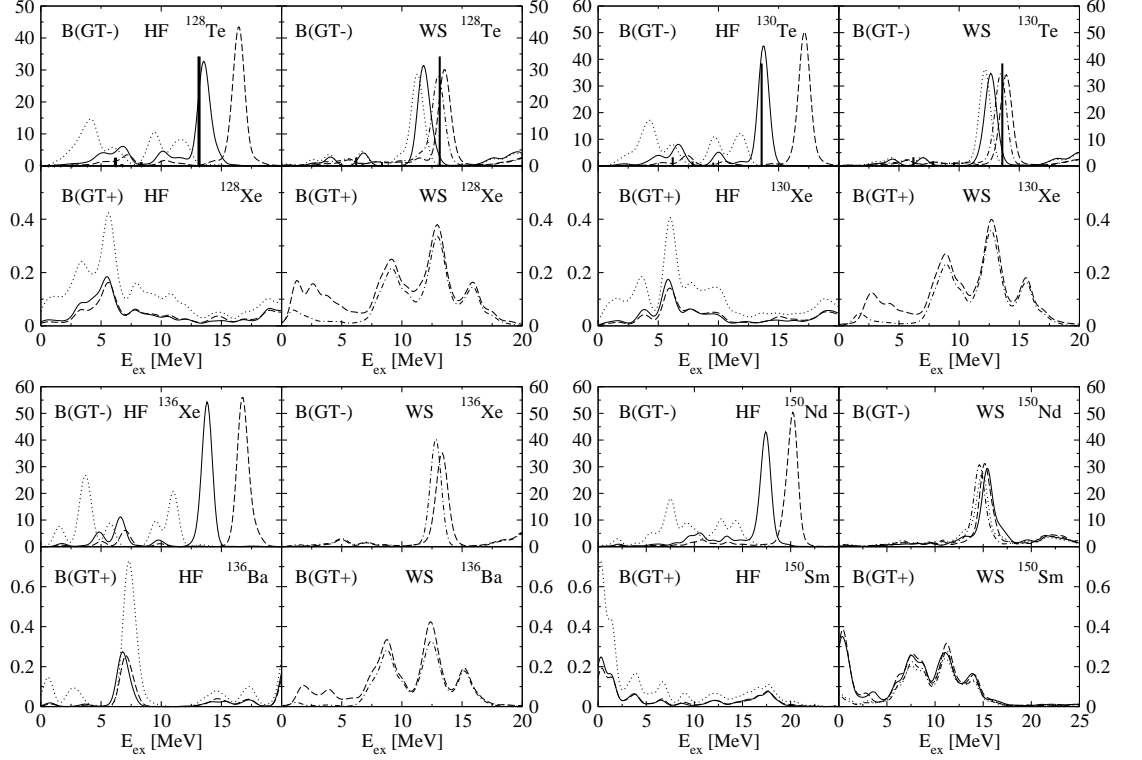
Figure 4.13: Same as in Fig. 4.12.

In the case of calculations with the WS potentials shown on the right hand panels, the results are for the two different experimental deformations as obtained from Refs. [147] and [148], which are given in Table 7.5.2.

The results for two different values of the κ_{GT}^{pp} coupling constant, the values obtained from Ref.[102] (set 1 in Table 4.4) and the values that reproduce the double beta-decay half-lives within a spherical formalism (set 2 in Table 4.4) are shown. The calculations are done for a fixed value of the χ_{GT}^{ph} constant as obtained from Ref. [102]. Table 4.4 shows the parameters used for these calculations. The meaning of the curves is as follows: Solid lines correspond to the deformation from [147] and to the κ_{GT}^{pp} from [102]. Dotted lines are for the same deformation with the new κ_{GT}^{pp} as obtained from the double beta-decay fitting procedure (set 2). Dashed lines are for the deformation of Ref.[148] and κ_{GT}^{pp} from [102] and finally dash-dotted lines are for the deformation of Ref.[148] and κ_{GT}^{pp} from set 2 in Table 4.4.

Some common features to all figures can be established first. For the HF calculations, there is a noticeable effect of χ_{GT}^{ph} on the GT distribution for fixed κ_{GT}^{pp} and deformation. In general, the value of χ_{GT}^{ph} given by the parametrization of Ref. [102] is an overestimation when dealing with selfconsistent Skyrme HF calculations. Actually, a small value of $\chi_{GT}^{ph} = 0.1$ MeV is already able to reproduce the experi-

Table 4.4: Parameters χ_{GT}^{ph} and κ_{GT}^{pp} used in Figs. 4.12, 4.13

	χ_{GT}^{ph}	κ_{GT}^{pp}	κ_{GT}^{pp}
	Ref.[102]	set 1 [102]	set 2
A=48	0.346	0.039	0.097
A=76	0.251	0.028	0.060
A=82	0.238	0.027	0.057
A=96	0.213	0.024	0.081
A=100	0.207	0.023	0.074
A=116	0.187	0.021	0.060
A=128	0.174	0.019	0.049
A=130	0.172	0.019	0.050
A=136	0.167	0.019	0.050
A=150	0.156	0.017	0.050

mental position of the GT resonance. This is a consequence of the structure of the two-body density-dependent Skyrme force that contains terms like spin exchange operators leading to a spin-spin interaction in the selfconsistent mean field, which is absent in the WS potential.

The agreement with the experimental energy of the GT resonance is very good in this calculation, as it can be seen in the cases A=76,82,100,116,128,130, where this information is available. Indeed, the experimental giant GT resonance shown in these figures represent the centroids of broad bumps. The resonance in ^{48}Ca reported at 10 MeV in Ref.[3] and used in the fitting procedure of Ref. [102], is also in good agreement with this results. In Table 4.5 the total GT strength measured and calculated is presented, taking into account a quenching factor of 0.6.

Regarding the calculations performed with the WS potential, comparing the results obtained from different deformations but using the same κ_{GT}^{pp}, it can be seen that larger deformations produce peaks in the GT distributions displaced to higher energies. This is a consequence of the larger separation of the single particle energies when the deformation increases. Thus, since the deformation derived from Ref. [148] is larger than that of Ref. [147], the solid lines appear on the left of the dashed ones as well as the dotted lines appear at lower energies than dash-dotted lines.

On the other hand, when the curves with the same deformation but different κ_{GT}^{pp} are compared, one expects that larger κ_{GT}^{pp} produce peaks slightly shifted to lower energies and containing less strength. Again, since in general the κ_{GT}^{pp} from set 2 in Table 4.4 are larger than the κ_{GT}^{pp} from Ref. [102], it can be observed that dotted peaks appear at lower energies than solid peaks and are smaller. Similarly,

dash-dotted peaks are smaller than dashed peaks and displaced to the left. It is also

Table 4.5: Experimental and calculated (HF-Sk3 and WS) summed GT strength. A standard quenching factor 0.6 has been included in the theoretical results.

		exp	HF-Sk3	WS
$\sum B(GT_+)$	^{48}Ti	1.42 ± 0.2	2.44	1.79
	^{76}Se	1.45 ± 0.07	1.29	2.06
$\sum B(GT_-)$	^{76}Ge	19.89	22.30	22.65
	^{82}Se	21.91	25.68	26.09
	^{100}Mo	26.69	29.67	29.93
	^{116}Cd	32.70	36.42	36.41
	^{128}Te	40.08	43.33	43.44
	^{130}Te	45.90	47.21	46.66

remarkable to see the good agreement with experiment obtained in this case. This agreement is mainly caused by the fixed value of χ_{GT}^{ph} from Ref. [102]. Contrary to the situation in the HF case, it is still valid when describing the mean field with a WS potential. One should keep in mind that the parametrization of Ref. [102] was obtained using a Nilsson potential. The summed $B(GT)$ strengths are compared with experiment in Table 4.5. Comparing the results obtained at different deformations with the selfconsistent mean fields (HF with Sk3) in Figs. 4.12, 4.13 and Table 4.4, one can see that there is a strong dependence on deformation of the strength distributions. However, the total strength does not depend so much on deformation. There is an increase of a few percent in going from the spherical to the oblate and prolate shapes. The latter observation is in contradiction with SU(3) and shell model calculations by previous authors [9] studying the dependence of the GT strengths on deformation in ^{20}Ne and ^{44}Ti. This is due to the much larger and richer single particle basis used in the present calculations. In the present case each single particle state contains mixtures from many harmonic oscillator shells (up to $N = 10$), while in the above mentioned calculations [9], the single particle basis is restricted to a single harmonic oscillator major shell (the sd shell in ^{20}Ne and the fp shell in ^{44}Ti). On the other hand, one may question whether in the deformed cases the total strengths calculated here may contain spurious contributions from higher angular momentum components in the initial and final nuclear wave functions. Since the matrix elements of the transition operator, which is a dipole tensor operator, are taken between the states considered in the laboratory frame (see eqs. 3.45, 3.46), the effect of angular momentum projection taken into account to a large extent.

4.4 The $2\nu\beta\beta$–decay matrix elements

The formalism described in the previous sections and the values of deformations and strengths are used for the calculation of the $2\nu\beta\beta$-decay ground state transition $^{76}Ge \rightarrow ^{76}Se$. The results are obtained with a deformed, axially symmetric Woods-Saxon potential [41]. The deformation independent Woods-Saxon parameters (well depth, skin thickness, radius and spin–orbit constants) are taken from [186]. This parametrization of the Woods-Saxon potential were used previously in different RPA calculations, where a good agreement was achieved with experimental data, in particular for single M1 transitions at low energy, which are observed in (e, e') and (γ, γ') experiments [155, 156]. More details are given in Appendix F. As it has been shown in the previous chapter, the deformation parameter β_2 can be deduced from the nuclear electric quadrupole laboratory moment ($Q_p = -(7/2)Q$, Q and Q_p are laboratory and intrinsic quadrupole moments, respectively) or extracted from values based on the measured E2 probability ($Q_p = \sqrt{16\pi B(E2)/5e^2}$, the sign can not be extracted) via the intrinsic quadrupole moments Q_p: $\beta_2 = \sqrt{\pi/5}Q_p/(Zr_c^2)$ (r_c is the charge root mean square radius). However, the available experimental [5] data [11, 147, 148] lead to a ambiguous quadrupole deformations both for ^{76}Ge and ^{76}Se. In particular, the quadrupole moments measured by Coulomb excitation reorientation [147] imply $\beta_2 = 0.1$ (^{76}Ge) and $\beta_2 = 0.16$ (^{76}Se) [158], but from the measured values of $B(E2)$ strengths [148] one finds $|\beta_2| = 0.26$ (^{76}Ge) and $|\beta_2| = 0.29$ (^{76}Se) [158]. A lack of accurate experimental information on the deformation of ^{76}Ge and ^{76}Se suggests that it is necessary to study the associated $2\nu\beta\beta$-decay matrix element as a function of deformation parameters of both initial and final nucleus. In the deformed QRPA calculation, a truncated model space is used by considering only single particle states with maximal allowed value of the asymptotic quantum number N=5. This truncation works just for light nuclei with A<100. For heavier nuclei, the model space has to be enlarged. Unfortunately this enlargement brings difficulties about numerical, namely in the size of the matrices and the resulting increase of CPU time and storage allocation.

In contrast to many other microscopic calculations, energies of single particle levels are not shifted but taken exactly as provided by the deformed Woods-Saxon potential.

The BCS equations are solved for protons and neutrons. The proton and neutron pairing gaps are determined phenomenologically to reproduce the odd-even mass differences through a symmetric five-term formula [8]. For both spherical and deformed shapes of the studied A=76 nuclei, the values of the gap parameters are given in Table 7.5.1

In Fig. 4.14 the calculated proton and neutron occupation probabilities close
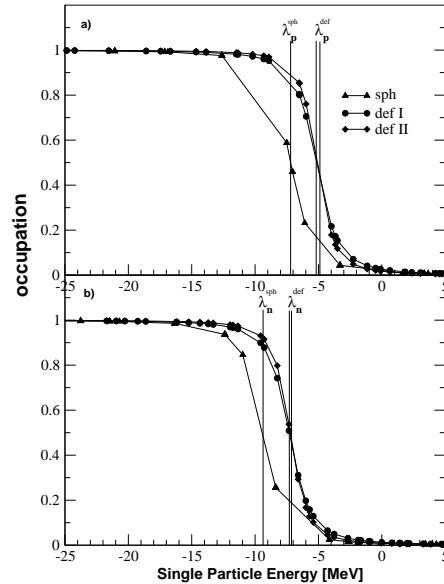
---

[5]See appendix E

Figure 4.14: The proton (a) and neutron (b) occupation probabilities close to the Fermi level for ^{76}Se. The spherical (sph, triangle up) and deformed (def, closed circle) BCS results correspond to pairing gaps. The vertical lines denote Fermi energy for protons (λ_p) and neutrons (λ_n)

.

to the Fermi level are presented for ^{76}Se. One can see that both for protons and neutrons the BCS solutions associated with spherical and deformed nuclear shapes differ significantly each from other. This deformation dependence of the BCS results is expected to have strong impact on the QRPA solution. The calculation of the QRPA energies and wave functions requires the knowledge of the particle-hole χ and particle–particle κ strengths of the residual interaction. The optimal value of χ is determined by reproducing the systematics of the empirical position of the Gamow-Teller giant resonance in the odd-odd intermediate nucleus as obtained from the (p, n) reactions [102, 183]. The parameter κ can be determined by exploiting the systematics of single β-decay feeding the initial and final nucleus. In Ref. [102] the strengths of the particle–hole and particle–particle terms of the separable Gamow-Teller force were fixed as smooth functions of mass number A by reproducing the β-decay properties of nuclei up to A=150 within the spherical pn-QRPA model. The recommended values of χ and κ of Ref. [102], used in the numerical calculations are presented in Table 4.4

The QRPA calculations for the $K = 0, \pm 1$ states are performed by following the procedure described in the previous section. The number of zeros of the non-linear RPA secular equation in equation (3.83) is equal to the number of the two-
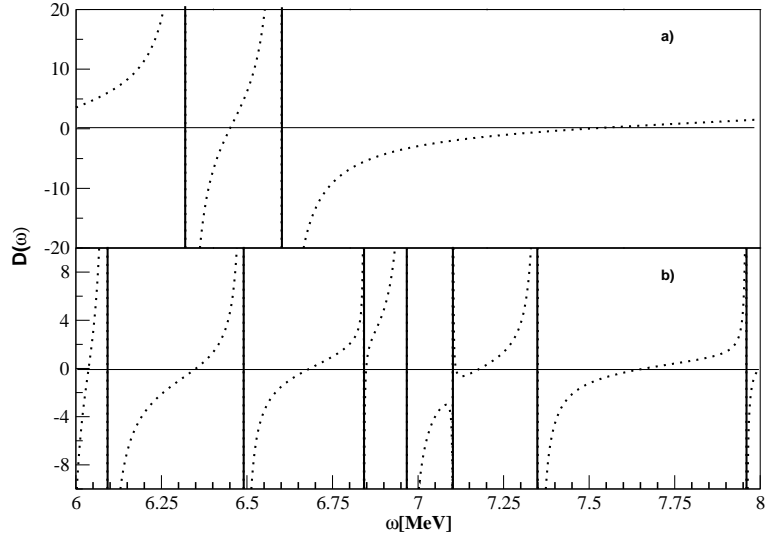
Figure 4.15: The l.h.s. of equation (3.83) $D(\omega)$ is plotted as function of the energy ω for ^{76}Ge. The calculation has been performed within spherical (a) and deformed (b) QRPA for $\chi = 0.25$ and $\kappa = 0$. In case (b) the K=0 results are presented.

quasiparticle configurations included in the microscopic sums (3.50). In the case of $K = 0$ ($K = \pm 1$) the dimension of the configuration space is of the order of 450 (900) quasiparticle pairs excitation. To each zero of the RPA secular equation corresponds one RPA energy ω_K^m. It is worthwhile to notice that by introducing the deformation degrees of freedom the zeros are not found in each subinterval of energy ω determined by the two subsequent two-quasiparticle excitation energies and that in some subintervals two or more zeros are found. This situation is illustrated in Fig. 4.15. The vertical axis is the left-hand side (l.h.s.) of equation(3.83) and the horizontal one is the energy $\omega_{K=1}$ in the range $6 \ MeV \le \omega_{k=1} \le 8 \ MeV$. The upper (a) and lower (b) subfigures show results for A=76 obtained within the spherical and deformed QRPA, respectively. A similar phenomenon was found also in Ref. [143] in a different context.

The main drawback of the QRPA is the overestimation of the ground state correlations leading to a collapse of the QRPA ground state, which may lead to an ambiguity in the β and $\beta\beta$-decay matrix elements. The QRPA collapses, because it generates too many correlations with increasing strength of the attractive proton-neutron interaction as a result of the quasiboson approximation used. An interesting issue is the dependence of the appearance of the collapse of the QRPA solution on the deformation degrees of freedom.

In Fig. 4.16 the energies of the lowest $K = 0$ and $|K| = 1$ states in ^{76}As calculated within the deformed QRPA are plotted as a function of particle-particle inter-
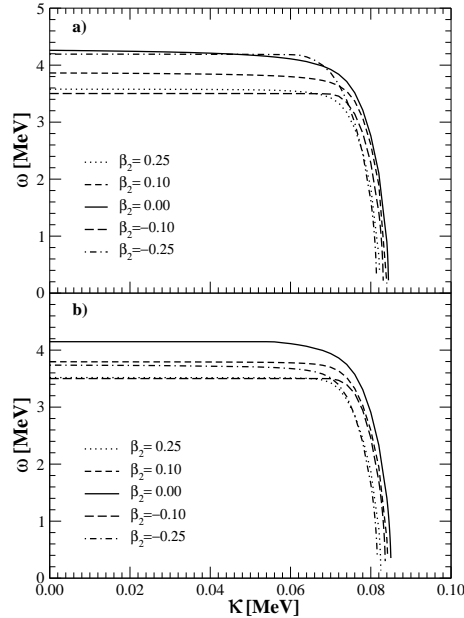
Figure 4.16: The energy of the lowest QRPA state as function of particle–particle interaction strength κ. The K=0 and K=1 deformed QRPA results for ^{76}Se are presented in subfigures (a) and (b), respectively.

action strength κ. The calculations were performed for different values of quadrupole deformation β_2, namely $\beta_2 = -0.25, -0.10$, $\beta_2 = 0.0$ and $\beta_2 = 0.10, 0.25$ representing oblate, spherical and prolate shapes of ^{76}Se, respectively. In the spherical limit the energies of $K = 0$ and $|K| = 1$ states of the intermediate nucleus coincide with each other. Fig. 4.16 shows that for a deformed nucleus the collapse of the QRPA solution appears for a slightly smaller value of κ. For the strongly deformed ^{76}Se this effect is more pronounced than for the less deformed one. Thus the deformation degrees of freedom do not improve the stability of the QRPA solution. The violation of the Pauli exclusion principle affects the QRPA results strongly in the range of particle-particle interaction κ above 0.7 MeV.

The half-life of the $2\nu\beta\beta$-decay of ^{76}Ge is known with high accuracy from the Heidelberg-Moscow experiment, in particular $T_{1/2}^{2\nu} = [1.55 \pm 0.01(stat)_{-0.15}^{+0.19}syst.)] \times 10^{21}$ years [110]. All existing positive results on the $2\nu\beta\beta$-decay were analyzed by Barabash [14], who suggested to consider the average value $T_{1/2}^{2\nu} = 1.43_{-0.07}^{+0.19} \times 10^{21}$ years for the ground state transition $^{76}Ge \rightarrow ^{76}Se$. Using equation (3.60) and the knowing the kinematical factor $G^{2\nu}$ [$G^{2\nu}(^{76}Ge) = 1.49 \times 10^{-20}\ year^{-1}\ MeV^2$] one can deduce the absolute value of the nuclear matrix element $|M_{GT}^{2\nu-exp.}|$ from the $2\nu\beta\beta$-decay half-life of ^{76}Ge.

This yields to a value of 0.138 MeV^{-1} when assuming $g_A = 1.25$. If the value of

the axial coupling constant g_A is considered to be unity, the approximately value of $|M_{GT}^{2\nu-exp.}|$ deduced from the average half-life for A=76 is larger 0.216 MeV^{-1}.
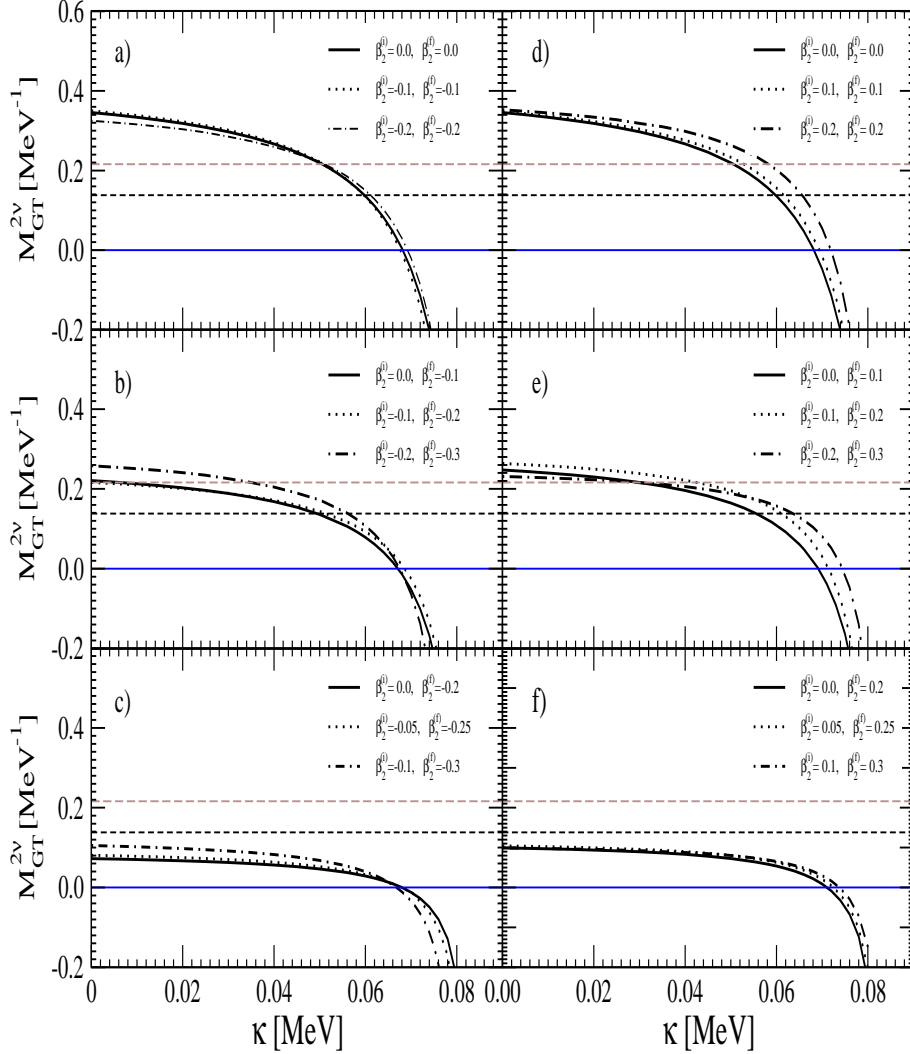
Figure 4.17: $2\nu\beta\beta$-decay matrix element of ^{76}Ge as function of particle–particle interaction strength κ. In the subfigures (a), (b) and (c) [(d), (e) and (f)] the results corresponding to oblate [prolate] deformation of both initial and final nucleus are presented. Please note that if the deformation of the initial and final nucleus is comparable, there is only minimal difference between the calculated values of $M_{GT}^{2\nu}$. With increasing difference in the deformations of parent and daughter nuclei the suppression of $M_{GT}^{2\nu}$ is increased in the range $0\ MeV \leq \kappa \leq 0.6\ MeV$. The two dashed horizontal lines correspond to $M_{GT}^{2\nu-exp} = 0.216\ MeV^{-1}$ ($g_A = 1.0$) and $M_{GT}^{2\nu-exp} = 0.138\ MeV^{-1}$ ($g_A = 1.25$).

In Fig. 4.17 the effect of the deformation on the $2\nu\beta\beta$-decay matrix element $M_{GT}^{2\nu}$ is analyzed. The results for the $2\nu\beta\beta$-decay matrix element are displayed as function of the particle–particle strength κ. The curves drawn in subfigures a), b) and c) [subfigures d), e) and f)] correspond to the case with both initial and final nuclei being oblate [prolate]. The two horizontal lines represent $M_{GT}^{2\nu-exp.} = 0.138 \; MeV^{-1}$ ($g_A = 1.25$) and $M_{GT}^{2\nu-exp.} = 0.216 \; MeV^{-1}$ ($g_A = 1.0$) respectively. Fig. 4.17 shows that within the whole range of κ there is only a small difference between values of $M_{GT}^{2\nu}$ corresponding to the same value of $\Delta\beta_2$, which is defined as

$$\Delta\beta_2 = |\beta_2(^{76}Ge) - \beta_2(^{76}Se)|. \tag{4.3}$$

In addition, one finds that by increasing the value of $\Delta\beta_2$ the suppression of $M_{GT}^{2\nu}$ becomes stronger within the range $0 \; MeV \; \leq \kappa \leq 0.06 \; MeV$. This a new suppression mechanism of the $2\nu\beta\beta$-decay matrix element namely, $M_{GT}^{2\nu}$ depends strongly on the difference in the deformations of parent and daughter nucleus.

One might wander about is the origin of this suppression. In Fig. 4.18 this point is clarified by presenting the overlap factor of two BCS vacua for different values of $\beta_2(^{76}Ge)$. The approximate calculation of $< BCS(^{76}Ge)|BCS(^{76}Se) >$ is slightly sensitive to the used approximations in case one of the nuclei is oblate and the second prolate. Therefore, the smoothed curves corresponding to a polynomial function are presented.[6]

For a given $\beta_2(^{76}Ge)$ the curve has a maximum for $\beta_2(^{76}Se) = \beta_2(^{76}Ge)$ and with increasing difference in deformations of initial and final nuclei, i.e., $\Delta\beta_2$, the value of the BCS overlap factor decreases rapidly.

From Fig. 4.18 it follows that oblate-prolate (or prolate-oblate) $2\nu\beta\beta$-decay transitions are disfavored in comparison with prolate-prolate or oblate-oblate ones. In particular, by assuming the β_2 and β_4 parameters of Ref. [113] one obtains $< BCS(^{76}Ge)|BCS(^{76}Se) >= 0.034$. This suppression is too strong to achieve agreement with experimental data for the calculated $M_{GT}^{2\nu}$. However, by changing the deformation of ^{76}Se from oblate to prolate ($\beta_2(^{76}Se) = 0.244$) the value of the BCS overlap factor: $< BCS(^{76}Ge)|BCS(^{76}Se) >= 0.69$ is significantly large. The presented suppression mechanism is expecting to work also for other $2\nu\beta\beta$-decay transitions.

In Fig. 4.19 different values of the BCS overlap factor for the $2\nu\beta\beta$-decay of ^{76}Ge, ^{100}Mo, ^{130}Te and ^{136}Xe are plotted. The quadrupole deformation of the initial nucleus was taken to be $\beta_2 = 0.1$ and β_2 of the the final nucleus was considered to be a free parameter within the range $-0.4 \leq \beta_2 \leq 0.4$. The pairing gaps, which entered the BCS equations, are given by in Table 7.5.1 for A=76 and for A=100, 130 and 136.

---

[6]The analytical expression of the overlap is presented in Appendix F.

Figure 4.18: The overlap factor of the initial and final BCS vacuum as function of the quadrupole deformation parameter β_2 of ^{76}Se. The results are presented for spherical ($\beta_2 = 0.0$), oblate ($\beta_2 = -0.25, -0.10$) and prolate ($\beta_2 = 0.10, 0.25$) deformations of ^{76}Ge.

One can see that the behavior of the overlap factor is qualitatively the same for all considered nuclear systems. The maximum of this factor appears for equal quadrupole deformation of the initial and final nucleus. This fact implies that the deformation of the nuclei plays an important role in the calculation of the $2\nu\beta\beta$-decay transitions and should be known with high reliability.

There are two suppression mechanisms of the $2\nu\beta\beta$-decay matrix element. Already long ago Vogel and Zirnbauer showed that $M_{GT}^{2\nu}$ is strongly suppressed when a reasonable amount of particle-particle interaction is taken into account [202], established close to the collapse of the QRPA solution. This is one suppression mechanism. Here the second suppression mechanism that $M_{GT}^{2\nu}$ depends strongly on the difference in deformations of the initial and final nucleus has been found. A criteria on to decide which of the mechanism dominates, is necessary for a common description of both single β and $2\nu\beta\beta$-decay within the same nuclear Hamiltonian. Three different cases are considered:

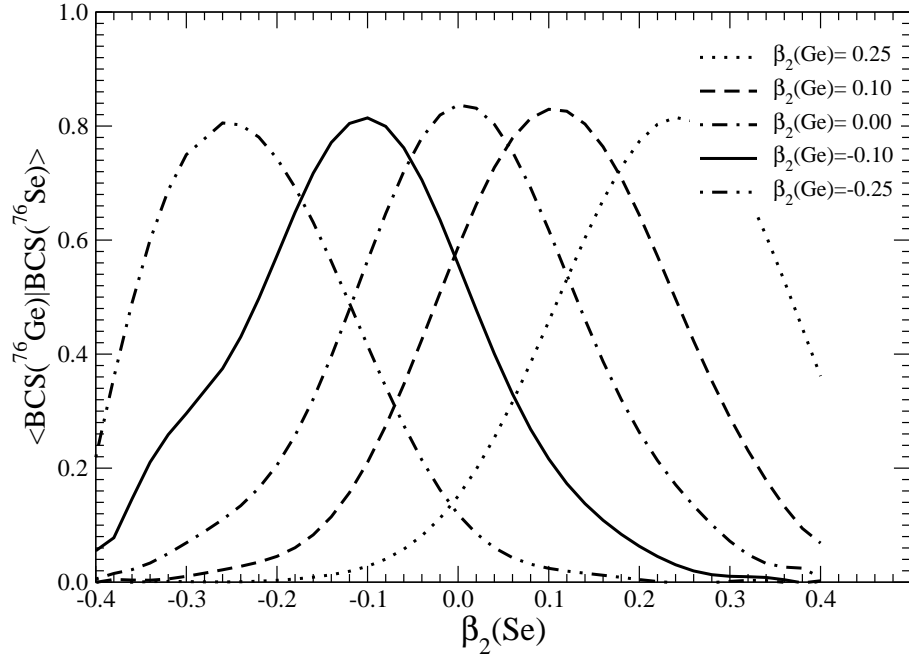i) Sphericity of both initial and final nucleus, i.e., $\beta_2(^{76}Ge) = 0$ and $\beta_2(^{76}Se) = 0$.
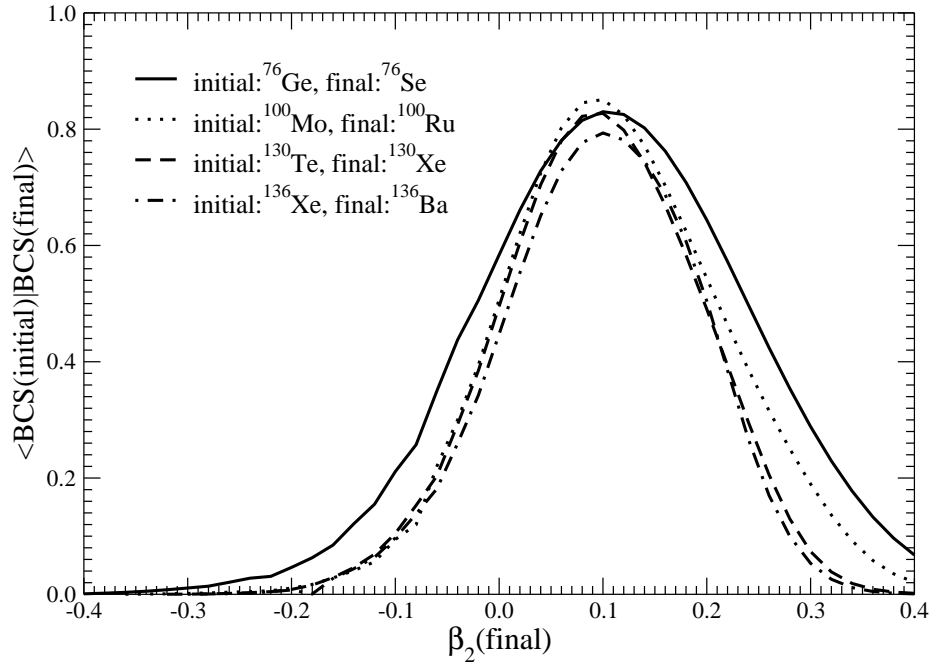
Figure 4.19: The overlap factor of the initial and final BCS vacuum as function of the quadrupole deformation parameter β_2 of the final nucleus for double beta decay of ^{76}Ge, ^{100}Mo, ^{130}Te, and ^{136}Xe. The deformation parameter of the initial nucleus is chosen to be $\beta_2(initial) = 0.1$.

ii) Deformations of parent and daughter nuclei are as follows: $\beta_2(^{76}Ge) = 0.09$ and $\beta_2(^{76}Se) = 0.23$.

iii) Deformations of ^{76}Ge and ^{76}Se are: $\beta_2(^{76}Ge) = 0.09$ and $\beta_2(^{76}Se) = 0.28$.

In Fig. 4.20 the $2\nu\beta\beta$-decay of ^{76}Ge is presented as function of particle-particle interaction strength κ for the above three cases. In case i) (spherical nuclei) $M_{GT}^{2\nu-exp.}$ equal to 0.138 MeV^{-1} ($g_A = 1.25$) is reproduced for $\kappa = 0.06\ MeV$. The corresponding set of nuclear structure input parameters in this calculation is denoted by capital letter A (see Table 7.6 Appendix F). This value of κ is significantly larger than the average value $\kappa_\beta = 0.028\ MeV$ deduced from the systematic study of the single β^+-decays [102]. One can hardly suppose that it is because ^{76}Ge and ^{76}Se are peculiar nuclear systems. They are no other indications to support this. In fact this seems to be a general problem within the spherical QRPA: the calculated nuclear matrix elements reproduce the experimental $2\nu\beta\beta$-decay half-life only for a particle-particle strength close to the critical value for the QRPA collapse.

In case ii) the situation is different. $M_{GT}^{2\nu-exp.}$ is reproduced for a considerable smaller value of particle-particle strength $\kappa = 0.025\ MeV$, which is very close to that of Homa et al. [102] and assuming $g_A = 1.25$. The letter B denotes the corresponding set of nuclear parameters, listed in Table 7.6. Since the effective axial coupling constant has not been determined uniquely $g_A = 1$ is also considered.

Then $M_{GT}^{2\nu-exp.}$ becomes larger, namely $0.216\ MeV^{-1}$. With this, a smaller difference in parent daughter deformation is needed to reproduce this value for $\kappa \approx \kappa_\beta$. This is done in case iii) yielding $\kappa = 0.019\ MeV$ (nuclear parameter set C). Nevertheless, one should keep in mind that the coupling strength of [102] has been adjusted by using a deformed Nilsson single-particle model and $g_A = 1.25$. Thus it is not necessarily the best possible choice. It is supposed that this prediction for κ is more accurate for nuclei with shorter β-decay half-lifes. The curves corresponding to cases ii) and iii) change only weakly in the range $0 \leq \kappa \leq \kappa_\beta$. It means that the role of the particle-particle interaction is negligible within this interval.
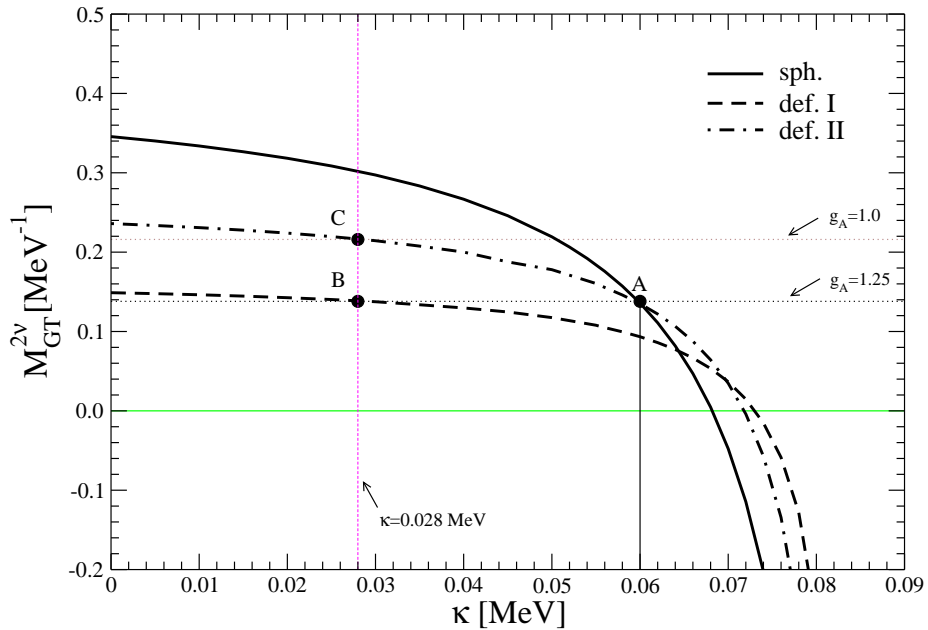
Figure 4.20: $2\nu\beta\beta$-decay matrix element of ^{76}Ge as function of particle–particle interaction strength κ. The solid (sph.) line corresponds to spherical shape of initial and final nuclei. The dashed (def. I) and dot-dashed (def. II) are asociated with a set of deformation parameters ($\beta_2(^{76}Ge) = 0.1$, $\beta_2(^{76}Se) = 0.266$) and ($\beta_2(^{76}Ge) = 0.1$, $\beta_2(^{76}Se) = 0.216$), respectively. The points indicated by letters A, B and C determine κ for which the value of $M_{GT}^{2\nu-exp.}$ deduced from the $2\nu\beta\beta$-decay half-life of ^{76}Ge is obtained. For $g_A = 1.25$ ($g_A = 1.0$) one finds $M_{GT}^{2\nu-exp} = 0.138\ MeV^{-1}$ ($M_{GT}^{2\nu-exp} = 0.216\ MeV^{-1}$) by assuming $T_{1/2}^{2\nu}(^{76}Ge) = 1.43 \times 10^{21}$ years [14].

It is worthwhile to notice that for a large value of κ of about 0.07 MeV the agreement with $|M_{GT}^{2\nu-exp}|$ deduced from the $2\nu\beta\beta$-decay half-life is also achieved and that in this case the sign of $M_{GT}^{2\nu}$ is negative. However, for negative values of $M_{GT}^{2\nu}$ a correspondence with κ_β from systematic studies of the single beta decay [102] is not achieved. Thus negative values of $M_{GT}^{2\nu}$ are ruled out. There is a longstanding
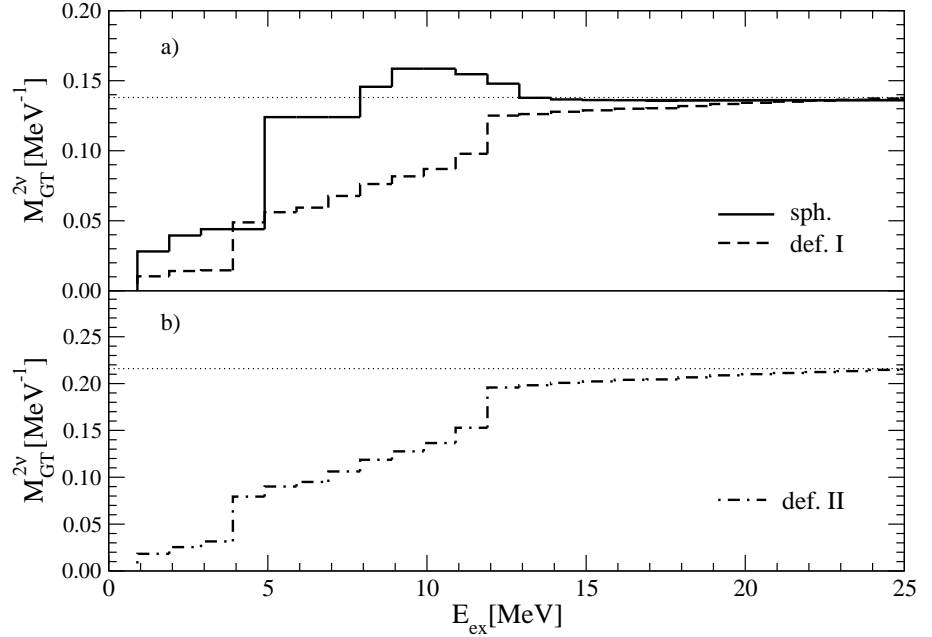
Figure 4.21: Running sum of the $2\nu\beta\beta$-decay matrix element $M_{GT}^{2\nu}$ as a function of the excitation energy E_{ex} in ^{76}As. In the upper figure (a) results corresponding to input parameter sets A (solid line) and B (dashed line) are presented. In the lower figure (b) results obtained with input parameter set C (dot-dashed line) are drawn. The dotted horizontal line in subfigure (a) [subfigure (b)] denotes the value of the matrix element $M_{GT}^{2\nu-exp} = 0.138 \ MeV^{-1}$ ($M_{GT}^{2\nu-exp} = 0.216 \ MeV^{-1}$) deduced from the experimental $2\nu\beta\beta$-decay half-life of ^{76}Ge by assuming $g_A = 1.25$ ($g_A = 1.0$).

question whether in the calculation of the $2\nu\beta\beta$-decay matrix element $M_{GT}^{2\nu}$ the transitions to higher lying states of the intermediate nucleus play an important role. The is so called "Single State Dominance Hypothesis" (SSDH), assumes that only the lowest 1^+ state of the intermediate nucleus is of major importance in the evaluation of $M_{GT}^{2\nu}$. The SSDH can be realized, e.g., through cancellation among the higher lying 1^+ states of the intermediate nucleus. Ref. [175] discussed a possibility to experimentally study the validity of the SSDH by measuring the single electron spectra and the angular distribution of the emitted electrons. The SSDH is suitable for the $2\nu\beta\beta$-decay transitions with low-lying 1^+ ground state of the intermediate nucleus. But this is not the case in $2\nu\beta\beta$-decay of ^{76}Ge. In Fig. 4.21 the QRPA

model dependent study of this problem is presented by drawing the running sum of the matrix element $M_{GT}^{2\nu}(E)$ as a function of the 1^+ excitation energy E_{ex} of the intermediate nucleus. It can be seen that for the spherical calculation the main contribution to $M_{GT}^{2\nu}$ comes from states in the intermediate nucleus lying below 5 MeV scale and that there is a partial cancellation among contributions to $M_{GT}^{2\nu}$ from higher lying states. In the case of deformed QRPA calculations there is a different situation. Important contributions to $M_{GT}^{2\nu}(E)$ arise even from relatively high energies of the intermediate states around the position of the Gamow-Teller resonance (about 12 MeV), which can not be described in the framework of the shell model. These results contradict the SSDH and indicate that a strong truncation of the complete set the states in the intermediate nucleus is not appropriate.

4.5   The $2\nu\beta\beta$–decay within the FR-QRPA

In this section, the results obtained within the FR-QRPA in comparison with the QRPA and SCQRPA ones are presented for 6 nuclei, ^{76}Ge, ^{82}Se, ^{100}Mo, ^{116}Cd, ^{128}Te and ^{130}Xe. Rather small model bases, listed in the Table 4.6, are used in order to get a full convergence in the FR-QRPA.

Table 4.6: The proton and neutron pairing gaps determined phenomenologically to reproduce the odd-even mass difference and the particle-hole strength g_{ph} chosen to reproduce the experimental position of Gamov-Teller resonance. The single particle basis for all nuclei under consideration is also shown.

	^{76}Ge	^{76}Se	^{82}Se	^{82}Kr	^{100}Mo	^{100}Ru
Basis	1p, 0f, 0g		1p, 0f, 0g		1p, 2s, 1d, 0g	
Δ_p MeV	1.561	1.751	1.401	1.734	1.612	1.548
Δ_n MeV	1.535	1.710	1.544	1.644	1.358	1.296
χ, MeV	0.21		0.18		0.17	
	^{116}Cd	^{116}Sn	^{128}Te	^{128}Xe	^{130}Te	^{130}Xe
Basis	1p, 2s, 1d, 0g, 0h		2s, 1d, 0g, 0h		2s, 1d, 0g, 0h	
Δ_p MeV	1.493	1.763	1.127	1.177	1.299	1.043
Δ_n MeV	1.377	1.204	1.307	1.266	1.243	1.180
χ, MeV	0.14		0.14		0.12	

The levels are considered in the vicinity of the Fermi levels and spin-orbit partners are always taken into account. The FR-QRPA method is rather sensitive to the differences between occupation probabilities for protons and neutrons, entering

the denominator in the expression of the bifermionic operators $\bar{A}^\dagger, \bar{A}$ and in the expression for the $\mathcal{R}_{\tau\tau'}$ factor of the renormalization matrices.
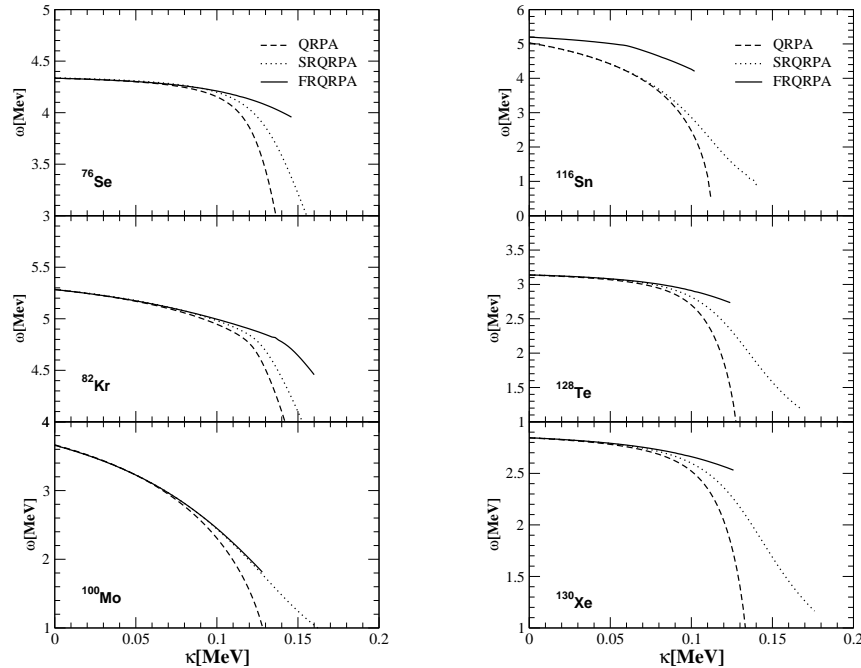
Figure 4.22: The energy of the first excited Gamov-Teller state as function of particle-particle interaction strength g_{pp} for all nuclei

It can be noticed from (3.78) that for levels far from the Fermi, the values of the occupation probabilities for protons and neutrons become small as well as their difference. Nevertheless the dominator in the expression of $\mathcal{R}_{\tau\tau'}$ goes to zero providing a finite result for $\mathcal{R}_{\tau\tau'}$. It is clear that in such situation the quantity $\mathcal{N}_\vee - \mathcal{N}_\backslash$ has to be calculated very accurately while the approximation (3.80) may be not good enough to guarantee that. This is why using the equation (3.80) the full convergence cannot be achieved.

This causes numerical problems, in particular concerning convergence for large values of particle-particle strength. Therefore, the bases are chosen in order to obtain convergence for a larger interval of the particle-particle strength, in particular up to the point of the collapse of the $2\nu\beta\beta$ matrix elements. The single-particle basis for each nucleus is shown in Table 4.6.

The single particle energies are obtained by using a Coulomb-corrected Woods-Saxon potential with Bertsch parametrization. The proton and neutron pairing gaps are determined phenomenologically to reproduce the odd-even mass differences through a symmetric five-term formula [8]. Then the equations for the chemical

potentials (3.81) are solved for proton and neutron subsystems. The pairing gaps entering the BCS equations are given in the Table 4.6

The calculation of the QRPA energies and wave functions requires the knowledge of the particle-hole χ and particle-particle κ strengths of the residual interaction. The value of particle-hole strength χ parameter for each nucleus is chosen in order to reproduce the experimental position of the Gamow-Teller giant resonance in the odd-odd intermediate nucleus [52, 117]. Those values are also given in the Table 4.6. The particle-particle strength κ is considered as a free parameter.

The main drawback of the QRPA is the overestimation of the ground state correlations leading to the collapse of the QRPA ground state near a certain critical interaction strength. Around this point the backward-going RPA amplitudes Y_{pn} of the first 1^+ states become overrated and too many correlations in the ground state are generated with increasing strength of the particle-particle interaction. This phenomenon, a result of the quasiboson approximation, leads to QRPA collapse and implies an ambiguous determination of the β and $2\nu\beta\beta$-decay matrix elements. In Fig. 4.22 the dependence of the energy of the first excited Gamow-Teller state in daughter nuclei is plotted versus the κ parameter. Hereafter, the dashed line corresponds to the QRPA case, the dotted line represents the SCQRPA case and the solid line describes the FR-QRPA case. For all studied nuclei the collapse of the first excited state is shifted to higher values of κ for each method and the stability increases in the FR-QRPA.

In Fig. 4.23 the $2\nu\beta\beta$-decay matrix elements are shown as function of the particle-particle strength κ. The calculations are done for all nuclei within the three methods. The horizontal dashed line indicates the experimental values taken from [122].

For all nuclei there is a similar behaviour in the sense that QRPA and SCQRPA collapse a bit earlier than the FR-QRPA does. Although the chosen bases are rather small, the new differences between QRPA extensions are evident. The FR-QRPA method offers considerably less sensitive dependence of $M_{GT}^{2\nu}$ on κ and shifts the collapse to larger values of particle- particle strength.

In the following the conservation of the Ikeda sum rule $ISR = S_- - S_+ = 3(N-Z)$ is discussed in the FR-QRPA framework and compared with the previous calculations for QRPA and SCQRPA. According with the definition (3.86) S^- (S^+) is the total summed Gammov-Teller $\beta^-(\beta^+)$ transition strength from the ground state of an even-even nucleus. In Fig. 4.24 the relative β^- strength $S^-/3(N-Z)$ is shown for the mother nucleus (left side) and relative β^+ strength, $S^+/3(N-Z)$ for the daugther (right side). The total strength is plotted as a function of particle-particle interaction parameter in order to show the magnitude and the nature of the ISR violation.

Finally the ratio of SCQRPA and FRQRPA sum $ISR/3(N-Z)$ is shown as a function of κ in Fig 4.25. In QRPA the Ikeda sum rule is exactly conserved as
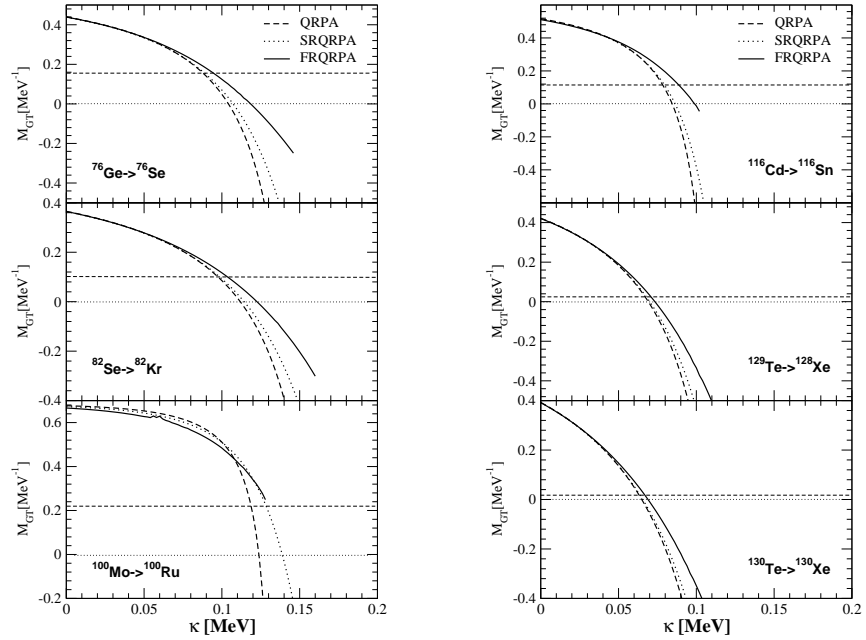
Figure 4.23: $2\nu\beta\beta$-decay matrix elements as a function of particle-particle strength g_{pp} for all nuclei

long as all spin-orbit partners of the single-particle orbitals are included. In the other extended versions of QRPA the sum rule is violated with a degree of deviation lying between 17% (RQRPA) and 3% [180]. In summary, following the analytical calculation of [149], it has been numerically shown that Ikeda sum rule is exactly fulfilled within FR-QRPA formalism. In this part the new results obtain within a selfconsistent formalism have been shown. The numerical applications were done for 6 double beta decay partners (^{76}Ge, ^{82}Se, ^{100}Mo, ^{116}Cd, ^{128}Te and ^{130}Xe). The method is interesting from qualitative point of view and in spite of the use of rather small model space, the effect of the restoration of the Ikeda sum rule on the decay amplitudes within FR-QRPA has been analyzed in comparison with the corresponding results in both QRPA and the self-consistent QRPA. Within the present work the following important conclusions are drown:

i) The SCQRPA violates the Ikeda sum rule. This phenomenon has been indicated in the previous studies [180], but the degree of violation we obtained is less than in the other calculations because we did not include all multipolarities.

ii) In the limit when the difference between proton and neutron quasiparticle occupation numbers is neglected the FR-QRPA coincides with SCQRPA.

iii) From a comparison of FR-QRPA with SCQRPA results we conclude that the effect of the restoration of the Ikeda sum rule is important in the range of large value
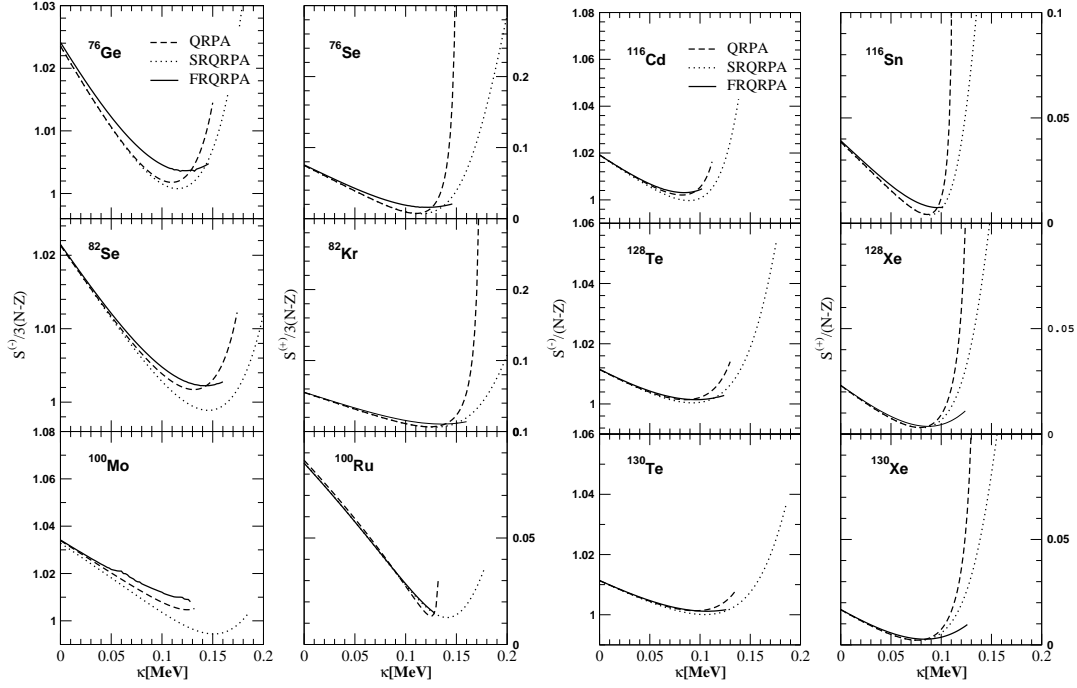
Figure 4.24: The dependence of the total β^- and β^+ strength on the g_{pp} parameter for mother and daughter nuclei respectively. The total strength is normalized to 3(N-Z)

of particle-particle strength beyond the point of collapse of the standard QRPA.

It is worth to mention that the FR-QRPA approach is sensitive to the precise evaluation of the proton and neutron quasiparticle occupation numbers. Due to the limitation of the approximate expression given in ([149]) (motivated by a similarity to the SQRPA approach) the convergence of the FR-QRPA is achieved only for relatively small model space. However, even for such a model space the differences among the standard QRPA, SCQRPA, FR-QRPA approach are evident for κ close to the point the standard QRPA breaks up. Also the question of the $2\nu\beta\beta$ collapse was open, unfortunately the actual calculations don't bring a satisfactory solution. There is a new attempt to solve this problem, namely the idea to use the concept of softly broken $SU(4)$ symmetry as a basis for describing the decay-amplitudes within a realistic a realistic nuclear model ([150, 151]).
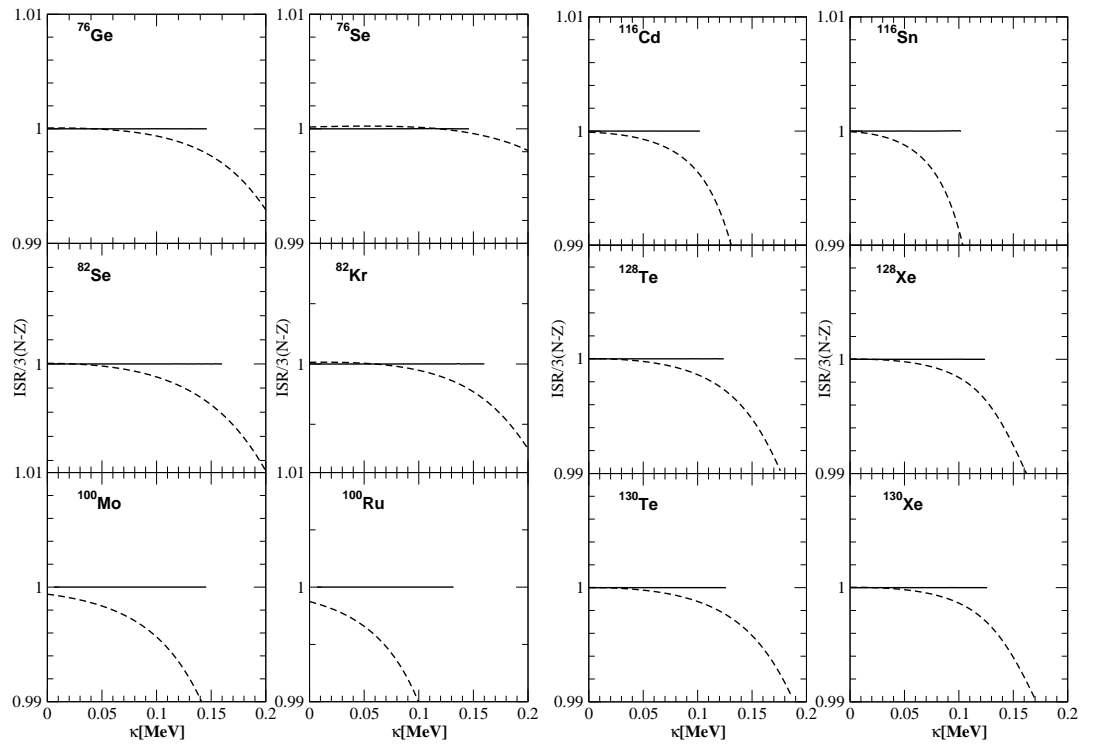
Figure 4.25: Ikeda sum rule as function of particle-particle interaction strength g_{pp}. The dashed line coresponds to SCQRPA and the continuous one coresponds to FRQRPA.

Chapter 5

Summary and Conclusions

The question whether the neutrino is a Majorana or a Dirac particle is still a major focus in particle physics research. Double beta decay is one of the most popular methods which try to answer this question. There are different possible modes of $\beta\beta$–decay which differ from each other by the light particles accompanying the emission of two electrons. We distinguish the $\beta\beta$–decay modes with and without lepton-number violation. The $2\nu\beta\beta$–decay conserves the lepton number and is fully consistent with the Standard Model (SM). This process involves the emission of two electrons and two antineutrinos. The half-lives, already well established experimentally for a couple of isotopes, range from 10^{19} up to 10^{24} years. The other decay mode, $0\nu\beta\beta$–decay, involves the emission of two electrons and no neutrinos. This process violates lepton number conservation and therefore is forbidden in the SM of the electroweak interaction. So far the neutrinoless double beta decay has not been experimentally observed. Nowadays there are many experiments running and the experimental evidences of this process will prove that neutrinos are Majorana particles.

Also closely connected to the above is the question concerning the amount of mass to be assigned to the neutrinos. Although the neutrinoless double beta decay has not been seen yet, it is possible to extract from the lower limits of the lifetime upper limits for the effective electron-neutrino mass and for the effective mixing angle of the right-handed and the left-handed vector bosons mediating the weak interaction. One can also obtain an effective upper limit for the mass ratio of the light and the heavy vector bosons. A condition to obtain reliable limits for these fundamental quantities from the measured lower limits of the half-lives of the $0\nu\beta\beta$–decay is that the nuclear matrix elements are correctly estimated. The nuclear structure calculations can be tested by calculating the $2\nu\beta\beta$–decay for which there are experimental data and not just lower limits like in $0\nu\beta\beta$–decay.

The $2\nu\beta\beta$–decay rate is governed by the Gamow-Teller matrix elements connecting the final and initial nucleus. The difficulty therein is that all intermediate 1^+ states have to be taken into account. The Quasiparticle Random Phase Approximation (QRPA) has been the most popular theoretical tool to theoretically study the $2\nu\beta\beta$–decay in the recent past. Its main ingredients, the repulsive particle-hole spin-isospin interaction and the attractive particle-particle interaction, clearly play a decisive role in describing the concentration of the β^- strength in the giant GT resonance, as well as in the relative suppression of the β^+ strength and its concentration at low excitation energies. Together, these two ingredients are able to explain the suppression of the $2\nu\beta\beta$ matrix element when expressed in terms of the corresponding sum rule. Previous calculations suggested that the nuclear deformation might be the reason for the suppression mechanism, beside the particle-particle interaction. In order to clarify this aspect, the study of the behavior of the double beta decay transition amplitudes with respect to the deformation constitute the main goal of this thesis.

In order to perform QRPA calculations for the deformed nuclei, the main effects of the deformation on the ground state properties of the double beta decay emitters have to be clarified. The pairing interactions between proton–proton, neutron–neutron and proton–neutron (pn) smear out the nuclear Fermi surface over a relatively large number of orbitals. The occupation probabilities for protons and neutrons enter the single and double beta decay matrix elements. One question is whether the effect of pn pairing becomes significant for deformed neutron-rich nuclei. Another one is, if due to the deformation a coexistence between T=0 and T=1 pn pairing might occur. Therefore, generalized BCS calculations were performed assuming an axially symmetric mean field and a Hamiltonian with schematic T=1 and T=0 pairing forces [176]. The competition between like-particle and pn pairing was studied in even-even Ge isotopes[1]. The system of BCS equations allows three different solutions. There is one solution with only like–particle pairs, and two solutions in which like and unlike particle pairs coexist, first with T=1 and second with T=0 pn–pairs. None of the observed pairing modes allows simultaneous presence of both T=0 and T=1 pn–correlations. The effect of pn pairing becomes important for isotopes with large neutron excess N-Z, in particular for ^{76}Ge which undergoes double beta decay. This result contrasts with the general belief that pn pairing correlations are restricted only to the vicinity of N=Z line.

It is also interesting to see the effect of deformation in single β^+ and β^- transitions. The β^- transition amplitudes from initial to intermediate nucleus and β^+ amplitudes from the intermediate to the final nucleus enter the final formula of the double beta decay matrix elements. The β^+ amplitudes are strongly suppressed due to the Pauli principle and thus implicitly also the $2\nu\beta\beta$–decay matrix elements. The GT strength distribution was studied for the two decay branches β^- and β^+ in all double beta decay emitters [158, 159]. This was done within a deformed QRPA formalism which includes particle–hole (ph) and particle–particle (pp) separable residual interactions. The quasiparticle mean field includes pairing correlations in the BCS approximation and it is generated, for comparison, by two different methods, a deformed Hartree-Fock (HF) approach with Skyrme interactions and a phenomenological deformed Woods-Saxon (WS) potential. Among the similarities between the HF and WS results, one can mention the structure of peaks found in the strength distributions and among the differences the displacement in the excitation energies found between HF and WS results. A significant part of the total β^+ strength is concentrated in the energy region above 10 MeV for the WS calculations. This discrepancy has its origin in the structure of the single–particle wave functions and energies generated by the deformed mean fields. This also implies that different mean fields require different residual interactions to reproduce the experimental GT resonances. Therefore, in order to obtain reliable GT strength

---

[1]The ^{76}Ge nucleus is a double beta decay emitter.

distributions and consequently reliable estimates for double β–decay half-lives, it is important to have not only the proper residual interactions but also a good deformed single-particle basis as a starting point. In the case of HF the standard Skyrme forces, such as SG2 or Sk3, give a good description of the GT strength distributions when the proper residual interactions are included. Even though the selfconsistent HF approach is a more sophisticated type of calculation, the deformed WS potential produces comparable results when the parameters of the potential and the residual interactions for a given mass region are chosen properly. Then the input parameters are adjusted so that the experimental data (position of GT giant resonance) are reproduced. The systematics of deformations, ph and pp strengths for all double beta decay emitters is shown in this thesis. These results are useful for the calculations of the $2\nu\beta\beta$ matrix elements in deformed ^{76}Ge described in the following.

The double beta decay matrix elements were calculated for both spherical and deformed Ge nuclei within the deformed QRPA with separable spin–isospin interactions in the ph and pp channels [177, 134]. It is shown that the suppression of the $2\nu\beta\beta$-decay matrix elements is large for a significant difference in the deformations of the parent and daughter nucleus and is not related to the increasing amount of the ground state correlations close to the collapse of the QRPA solution. A new mechanism of the suppression of the double beta decay nuclear matrix elements due to deformation is found. The origin of this new mechanism is a strong sensitivity of the overlap of the initial and final BCS vacuum to the deformations of the initial and final nucleus. This enters directly into the overlap of the intermediate nuclear states generated from the initial and final nuclei via the QRPA diagonalization. A study of other double beta decay transitions as a function of this deformation dependent overlap indicates the general importance of the new suppression mechanism for the $2\nu\beta\beta$-decay and $0\nu\beta\beta$-decay matrix elements. It is also shown that by assuming spherical nuclei there is a strong disagreement between the pp strength κ needed to reproduce the $2\nu\beta\beta$-decay half-life of ^{76}Ge and the κ deduced in Ref. [102] from a systematic study of the single β-decay transitions. With the new suppression mechanism of the $2\nu\beta\beta$-decay matrix element, a simultaneous description of both single β and $2\nu\beta\beta$-decay is possible.

The detailed study of contributions to $2\nu\beta\beta$–matrix elements from different 1^+ intermediate nuclear states shows that for the A=76 nuclei it is necessary to consider all 1^+ states of ^{76}As up to an energy of $15 - 20$ MeV. This fact disfavors theoretical studies of the $2\nu\beta\beta$-decay of medium and heavy nuclei in models with a strongly truncated basis, like the shell model. The investigation of the deformation dependence yielded insight into a new suppression mechanism but still did not help to overcome the main problem in the QRPA approximations, as it was hoped initially. The collapse of the QRPA solutions, and thus of the $2\nu\beta\beta$ matrix elements, cannot be avoided for deformed nuclei and also cannot be much shifted to larger

values of pp strength. The origin of this behavior is in the Quasiboson Approximation violating the Pauli principle. Furthermore, in calculations using separable forces and the secular dispersion equation, the Ikeda sum rule (ISR) is fulfilled only on the level of 90-95%.

In this thesis, the new extension of the QRPA [135, 149], the Fully Renormalized-QRPA, which can overcome the inconvenient aspects of the QRPA, has been applied. The Pauli principle violation and the collapse of matrix elements are particulary studied. It is shown analytically that the phonon operator includes the scattering terms restoring the ISR. Moreover, the collapse of the FR-QRPA solutions and double beta decay matrix elements occurs for large values of pp strength. It has to be mentioned that the FR-QRPA approach is sensitive to the precise evaluation of the proton and neutron quasiparticle occupation numbers. Due to numerical problems, convergence of the FR-QRPA is achieved only for a relatively small model space. Nevertheless, it is shown numerically that the ISR is fulfilled also in a limited space. Already for such a model space the differences between the standard QRPA, its extensions, and the FR-QRPA are evident when the pp strength is close to the point where the standard QRPA collapses. There is hope that for a proper ansatz of the RPA ground state the FR-QRPA approach can work also for large model spaces.

The Gamow-Teller β^+ strengths and double beta decay matrix elements in medium and heavy nuclei continue to be a challenge for nuclear structure models. Further theoretical studies are needed to clarify the role of deformation in the calculation of other double beta decay transitions, especially those including heavier nuclear systems which are known to be strongly deformed. Future work should investigate the $2\nu\beta\beta$-decay matrix elements also within different possible extensions of the deformed QRPA, e.g., those including proton-neutron pairing [176]. In this way one expects to develop a reliable many-body approach with well–defined nuclear structure parameters for the calculation of the $0\nu\beta\beta$-decay matrix elements. Their accurate values are highly required to determine the neutrino mixing pattern and to answer the question of the dominant mechanism in the $0\nu\beta\beta$-decay [21, 64].

Chapter 6

Zusammenfassung

Diese Arbeit beschäftigt sich mit neuen Aspekten der Berechnung von $2\nu\beta\beta$ Matrixelementen im Rahmen der deformierten QRPA. Dabei wurde ein neuer Mechanismus gefunden, der die $\beta\beta$ Matrixelemente in Abhängigkeit von der Deformation unterdrückt.

Das Studium des doppelten β-Zerfalls kann neues Licht auf eine der wichtigsten Fragen der Teilchenphysik werfen, nämlich, ob das Neutrino ein Majorana oder Dirac Teilchen ist. Beim $\beta\beta$-Zerfall kann man einen Zerfallsmodus mit und einen ohne Verletzung der Leptonenzahl definieren. Der die Leptonenzahl erhaltende $2\nu\beta\beta$-Zerfall (Aussendung zweier Elektronen und zweier Antineutrinos) ist mit dem Standardmodell der Teilchenphysik verträglich. Die für einige Kerne bereits experimentell bestimmten Halbwertszeiten liegen im Bereich zwischen 10^{19} und 10^{24} Jahren für diese Art von Zerfalls. Beim anderen Modus, dem $0\nu\beta\beta$-Zerfall oder neutrinolosen β-Zerfall, werden nur zwei Elektronen, aber keine Neutrinos emittiert. Dieser Prozess verletzt den Erhaltungssatz der Leptonenzahl und ist deshalb im Standardmodell der schwachen Wechselwirkung verboten. Bis heute gibt es keine experimentelle Bestätigung dieser Zerfallsart. Es sind jedoch eine Reihe von Experimenten im Gange, da durch den Nachweis des neutrinolosen β-Zerfalls das Neutrino als Majorana Teilchen festgelegt werden könnte.

Eng verknüpft mit obiger Frage ist auch die Bestimmung der Neutrinomassen. Obwohl noch kein doppelter β-Zerfall direkt beobachtet werden konnte, ist es doch mglich, Untergrenzen der für diesen Zerfall relevanten Lebensdauern anzugeben. Aus diesen wiederum können Obergrenzen der effektiven Neutrinomasse und Grenzwerte für den effektiven Mischungswinkel der rechts- und links-händigen Vektorbosonen, welche die schwache Wechselwirkung vermitteln, abgeleitet werden. Es ist auch möglich, eine effektive Obergrenze des Massenverhältnisses der leichten und schweren Vektorbosonen anzugeben. Verlässliche Grenzwerte dieser fundamentalen Größen können jedoch nur bestimmt werden, wenn die Matrixelemente des $0\nu\beta\beta$-Zerfalls präzise berechnet werden können. Die dazu nötigen Kernstrukturrechnungen können in Rechnungen zum $2\nu\beta\beta$-Zerfall durch Vergleich mit dem Experiment direkt getestet werden, im Gegensatz zum $0\nu\beta\beta$-Zerfall für den es nur Untergrenzen der Halbwertszeiten gibt.

Die $2\nu\beta\beta$-Zerfallsrate wird durch die Gamow-Teller Matrixelemente bestimmt, die Zustände im zerfallenden Kern mit jenen im Endkern verknüpfen. Die Schwierigkeit hierbei liegt darin, dass alle 1^+ Zwischenzustände berücksichtigt werden müssen. In der theoretischen Behandlung des $2\nu\beta\beta$-Zerfalls war bislang üblicherweise QRPA die Methode der Wahl. Deren Hauptbestandteile, die abstoßende Teilchen-Loch, Spin-Isospin Wechselwirkung und die anziehende Teilchen-Teilchen Wechselwirkung, spielen eindeutig eine entscheidende Rolle in der Beschreibung der Konzentration der β^- Stärke in der GT Riesenresonanz und bei relativen Unterdrückung der β^+ Stärke, die hauptsächlich bei niedrigen Anregungsenergien liegt. Zusammen können diese beiden Wechselwirkungen die Unterdrückung der $2\nu\beta\beta$ Matrixelemente

in der dazugehörigen Summenregel erklären. Frühere Rechnungen deuteten darauf hin, dass die Kerndeformation neben der Teilchen-Teilchen Wechselwirkung ebenfalls eine Rolle in der Unterdrückung der Matrixelemente spielt. Aus diesem Grund ist der Hauptaspekt der vorliegenden Arbeit die Untersuchung des Verhaltens der Übergangsamplituden des doppelten β-Zerfalls in Abhängigkeit von der Deformation.

Um überhaupt QRPA Rechnungen für deformierte Kerne machen zu können, müssen zunächst die Haupteinflüsse der Deformation auf die Grundzustandseigenschaften der Mutterkerne verstanden werden. Die Paarungskräfte zwischen Protonen unter sich, Neutronen unter sich und zwischen Proton-Neutron (pn) verschmieren die Fermioberfläche über eine relativ große Anzahl von Orbitalen. Die Besetzungswahrscheinlichkeiten der Protonen und Neutronen gehen in die Matrixelemente für einfachen und doppelten β-Zerfall ein. Eine der bedeutsamen Fragen ist, ob der pn Paarungseffekt für neutronenreiche, deformierte Kerne von Bedeutung ist. Eine andere Frage ist, ob T=0 und T=1 pn Paarung wegen der Deformationseffekte koexistieren kann. Um diese Fragen zu untersuchen wurden in dieser Arbeit Rechnungen im verallgemeinerten BCS Modell durchgeführt, wobei ein axialsymmetrisches gemitteltes Potenzial und ein Hamiltonoperator mit vereinfachten T=1 und T=0 Paarungskräften verwendet wurde [176]. Der Wettbewerb zwischen Paarung gleicher Teilchen und pn Paarung wurde in geraden Ge-Isotopen studiert (^{76}Ge kann doppelten β-Zerfall machen). Das BCS Gleichungssystem hat drei verschiedene Lösungen. Eine davon enthält nur Paare gleicher Teilchen, in den beiden anderen koexistieren Paare gleicher und ungleicher (pn) Teilchen, in einer mit T=1 und in der anderen mit T=0 pn-Paaren. Keine der beobachteten Paarungsmoden erlaubt die gleichzeitige Realisierung von T=0 und T=1 pn-Korrelationen. Der Effekt der pn-Paarung ist wichtig in Isotopen mit großem Neutronüberschuss (N-Z groß), besonders auch im Falle des ^{76}Ge. Dieses Ergebnis steht im Gegensatz zur verbreiteten Annahme, pn-Paarungseffekte wären nur auf die Umgebung der N=Z Linie beschränkt.

Es ist auch interessant, den Einfluss der Deformation auf einzelne β^+ und β^- Übergänge zu betrachten. Die Formel für die Matrixelemente des doppelten β-Zerfalls enthält die β^- Übergangsamplituden vom Anfangs– zum Zwischenkern und die β^+ Amplituden vom Zwischen– zum Endkern. Wegen des Pauliprinzips sind die β^+ Amplituden stark unterdrückt und deshalb implizit die Matrixelemente des $2\nu\beta\beta$-Zerfalls. In dieser Arbeit wurde die Verteilung der GT Stärke in den β^- und β^+ Zerfallszweigen aller Kerne, die doppelten β-Zerfall machen können, untersucht. [158, 159]. Dazu wurde eine Formulierung der deformierten QRPA benutzt, welche separable Teilchen-Loch (TL) und Teilchen-Teilchen (TT) Restwechselwirkungen enthält. Paarungskorrelationen werden darin im BCS Modell beschrieben. Das "mean field" der Quasiteilchen wurde zu Vergleichszwecken auf zwei verschiedene Arten erzeugt, einmal über die deformierte Hartree-Fock Methode

(HF) mit Skyrme Wechselwirkungen, und einmal mittels eines phänomenologischen, deformierten Woods-Saxon (WS) Potenzials. Den Ergebnissen beider Rechnungen ist gemeinsam, dass sie die gleiche Struktur der peaks in den Stärkeverteilungen aufweisen. Unterschiede ergeben sich in der Anregungsenergie, bei der die peaks liegen. Der Großteil der totalen β^+ Stärke ist in der WS Rechnung im Energiebereich oberhalb von 10 MeV konzentriert. Dieser Unterschied in den HF und WS Rechnungen liegt in der Struktur der Einteilchenwellenfunktionen und -energien begründet, die durch die unterschiedlichen "mean fields" erzeugt werden. Daraus folgt, dass mit verschiedenen "mean fields" auch unterschiedliche Restwechselwirkungen benötigt werden, um die gleichen experimentellen GT Resonanzen zu beschreiben. Daher ist es für eine verlässliche Beschreibung der Verteilung der GT Stärke und somit der β Halbwertszeiten nicht nur wichtig adäquate Restwechselwirkungen zu benutzen, sondern auch eine gute Einteilchen-Basis als Startpunkt zu haben. In der HF Rechnung ergeben die Standard-Skyrme Kräfte, wie SG2 oder Sk3, eine gute Beschreibung der GT Stärkeverteilung, wenn man passende Restwechselwirkungen hat. Obwohl die selbstkonsistente HF Methode grundlegender erscheint, ergeben sich mit dem deformierten WS Potenzial vergleichbar gute Ergebnisse wenn die Potenzialparameter und die Restwechselwirkungen für den gegebenen Massenbereich vernünftig gewählt werden. Das heisst, die Parameter werden so angepasst, dass experimentelle Daten (Position der GT Riesenresonanz) reproduziert werden. Systematiken der sich daraus ergebenden Deformationen, sowie TL- und TT-Stärken aller im doppelten β-Zerfall wichtigen Kerne sind in der vorliegenden Arbeit angegeben. Diese Ergebnisse sind für die unten beschriebene Berechnung der $2\nu\beta\beta$ Matrixelemente für das deformierte ^{76}Ge nützlich.

Im weiteren Verlauf wurden die Matrixelemente des doppelten β-Zerfalls für sphärische und deformierte Ge-Kerne mittels QRPA und mit separablen Spin-Isospin Wechselwirkungen in den TL- und TT-Kanälen berechnet [177, 134]. Es stellt sich heraus, dass die Unterdrückung der $2\nu\beta\beta$ Matrixelemente stark ist, wenn ein signifikanter Unterschied in der Deformation des Mutter- und des Tochterkerns besteht. Es zeigt sich auch, dass diese Unterdrückung nichts mit dem wachsenden Anteil von Grundzustandskorrelationen nahe des Kollapses der QRPA Lösung zu tun hat. Es wurde also ein neuer Mechanismus zur Unterdrückung der Matrixelemente des doppelten β-Zerfalls gefunden. Dieser neue Mechanismus gründet sich auf die starke Empfindlichkeit des Überlapps zwischen den BCS Vakua des Anfangs- und Endzustands auf die Deformation des Anfangs- bzw. Endkerns. Diese setzt sich auch fort bis in den Überlapp der Zwischenzustände, die aus den Anfangs- und Endkernen mittels Diagonalisierung der QRPA erzeugt werden. Die Ergebnisse einer weitergehenden Untersuchung anderer Übergänge im doppelten β-Zerfall als Funktion dieses deformationsabhängigen Überlapps deuten auf eine Allgemeingültigkeit dieses Unterdrückungsmechanismus und unterstreichen seine Bedeutung in der Berechnung von Matrixelementen des $2\nu\beta\beta$- und $0\nu\beta\beta$-Zerfalls. Es wird auch deutlich, dass die

Annahme von Spherizität aller Kerne zu einem großen Widerspruch zwischen der TT-Stärke κ führt, die benötigt wird, die Halbwertszeit von ^{76}Ge im $2\nu\beta\beta$-Zerfall zu reproduzieren, und jener Stärke κ, die in Ref. [102] aus einer systematischen Studie von einzelnenβ-Übergängen abgeleitet wurde. Mit dem neuen Mechanismus zur Unterdrückung der $2\nu\beta\beta$ Matrixelemente ist hingegen eine gleichzeitige, konsistente Beschreibung sowohl von β- als auch von $2\nu\beta\beta$-Zerfall möglich.

Untersucht man detailliert die Beiträge verschiedener 1^+ Zwischenzustände zu den $2\nu\beta\beta$ Matrixelementen, so zeigt sich, dass man in den A=76 Kernen alle 1^+ Zustände in ^{76}As bis zu einer Energie von $15-20$ MeV berücksichtigen muss. Diese Tatsache verbietet theoretische Studien des $2\nu\beta\beta$-Zerfalls von mittelschweren und schweren Kernen in Modellen mit stark verkleinerter Basis, wie etwa im Schalenmodell. Mit der oben beschriebenen Untersuchung der Abhängigkeit von der Deformation erhält man Einsicht in den neuen Unterdrückungsmechanismus, aber das hilft trotzdem noch nicht, die Schäche der QRPA zu überwinden, wie es ursprünglich erhofft wurde. Der Kollaps der QRPA Lösungen, und somit auch der $2\nu\beta\beta$ Matrixelemente kann auch in deformierten Kernen nicht vermieden werden und kann auch nicht viel zu grösseren Werten der TT-Stärke hin verschoben werden. Der Grund für dieses Verhalten liegt in der quasibosonischen Näherung, die das Pauliprinzip verletzt. Ausserdem wird die Summenregel von Ikeda (ISR) in Modellen, die separable Kräfte und die säkulare Dispersionsgleichung benutzen, nur zu $90-95\%$ erfüllt.

Deshalb wurde im Rahmen der vorliegenden Arbeit schließlich eine neue Erweiterung der QRPA entwickelt [135, 149]. In der "Fully Renormalized-QRPA" (FR-QRPA) sind die unhandlichen Aspekte der QRPA eliminiert. Die Verletzung der Pauliprinzips und der Kollaps der Matrixelemente bei kleiner TT-Stärke wird vermieden. Analytisch wurde hier gezeigt, dass der Phononoperator Streuterme enthält, sodass die ISR wieder erfüllt ist. Somit erfolgt der Kollaps der FR-QRPA Lösungen and Matrixelemente des doppelten β-Zerfalls erst für große Werte der TT-Stärke. Man muss jedoch anmerken, dass die FR-QRPA Methode empfindlich auf die genaue Berechnung der Besetzungszahlen der Proton- und Neutron-Quasiteilchen ist. Wegen numerischer Probleme erhält man Konvergenz nur in einem vergleichsweise kleinen Modellraum. Trotzdem konnte numerisch gezeigt werden, dass die ISR auch im beschränkten Modellraum erfüllt wird. Selbst im limitierten Modellraum werden große Unterschiede zwischen der Standard-QRPA, ihren Erweiterungen und der FR-QRPA deutlich, wenn die TT-Stärke nahe dem Wert ist, an dem die Standard-QRPA zusammenbricht. Es besteht die Hoffnung, dass die FR-QRPA Methode mit einem geschickten Ansatz des RPA Grundzustands auch in großen Modellräumen funktionieren wird.

Die Berechnung der Gamow-Teller β^+ Stärken und der Matrixelemente des doppelten β-Zerfalls in mittelschweren und schweren Kernen bleibt auch weiterhin eine Herausforderung für Kernstrukturmodelle. Es sind noch weitere theoretische Arbeiten nötig, um die Rolle der Deformation in anderen Übergängen im doppel-

ten β-Zerfall zu klären, insbesonders in jenen schwereren kernphysikalischen Systemen, von denen man weiss, dass sie deformiert sind. Zukünftige Studien sollten die $2\nu\beta\beta$ Matrixelemente auch mit weiteren, unterschiedlichen Erweiterungen der deformierten QRPA untersuchen, zum Beispiel solche, die auch Proton-Neutron Paarung enthalten [176]. Auf diese Weise kann man erwarten, eine verlässliche Vielteilchen-Methode mit wohldefinierten Kernstrukturparametern für die Berechnung der Matrixelemente des $0\nu\beta\beta$-Zerfalls zu erhalten. Genaue Werte dieser Matrixelemente werden zur Bestimmung der Neutrinomischungsverhältnisse und zur Beantwortung der Frage benötigt, welches der dominante Mechanismus im $0\nu\beta\beta$-Zerfall ist [21], [64].

Chapter 7

Appendix

7.1 Appendix A

7.1.1 History of the $2\nu\beta\beta$–decay

"Liebe Radioaktive Damnen und Herren,

wie der Überbringer dieser Zeilen, den ich huldvollst anzuhören bitte, Ihnen des näheren auseinandersetzen wird, bin ich angesichts der "falschen" Statistik der N und Li 6 Kerne, sowie des kontinuierlichen β-Spektrums auf einen verzweifelten Ausweg verfallen, um den "Wechselsatz" der Statistik und den Energiesatz zu retten. Nämlich die Möglichkeit, es könnten elektrisch neutrale Teilchen, die ich Neutronen nennen will, in den Kernen existieren, welche den Spin 1/2 haben und das Ausschließungsprinzip befolgen und sich von Lichquanten außerdem noch dadurch unterscheiden, daß sie nicht mit Lichtgeschwindigkeit laufen. Die Masse der Neutronen müß te von derselben Größ enordnung wie die Elektronenmasse sein und jedenfalls nicht größer als 0.01 Protonenmasse. Das kontinuierliche β-Spektrum wäre dann verständlich unter der Annahme, daß beim β-Zerfall mit dem Elektron jeweils noch ein Neutron emittiert wird, derart, daß die Summe der Energien von Neutron und Elektron konstant ist.

Nun handelt es sich weiter darum, welche Kräfte auf die Neutronen wirken. Das wahrschelischstes Modell für das Neutron scheint mir aus wellenmechanischen Gründen (näheres weiß der Überbringer dieser Zeilen) dieses zu sein, daß das ruhende Neutron ein magnetischer Dipol von einem gewissen Moment μ ist. Die Experimente verlangen wohl, daß die ionisierende Wirkung eines solchen Neutrons nicht größer sein kann als die eines γ -Strahls, und dann darf μ wohl nicht größ er sein als $e10^{-13}$ cm.

Ich traue mich vorläufig aber nicht, etwas über diese Idee zu publizieren, und wende mich erst vertrauensvoll an Euch, liebe Radioaktive, mit der Frage, wie es um den experimentellen Nachweis eines solchen Neutrons stände, wen dieses ein ebensolches oder etwas 10 mal größeres Durchdringungsvermögen besitzen würde wie ein γ -Strahl.

Ich gebe zu, daß mein Ausweg vielleicht von vornherein wenig wahrscheinlich erscheinen mag, weil man die Neutronen, wenn sie existierten wohl längst gesen hätte. Aber nur wer wagt, gewinnt und der Enst der Situation beim kontinuierlichen β Spektrum wird durch einen Ausspruch meines verehrten Vorgängers im Amte, Herrn Debye, bleuchtet, der mir kürzlich in Brüssel gesagt hat: "O, daran soll man am besten nicht denken, so wie an die neuen Steuern." Darum soll man jeden Weg zur Rettung ernstlich diskutieren. Also liebe Radioactive, prüfet, und richtet. - Leider kann ich nicht in Tüebingen erscheinen, da ich infolgeines in der Nacht von 6. zum 7. Dez. in Zürich stattfindenden Balles hier unabkömmlich bin. -Mit vielen grüß en an Euch, sowie auch Herrn Back, Eurer untertänigster Diener
W. Pauli"

7.2 Appendix B

The single particle wave functions of the deformed axially-symmetric Woods-Saxon potential are expanded in a basis of the deformed harmonic oscillator. Two types of Skyrme forces SG2 and Sk3 are described.

7.2.1 Deformed Woods-Saxon potential

The average field potential (deformed Woods-Saxon potential) is defined on a basis of implicit equation, which determines the shape of the nuclear surface. The hamiltonian used includes also a spin-orbit coupling and for charged particles, the coulomb potential. The starting point is the general definition of the nuclear surface which is given by an implicit equation in cylindrical coordinates

$$\Pi(u, v) = 0. \tag{7.1}$$

For the radial part of the potential it is assumed that this can be expressed by a single variable l, which in turn is a function of the spatial variables u and v. With l defined as a spatial distance, the Woods-Saxon potential has the following form

$$V(l) = \frac{V}{1 + exp(l/a)}. \tag{7.2}$$

Here a is the thickness of the nuclear surface.

$$l = \frac{Cs(u, v)}{|\nabla_{u,v} S(u, v)|}, \tag{7.3}$$

with:

$$
\begin{aligned}
S(u, v) &= (\Pi(u, v) - \Pi_{min})^{1/2} - (-\Pi_{min})^{1/2}, \\
\Pi(u, v) &= v^2 + u^2 - R^2(u, v), \\
R(u, v) &= R(\theta) = R_n(1 + \beta_2 Y_{20}(\theta) + \beta_4 Y_{40}(\theta)), \\
\Pi_{min} &= absolute \ \ minimum \ \ for \ \ \Pi(u, v),
\end{aligned}
\tag{7.4}
$$

where C and R_n are normalization constants as a function of β_2, β_4 and R_0 and respectively $R_0 = r_0 A^{1/3}$

$$z = Cu, \qquad \zeta = Cv. \tag{7.5}$$

The spin-orbit coupling field is assumed to be of the form

$$V^{s.o} = -\frac{\kappa}{\hbar^2} \vec{\nabla} V_{so}(l)[\vec{\sigma} \times \vec{p}], \tag{7.6}$$

with

$$V_{so}(l) = \frac{V_0}{1 + exp(\frac{l_{so}}{a_{so}})}, \tag{7.7}$$

and the Coulomb potential

$$V_c = \int \frac{\zeta_0}{1 + exp(\frac{l_c}{a_c})} \frac{1}{|\vec{r} - \vec{r'}|} d^3 r', \tag{7.8}$$

where κ is the coupling parameter and ζ_0 is a charge distribution inside of the nucleus.

In order to solve the Schrodinger equation:

$$H\Psi_i = [T + V^{w.s.} + V^{s.o.} + \Phi_C]\Psi_i = \epsilon_i \Psi_i, \tag{7.9}$$

where $V^{w.s.} = V^{w.s.}(\beta_2, \beta_4)$, the single-particle wave function is expanded in terms of the eigenstates of an axially symmetric harmonic oscillator. The single particle states $|i>$ and their time reversed $\widetilde{|i>}$ are characterized by the eingenvalues K of J_z, parity π_i and energy ϵ_i

$$|i> = \sum_N \frac{(-1)^N + \pi_i}{2} \sum_{n_r, n_z, \Lambda, \Sigma} C^i_{N, n_r, n_z, \Lambda, \Sigma} |N, n_r, n_z, \Lambda, \Sigma>, \tag{7.10}$$

with $K = \Lambda + \Sigma$ and

$$\widetilde{|i>} = \sum_N \frac{(-1)^N + \pi_i}{2} \sum_{n_r, n_z, \Lambda, \Sigma} C^i_{N, n_r, n_z, \Lambda, \Sigma} (-1)^{\frac{1}{2} - \Sigma} |N, n_r, n_z, -\Lambda, -\Sigma>. \tag{7.11}$$

The radius and potential parameters are taken from the literature. Here, is used the parametrization of Tanaka et al. [186]:

$$
\begin{aligned}
r_0 &= r_0^0 - r_0^1 A^{-1/3}, & a_0 &= a_0^0 + a_0^1 (N - Z)/A, \\
V_0 r^n &= v_0^0 + v_0^1 (N - Z)/A, \\
r_{so} &= r_{so}^0 - r_{so}^1 A^{-1/3} & a_{so} &= a_0 \\
V_{so} &= v_{so}^0 + v_{so}^1 (N - Z)/A, \\
r_c &= r_0 & a_c &= a_0,
\end{aligned} \tag{7.12}
$$

with $n = 1.6$, $a_0^0 = 0.60$, $a_0^1 = 0.47$, $\kappa V_0 = V_{so}(\frac{\hbar}{m_\pi c})^2 = 1.998063$ V_{so} fm^2 and the parameters from Table 7.1

Table 7.1: Radius and potentials parametrization for deformed Woods-Saxon potential

	$v_0^0[MeV]$	$v_0^1[MeV]$	$v_{so}^0[MeV]$	$v_{so}^1[MeV]$
Protons	74,74	50.32	6.315	-3.501
Neutrons	75.91	-53.43	6.829	2.287
	$r_0^0[fm]$	$r_0^1[fm]$	$r_{so}^0[fm]$	$r_{so}^1[fm]$
Protons	1.412	0.621	1.185	0.946
Neutrons	1.501	0.636	1.510	1.006

7.2.2 Deformed harmonic oscillator

Hamilton operator for a deformed axially symmetric harmonic oscillator in cylindrical coordinates (ρ, z, ϕ), ρ being the azimuth radius, with a quadrupole and hexadecapole parametrization

$$H_{DO} = -\frac{\hbar^2}{2m}\nabla^2 + \frac{m}{2}({\omega_\perp}^2\rho^2 + \omega_z^2 z^2). \qquad (7.13)$$

The basic wave functions are the eigenstates of an anisotropic harmonic oscillator and they are described by the quantum numbers n_ρ, n_z and Λ. For a deformed harmonic oscillator single particle energy is given by

$$\epsilon_0 = \hbar\omega_\perp(2n_\rho + \Lambda + 1) + \hbar\omega_z(n_z + \frac{1}{2}), \qquad (7.14)$$

where Λ and Σ are the projections of the orbital and spin angular momentum on the symmetry axis z. The axially symmetric deformed harmonic oscillator can be also describe using the Nilsson quantum numbers

$$[Nn_z\Lambda]K^\pi, \qquad (7.15)$$

with the folowing quantum numbers:

$$\begin{aligned} N &= n_z + 2n_\rho + |\Lambda|, \\ K &= \Lambda + \Sigma, \\ \pi &= (-1)^N. \end{aligned} \qquad (7.16)$$

Basis functions are a superposition of Hermite and associated Laguerre polynomials

$$\Psi(n_\rho, n_z, \Lambda, \Sigma) = \Psi_{n_\rho}^\Lambda(\rho)\Psi_{n_z}(z)\Psi_\Lambda(\varphi)\chi(\Sigma) = |N, n_z, \Lambda, \Sigma, K >, \qquad (7.17)$$

$$\Psi_\Lambda(\varphi) \;=\; \frac{1}{\sqrt{2\pi}}e^{i\Lambda\varphi},$$

$$\Psi_{n_z}(z) \;=\; N_{n_z}[\frac{M\omega_z}{\hbar}]^{\frac{1}{4}}e^{-\frac{1}{2}\xi^2}H_{n_z}(\xi),$$

$$\Psi_{n_\rho}^\Lambda(\rho) \;=\; N_{n_\rho}[\frac{2M\omega_\perp}{\hbar}]^{\frac{1}{2}}\eta^{\frac{1}{2}\Lambda}e^{-\frac{1}{2}\eta}L_{n_\rho}^\Lambda(\eta), \qquad (7.18)$$

where: $\eta^{\frac{1}{2}} = \sqrt{\frac{M\omega_\perp}{\hbar}}r$; $\xi = \sqrt{\frac{M\omega_z}{\hbar}}z$; $n_\perp = 2n_r + \Lambda$
$N_{n_z} = \frac{1}{\sqrt{\sqrt{\pi}2^{n_z}n_z!}}$; $N_{n_r}^\Lambda = \sqrt{\frac{n_r!}{(n_r+\Lambda)!}}$.

As it has been mentioned before $H_n(\xi)$ and $L_m^l(\eta)$ are associated polynomials. The frequencies $\omega_\perp$ and ω_z characterizing the deformed harmonic oscillator are two free parameters which are found from fitting the shape and size of the deformed harmonic oscillator potential to the average field. The time revers wave function is defined like

$$\tilde{|}N,n_z,\Lambda,\Sigma,K> = \hat{T}|N,n_z,\Lambda,\Sigma,K> = (-1)^{1/2-\Sigma}|N,n_z,-\Lambda,-\Sigma,-K>. \quad (7.19)$$

7.2.3 Skyrme forces

The density-dependent HF approximation gives a very good description of ground-state properties for both spherical and deformed nuclei [70] and it is at present the most reliable mean field description. Two different Skyrme forces were used for the numerical applications: on one hand the Skyrme force Sk3 [17] because it is the most extensively used Skyrme force and it is considered as a reference, on the other hand the SG2 force [78] of Van Giai and Sagawa. The two forces were designed to fit ground state properties of spherical nuclei and nuclear matter properties but, in addition, the force SG2 gives a good description of Gamow Teller excitations in spherical nuclei [78]. Recently [156], these two forces and were applied to make a rather extensive study of isoscalar and isovector spin M1 excitations in deformed nuclei obtaining a good description of the available data, particularly with SG2. The parameters of these two interactions are given in Table 7.2.3. The corresponding HF energy density functional for an even-even nucleus has the form

$$\begin{aligned}
\mathcal{E}\left(\mathbf{r}\right) \;=\; & \sum_{st}\rho_{st}\sum_{s't'}\left\{\frac{1}{2}t_0\rho_{s't'}\left[1-\delta_{ss'}\delta_{tt'}+x_0\left(\delta_{ss'}-\delta_{tt'}\right)\right]\right. \\
& +\frac{1}{4}t_2\left(\tau_{s't'}+\frac{1}{4}\nabla^2\rho_{s't'}\right)\left[1+\delta_{ss'}\delta_{tt'}+x_2\left(\delta_{ss'}+\delta_{tt'}\right)\right] \\
& +\frac{1}{16}t_1\left(4\tau_{s't'}-3\nabla^2\rho_{s't'}\right)\left[1-\delta_{ss'}\delta_{tt'}+x_1\left(\delta_{ss'}-\delta_{tt'}\right)\right] \\
& +\frac{1}{12}t_3\rho^\alpha\rho_{s't'}\left[1-\delta_{ss'}\delta_{tt'}+x_3\left(\delta_{ss'}-\delta_{tt'}\right)\right]
\end{aligned}$$

$$+\frac{i}{2}W_0\nabla\cdot\mathbf{J}_{s't'}\left(1+\delta_{tt'}\right)\Big\}+\mathcal{E}_C\left(\mathbf{r}\right), \tag{7.20}$$

with $\mathcal{E}_C$ the Coulomb energy density

$$\mathcal{E}_C\left(\mathbf{r}\right)=e^2\frac{1}{2}\int d\mathbf{r}'\frac{\rho_p\left(\mathbf{r}'\right)\rho_p\left(\mathbf{r}\right)}{\left|\mathbf{r}-\mathbf{r}'\right|}-\frac{3}{4}e^2\rho_p\left(\mathbf{r}\right)\left[\frac{3}{\pi}\rho_p\left(\mathbf{r}\right)\right]^{1/3}. \tag{7.21}$$

The spin-isospin (st) components of the nucleon, kinetic energy, and magnetization densities are

$$\rho_{st}\left(\mathbf{r}\right)=\sum_i v_i^2\left|\phi_i\left(\mathbf{r},s,t\right)\right|^2, \tag{7.22}$$

$$\tau_{st}\left(\mathbf{r}\right)=\sum_i v_i^2\left|\nabla\phi_i\left(\mathbf{r},s,t\right)\right|^2, \tag{7.23}$$

$$\mathbf{J}_{st}\left(\mathbf{r}\right)=\sum_{i,s'} v_i^2\phi_i^*\left(\mathbf{r},s',t\right)\left(-i\nabla\times\sigma\right)\phi_i\left(\mathbf{r},s,t\right), \tag{7.24}$$

with

$$\rho_t=\sum_s\rho_{st}, \tag{7.25}$$

$$\rho=\sum_{t=p,n}\rho_t, \tag{7.26}$$

and similarly for τ and $\mathbf{J}$. The single-particle energies ϵ_i and wave functions are obtained from the HF equations

$$\frac{\delta\mathcal{E}}{\delta\phi_i^*}=\epsilon_i\phi_i. \tag{7.27}$$

The HF theory gives a single solution which is the Slater determinant of the lowest energy. To allow for shape coexistence one has to extend the theory to a constrained HF theory [71]. Minimization of the HF energy under the constraint of holding the nuclear deformation fixed is carried out over a range of deformations. When more than one local minimum occurs for the total energy as a function of deformation, shape coexistence results. The energy surfaces as a function of deformation are obtained by this procedure including a quadratic quadrupole constraint [71].

Following Bertsch and Tsai [18] the particle-hole interaction consistent with the HF mean field can be obtained as

$$V_{ph}=\frac{1}{16}\sum_{sts't'}\left[1+(-1)^{s-s'}\sigma_1\cdot\sigma_2\right]\left[1+(-1)^{t-t'}\tau_1\cdot\tau_2\right]\frac{\delta^2\mathcal{E}}{\delta\rho_{st}\left(\mathbf{r}_1\right)\delta\rho_{s't'}\left(\mathbf{r}_2\right)}. \tag{7.28}$$

This gives a local interaction that can be put in the Landau-Migdal form [121]. For the study of β decay the relevant residual interactions are the isospin contact forces generating the allowed Fermi transitions $(\Delta L = 0, \Delta S = 0, \Delta I^\pi = 0^+)$

$$V_F(12) = \chi_F \left(t_1^+ t_2^- + t_1^- t_2^+ \right), \tag{7.29}$$

and the spin-isospin contact forces generating the allowed Gamow Teller transitions $(\Delta L = 0, \Delta S = 1, \Delta I^\pi = 1^+)$

$$V_{GT}(12) = \chi_{GT} \, \sigma_1 \cdot \sigma_2 \left(t_1^+ t_2^- + t_1^- t_2^+ \right), \tag{7.30}$$

where the used convention is $t^+ |p\rangle = |n\rangle, \ t^- |n\rangle = |p\rangle$. The latter (V_{GT}) is the charge changing component of the spin-spin interaction H_{SS}

$$H_{SS} = \frac{K_S}{4A} \left[(1+q) \, \mathbf{s}_1 \cdot \mathbf{s}_2 + (1-q) \, \mathbf{s}_1 \cdot \mathbf{s}_2 \, \tau_1 \cdot \tau_2 \right], \tag{7.31}$$

considered in Refs. [155, 156] for the study of spin $M1$ excitations. Not allowed transitions $(\Delta L > 0)$ produce strengths which are orders of magnitude smaller than the allowed ones $(\Delta L = 0)$ and will not be considered.

The coupling strengths result after the functional differentiation of Eqs. (7.20) and (7.28-7.30), assuming symmetric uniform nuclear matter and averaging over the nuclear volume V

$$\chi_F = \frac{3}{4\pi R^3} \left(-\frac{1}{2} \right) \left\{ t_0 (1+2x_0) - \frac{1}{2} k_F^2 \left[t_2 (1+2x_2) - t_1 (1+2x_1) \right] + \frac{1}{6} t_3 \rho^\alpha (1+2x_3) \right\}, \tag{7.32}$$

$$\chi_{GT} = \frac{3}{4\pi R^3} \left(-\frac{1}{2} \right) \left\{ t_0 + \frac{1}{2} k_F^2 (t_1 - t_2) + \frac{1}{6} t_3 \rho^\alpha \right\}, \tag{7.33}$$

where R is the nuclear radius and k_F the Fermi momentum $k_F = \left(3\pi^2 \rho/2 \right)^{1/3}$. These coupling strengths are related to the familiar Landau-Migdal parameters F_0' and G_0' (see for instance [78]) by

$$\chi_F = \frac{2F_0'}{V N_0} \, , \, \chi_{GT} = \frac{2G_0'}{V N_0}, \tag{7.34}$$

where $V = 4\pi R^3/3$ and $N_0 = \left(2m^\star k_F / \hbar^2 \pi^2 \right)$, with $m^\star$ the effective mass. For completeness the values of χ_F and χ_{GT} are also given in Tables.

Table 7.2: Parameters of the Skyrme forces SG2 and Sk3: t_0[MeVfm^3], t_1[MeVfm^5], t_2[MeVfm^5], t_3[MeV fm^6], W[MeVfm^5], x_0, x_1, x_2, x_3, and α.

	t_0	t_1	t_2	t_3	W	x_0	x_1	x_2	x_3	$\frac{1}{\alpha}$
SG2	-2645.0	340.0	-41.9	15595.0	105.0	0.09	-0.0588	1.425	0.06044	6.0
Sk3	-1128.75	395.0	-95.0	14000.0	120.0	0.45	0.0	0.0	1.0	1.0

Table 7.3: Strengths of the separable isospin χ_F[MeV] and spin-isospin χ_{GT} [MeV] residual interactions obtained from Eqs.(7.32) and (7.33) , respectively.

	χ_F	χ_{GT}
SG2	0.69	0.48
Sk3	0.88	0.46

7.3   Appendix C

In deformed nuclei the short range pairing correlations play a very important role, namely the smooth behavior of the occupation probabilities close to the Fermi level involve non-zero amplitudes for the beta transitions. This pairing correlation are described within the BCS theory starting from the variational principle.

7.3.1   The BCS Hamiltonian

The BCS wave function for even-even nuclei:

$$|BCS> = \prod_{k>0}(u_k + v_k a_k^\dagger a_{\bar{k}}^\dagger)|->$$
(7.35)

where u_k and v_k represent variational parameters. The product runs only over half of the configuration space as indicated by $k > 0$. For each state $k > 0$ there exists another "conjugate" state $\bar{k} < 0$ and the states $k, \bar{k}$ generate the whole single-particle space. The product can be written more suggestive as:

$$|BCS> = |-> + \sum_{k>0}\frac{v_k}{u_k}a_k^\dagger a_{\bar{k}}^\dagger|-> + 1/2\sum_{k,k'>0}\frac{v_k v_{k'}}{u_k u_{k'}}a_k^\dagger a_{\bar{k}}^\dagger a_{k'}^\dagger a_{\bar{k'}}^\dagger|->$$
(7.36)

The v^2 and u^2 represent the probability that a certain pair state is $(k, \bar{k})$ is occupied or not occupied.

7.3.2   The BCS equations

The BCS Hamiltonian has the following form:

$$H = \sum_{k>0} \epsilon_k (a_k^\dagger a_k + a_{\bar{k}}^\dagger a_{\bar{k}}) - G \sum_{k,k'} a_k^\dagger a_{\bar{k}}^\dagger a_{\bar{k}'} a_{k'}. \qquad (7.37)$$

The Bogoliubov-Valatin transformation:

$$\begin{aligned}
\alpha_k^\dagger &= u_k a_k^\dagger - v_k a_{\bar{k}} \\
\alpha_{\bar{k}}^\dagger &= u_k a_{\bar{k}}^\dagger - v_k a_k.
\end{aligned} \qquad (7.38)$$

As long as the number of particles is not conserved and the hamiltonian doesn't commute with the particle number operator $\hat{N}$ it is necessary to add a new term:

$$H' = H - \lambda \hat{N}, \qquad (7.39)$$

where λ is a Lagrange multiplier (in realistical calculations its value gives the value of the Fermi level). The expectation value of H':

$$< BCS|H'|BCS > = 2 \sum_{k>0} (\tilde{\epsilon}_k v_k^2 + \frac{1}{2} G v_k^4) - \frac{\Delta}{G}, \qquad (7.40)$$

with the gap parameter δ

$$\Delta = G \sum u_k v_k, \qquad (7.41)$$

and

$$\tilde{\epsilon}_k = \epsilon_k - \lambda - G v_k^2. \qquad (7.42)$$

Here $G v_k^4$ and $G v_k^2$ are renormalization terms. The BCS equations are obtained by the variation of Eq. 7.40 with respect with the occupation probabilities

$$2\tilde{\epsilon}_k u_k v_k + \Delta(v_k^2 - u_k^2) = 0, \quad k > 0. \qquad (7.43)$$

The parameters u$_k$ and v$_k$ are given by the following relations

$$\begin{aligned}
u_k^2 &= \frac{1}{2}[1 + \frac{\epsilon_k - \lambda}{\sqrt{(\epsilon_k - \lambda)^2 - \Delta^2}}], \\
v_k^2 &= \frac{1}{2}[1 - \frac{\epsilon_k - \lambda}{\sqrt{(\epsilon_k - \lambda)^2 - \Delta^2}}],
\end{aligned} \qquad (7.44)$$

$$(7.45)$$

and the gap parameter

$$\Delta = \frac{G}{2} \sum_{k>0} \frac{\Delta}{\sqrt{(\epsilon_k - \lambda)^2 - \Delta^2}} \tag{7.46}$$

7.4 Appendix D

The independent particle models (shell model and more elaborated methods like Hartree-Fock or Hartree-Fock-Bogoliubov) can explain very adequately a series of excited states in the nuclear spectrum by models like p-h and pp excitations but their applicability fails to explain the high-energy 1^- expiations like giant dipole resonances. This excitations can be explained as a coherent participation of many nucleons together. This excitations fulfill the following criteria.

- Their electromagnetic transition probabilities have a collective strength such that they one or two orders of magnitude larger than the single particle transitions

- They show up in the entire spectra of the different nuclei over the whole periodic table

7.4.1 The TDA formalism

The first approximation where one can build correlations in the excited states in Tamm-Dancoff, the ground state remanding however unchanged. This complete neglect of the residual interaction in the ground state certainly influence the results. To remove this draw-back of TDA method one could think of retaining also the (2p-2h) components. This is not practicable since the matrices will became prohibitory large. One way out is the generalization of TDA which one takes instead of HF ground state another ground state where certain correlations are considered. In the shell model representation the ground state of the nuclei is given by:

$$|0> = C_0^0 + \sum_{mi} C_{mi}^0 a_m^\dagger a_i |HF> + 1/4 \sum_{mnij} C_{mn,ij}^0 a_m^\dagger a_n^\dagger a_i a_j |HF> + ... \tag{7.47}$$

and the excited state is given by

$$|\nu> = C_0^\nu + \sum_{mi} C_{mi}^\nu a_m^\dagger a_i |HF> + 1/4 \sum_{mnij} C_{mn,ij}^\nu a_m^\dagger a_n^\dagger a_i a_j |HF> + ... \tag{7.48}$$

In the shell model framework the coefficients $C_{mi}^0, C_{mn,ij}^0$ are close to zero. Also as long as there are no correlations in the ground state is sufficient for the excited state to be reduced to

$$|\nu> = \sum_{mi} C_{mi}^\nu a_m^\dagger a_i |HF> \tag{7.49}$$

The starting point is s is a set of eigenvalues of a given hamiltonian H.

$$H|\nu> = E_\nu |\nu> \tag{7.50}$$

It is possible to define operators $Q_\nu^\dagger$ and Q_ν in such a way that:

$$|\nu> = Q_\dagger^\nu \qquad and \qquad Q_\nu |0> = 0 \tag{7.51}$$

From the Schrodinger equation we get the equation of motion:

$$[H, Q_\nu^\dagger]|0> = (E_{nu} - E_0) Q_{nu}^\dagger |0> \tag{7.52}$$

Multiplying from left and right with an arbitrary state of the form $< 0|\delta Q$ one gets:

$$< 0|[\delta Q, [H, Q_\nu^\dagger]]|0> = (E_{nu} - E_0) < 0|[\delta Q, Q_{nu}^\dagger |0> \tag{7.53}$$

In the TDA case one can define the collective ph-operator Q_ν by the following formula:

$$Q_\nu^\dagger = \sum_{mi} C_{mi}^{nu} a_m^\dagger a_i \tag{7.54}$$

By this approximation one restricts to the space of 1p-1h excitation and the excitation energy is given by:

$$\sum_{nj} < HF|[a_i^\dagger a_m, [H, a_n^\dagger a_j]]|HF> C_{nj}^\nu = E_\nu^{TDA} C_{mi}^\nu \tag{7.55}$$

7.4.2   The RPA formalism

In the space of 2p-2h correlations, one can not only create a ph pair but also destroy one. In this case the most straight forward generalization of the operator has the following form:

$$Q_\nu^\dagger = \sum_{mi} X_{mi}^{nu} a_m^\dagger a_i - \sum_{mi} Y_{mi}^{nu} a_i^\dagger a_m \tag{7.56}$$

It is obvious in this case that apart of correlations on the level of excitations, the ground state correlations are also taken into account, as they can be destroyed. But

in this case the ground state is not the $|HF>$ state anymore and this is a very important point in this approximation. The ground state $|RPA>$ is defined in correlation with the RPA operator

$$Q_\nu |RPA >= 0 \qquad (7.57)$$

and it has a an explicit expression. The matrix elements X_{mi}, Y_{mi} are called forwards and backwards amplitudes. The set of equations (7.55) gives:

$$
\begin{aligned}
< RPA|[a_i^\dagger a_m, [H, Q_\nu^\dagger]]|RPA > &= \hbar\Omega_\nu < |[a_i^\dagger a_m, Q_\nu^\dagger]|RPA > \\
< RPA|[a_m^\dagger a_i, [H, Q_\nu^\dagger]]|RPA > &= \hbar\Omega_\nu < |[a_m^\dagger a_i, Q_\nu^\dagger]|RPA >
\end{aligned} \qquad (7.58)
$$

where $\hbar\Omega_\nu$ is the excitation energy of the state $|\nu>$. Unfortunately the expectation values of fermi operators are not so easy to calculate as long as the RPA ground state is not known. Therefore the main approximation in the RPA formalism consists in assuming that the correlated ground state doesn't differ so much from the HF ground state (so called *"quasi-boson approximation"*).

$$
\begin{aligned}
< RPA|[a_i^\dagger a_m, a_n^\dagger a_j]|RPA > &= \delta_{ij}\delta_{mn} - \delta_{mn} < RPA|a_j a_i^\dagger|RPA > \\
&\quad -\delta_{ij} < RPA|a_n^\dagger a_m|RPA > \\
&\simeq < HF|[a_i^\dagger a_m, a_n^\dagger a_j]|HF >= \delta_{ij}\delta_{mn} \quad (7.59)
\end{aligned}
$$

It is obvious that in the relation (7.59) the ph creation and annihilation operators obey the commutation relations for boson field operators. Equation (7.59), however, violates the Pauli principle because the terms coming from the commutator are neglected. This is another drawback of RPA equation. Within the quasi-boson approximation, the amplitudes have a very direct meaning, their absolute squares gives the probability of finding the states $a_m^\dagger a_i|0>$ and $a_i^\dagger a_m|0>$ in the excited state $|\nu>$, that is the ph and hp matrix elements of the transition density.

$$
\begin{aligned}
\rho_{mi}^\nu &= < 0|a_i^\dagger a_m|\nu > \simeq < HF|[a_i^\dagger a_m, Q_\nu^\dagger]|HF >= X_{mi}^\nu \\
\rho_{im}^\nu &= < 0|a_m^\dagger a_i|\nu > \simeq < HF|[a_m^\dagger a_i, Q_\nu^\dagger]|HF >= Y_{mi}^\nu
\end{aligned} \qquad (7.60)
$$

The matriceal form of the last equation is:

$$
\begin{pmatrix} \mathcal{A} & \mathcal{B} \\ \mathcal{B}^* & \mathcal{A}^* \end{pmatrix} \begin{pmatrix} X^\nu \\ Y^\nu \end{pmatrix} = \hbar\Omega^\nu \begin{pmatrix} 1 & 0 \\ 0 & -1 \end{pmatrix} \begin{pmatrix} X^\nu \\ Y^\nu \end{pmatrix}, \qquad (7.61)
$$

with $(X^\nu)_{mi} = X_{mi}^\nu$ and $(Y^\nu)_{mi} = Y_{mi}^\nu$ and:

$$
\begin{aligned}
\mathcal{A}_{minj} &= < [a_i^\dagger a_m[H, a_n^\dagger a_j]]HF >= (\epsilon_m - \epsilon_i)\delta_{mn}\delta_{ij} + \bar{v}_{mjin} \\
\mathcal{B}_{minj} &= - < [a_i^\dagger a_m[H, a_j^\dagger a_n]]HF >= \bar{v}_{mnij}.
\end{aligned} \qquad (7.62)
$$

In the last representation the matrix $\mathcal{A}$ is Hermitian and the matrix $\mathcal{B}$ is symmetrical. Equation (7.61) together with (7.62) is called the RPA equation. For $Y_{mi}^{\nu} = 0$ the results of TDA approximation are obtained. Concluding the backwards amplitudes $Y_{mi}^{\nu} = 0$ are the measure of the correlations in the ground state. To solve the RPA equation mean to get the energy of the excited states and, the RPA amplitudes. Technically speaking this can be done either by diagonalizing the matrices using a different numerical procedures (LU decomposition), for rather small basis (Lanchotz formalism...) for larger basis but with a cut-off in excitation energies. For larger bases (for example in deformed nuclei) the best solution is to treat the residual interaction as a separable interaction (it works pretty good for quadrupole-quadrupole interactions and for spin-isospin interaction as well) and to solve the dispersion equation. As a conclusion, in general the main problem in RPA is the quasibosonic-approximation which violates the Pauli principle and also the ground state correlations which are pretty often overestimate. But the limits of applicability can be fixed just numerically. It has been proved that it works for very collective states, where basically each single particle component has a rather small probability to be excited alone, the violation of the Pauli principle can be neglected and the forwards amplitudes have the same order of magnitude.On the other hand, the amplitudes Y_{mi}^{ν} shall be small compared with X_{mi}^{ν} because they describe the ground state correlations. If their values will be large the replacement of the RPA ground state with the HF one is not justified.

7.5   Appendix E

7.5.1   Pairing gaps and charge radii

Table 7.4: Pairing gaps for protons and neutrons Δ_p, Δ_n (MeV) and charge radii r_c (fm).

Nucleus	Δ_p	Δ_n	exp r_c [205]	r_c Sk3	r_c SG2	r_c [113]
^{48}Ca	2.18	1.68	3.4736(8)	3.586	3.549	3.471
^{48}Ti	1.90	1.56	3.592	3.628	3.597	3.571
^{76}Ge	1.56	1.54	4.127(8)	4.130	4.083	4.057
^{76}Se	1.75	1.71	4.152(9)	4.170-4.180	4.113-4.143	4.119
^{82}Se	1.41	1.54	4.122(8)	4.204	4.159	4.131
^{82}Kr	1.72	1.64	4.1921(11)	4.196	4.196	4.173
^{96}Zr	1.53	0.84	4.3508(12)	4.433-4.443	4.342-4.389	4.376
^{96}Mo	1.53	1.03	4.377(10)	4.448-4.457	4.369-4.388	4.381
^{100}Mo	1.60	1.36	4.447(10)	4.516	4.439-4.466	4.448
^{100}Ru	1.55	1.30	4.453	4.516	4.457	4.449
^{116}Cd	1.47	1.37	4.625	4.703-4.715	4.653	4.643
^{116}Sn	1.77	1.20	4.625	4.709-4.753	4.702	4.609
^{128}Te	1.13	1.28	4.735	4.803-4.805	4.746	4.732
^{128}Xe	1.32	1.27	4.776	4.836-4.839	4.782-4.786	4.778
^{130}Te	1.06	1.18	4.742	4.812-4.816	4.750	4.739
^{130}Xe	1.31	1.25	4.783	4.845-4.846	4.796-4.801	4.784
^{136}Xe	0.98	1.44	4.799	4.878	4.815	4.804
^{136}Ba	1.27	1.03	4.833	4.902	4.847	4.837
^{150}Nd	1.23	1.05	5.047	5.114	5.055	5.046
^{150}Sm	1.44	1.19	5.047	5.108	5.046	5.047

7.5.2   Theoretical and experimental nuclear deformations

Table 7.5: Theoretical and experimental β values

Nucl.	Exp		Theory			
	Ref.[147]	Ref.[148]	(Sk3)	(SG2)	Ref.[113]	Ref.[126]
^{48}Ca	0.000	0.101(17)	-0.002	-0.001	0.000	0.000
^{48}Ti	+0.17(10)	0.269(7)	-0.002	-0.003	-0.009	0.000
^{76}Ge	+0.095(30)	0.2623(39)	0.161	0.157	0.157	0.143
^{76}Se	+0.163(33)	0.3090(37)	-0.181 [+0.157]	-0.191[+0.049]	-0.244	-0.241
^{82}Se	+0.104(32)	0.1944(26)	0.126	0.150	0.133	0.154
^{82}Kr		0.2022(45)	0.106	0.103	0.119	0.071
^{96}Zr		0.081(16)	0.207 [-0.167]	0.016 [+0.147]	0.223	0.217
^{96}Mo	+0.068(27)	0.1720(16)	0.147 [-0.164]	-0.006 [+0.119]	0.167	0.080
^{100}Mo	+0.139(30)	0.2309(22)	0.236	0.167 [-0.191]	0.253	0.244
^{100}Ru	+0.136(22)	0.2172(22)	0.175	0.157	0.194	0.161
^{116}Cd	+0.113(11)	0.1907(34)	0.206 [-0.207]	0.209	-0.258	-0.241
^{116}Sn	+0.043(10)	0.1118(16)	0.264 [-0.134]	0.251 [-0.034]	0.003	0.000
^{128}Te	+0.011(10)	0.1363(11)	-0.088 [+0.102]	0.094 [-0.091]	-0.002	0.000
^{128}Xe		0.1837(49)	0.148 [-0.122]	0.150 [-0.133]	0.160	0.143
^{130}Te	+0.035(23)	0.1184(14)	-0.076 [+0.051]	-0.039 [+0.066]	0.032	0.000
^{130}Xe		0.169(6)	0.108 [-0.098]	0.161 [-0.132]	0.128	-0.113
^{136}Xe		0.086(19)	0.001	0.016	-0.001	0.000
^{136}Ba		0.1242(8)	0.009	0.070	-0.002	0.000
^{150}Nd	+0.367(86)	0.2848(21)	0.266	0.271	0.221	0.243
^{150}Sm	+0.230(30)	0.1931(22)	0.207	0.203	0.176	0.206

7.6   Appendix F

The single-particle states are calculated by solving the Schrödinger equation with the deformed axially symmetric Woods-Saxon potential, which parameterization is given in Ref. [186]. They are characterized by their energy ε_τ, parity π_τ and by the projection Ω_τ ($\tau = p, n$) of the full angular momentum on the nuclear symmetry axis. The notation $|p\rho_p >$ and $|n\rho_n >$ is for protons and neutrons, respectively. $|\tau\rho_\tau >$ represents proton ($\tau = p$) or neutron ($\tau = n$) state with quantum numbers Ω_τ and π_τ. ρ_τ is the sign of the angular momentum projection Ω ($\rho_\tau = \pm 1$). The intrinsic states are twofold degenerate. The states with Ω_τ and $-\Omega_\tau$ have the same energy as consequence of the time reversal invariance. ρ_τ is taken to be positive for states and negative for time reversal states.

7.6.1   The single-particle matrix elements of the $\tau^+ \sigma_K$ operator

In order to solve the Schrödinger equation the eigenfunctions of a deformed symmetric harmonic oscillator are used as a basis for the diagonalization of the mean-field Hamiltonian [41]. These states are completely determined by a principal set of quantum numbers $(N, n_z, \Lambda, \Omega)$, where $N = n_x + n_z$, $n_x = 2n_r + |\Lambda|$ and $\Omega = \Lambda + \Sigma$. $n_z - 1$ and $n_x - 1$ are number of nodes of the basis functions in the z-direction and r-direction, respectively. Λ and Σ are the projections of the orbital and spin angular momentum on the symmetry axis z. The explicit form of single-particle harmonic oscillator wave functions in cylindrical coordinates (r, z, ϕ) can be found, e.g., in Ref. [133]. For a given shape of the nuclear surface, the shape of the deformed harmonic oscillator is automatically chosen in a way suitable for obtaining good accuracy with a smallest number of basis functions [41]. The deformation dependent cutt-off is chosen in such way as to assure numerical stability of the results. In our calculation we use 11 major shells.

In cylindrical coordinates the eigenfunctions of states and time-reversed states in deformed Woods-Saxon potential are expressed as follows:

$$|\tau\rho_\tau = +1 > \;\; = \;\; \sum_{Nn_z}[b^{(+)}_{Nn_z\Omega_\tau}|N, n_z, \Lambda_\tau, \Omega_\tau = \Lambda_\tau + 1/2 > +$$

$$b^{(-)}_{Nn_z\Omega_\tau}|N, n_z, \Lambda_\tau + 1, \Omega_\tau = \Lambda_\tau + 1 - 1/2 >] \quad (7.63)$$

and

$$|\tilde{\tau}\rho_\tau = +1 > \;\; = \;\; |\tau\rho_\tau = -1 >= \sum_{Nn_z}[b^{(+)}_{Nn_z\Omega_\tau}|N, n_z, -\Lambda_\tau, \Omega = -\Lambda_\tau - 1/2 > -$$

$$b^{(-)}_{Nn_z\Omega_\tau}|N, n_z, -\Lambda_\tau - 1, \Omega_\tau = -\Lambda_\tau - 1 + 1/2 >] \qquad (7.64)$$

with $\Lambda \geq 0$. $\sim$ indicates time reversal states.

The single-particle matrix elements of the $\tau^+\sigma_K$ operator are given by

$$< p\rho_p|\tau^+\sigma_{K=0}|n\rho_n > \quad = \quad \delta_{\Omega_p\Omega_n}\rho_p \sum_{Nn_z}[b^{(+)}_{Nn_z\Omega_p}b^{(+)}_{Nn_z\Omega_n} - b^{(-)}_{Nn_z\Omega_p}b^{(-)}_{Nn_z\Omega_n}], \qquad (7.65)$$

$$< p\rho_p|\tau^+\sigma_{K=+1}|n\rho_n > \quad = \quad -\sqrt{2}\delta_{\Omega_p\Omega_n+1}\sum_{Nn_z} b^{(+)}_{Nn_z\Omega_p}b^{(-)}_{Nn_z\Omega_n} \quad for \quad \rho_p = \rho_n = +1,$$

$$= \quad +\sqrt{2}\delta_{\Omega_p\Omega_n+1}\sum_{Nn_z} b^{(-)}_{Nn_z\Omega_p}b^{(+)}_{Nn_z\Omega_n} \quad for \quad \rho_p = \rho_n = -1,$$

$$= \quad -\sqrt{2}\delta_{\Omega_p\frac{1}{2}}\delta_{\Omega_n-\frac{1}{2}}\sum_{Nn_z} b^{(+)}_{Nn_z\Omega_p}b^{(+)}_{Nn_z\Omega_n} \quad for \quad \rho_p = +1, \ \rho_n = (7.66)$$

$$< p\rho_p|\tau^+\sigma_{K=-1}|n\rho_n > \quad = \quad \sqrt{2}\delta_{\Omega_p\Omega_n-1}\sum_{Nn_z} b^{(-)}_{Nn_z\Omega_p}b^{(+)}_{Nn_z\Omega_n} \quad for \quad \rho_p = \rho_n = +1,$$

$$= \quad -\sqrt{2}\delta_{\Omega_p\Omega_n-1}\sum_{Nn_z} b^{(+)}_{Nn_z\Omega_p}b^{(-)}_{Nn_z\Omega_n} \quad for \quad \rho_p = \rho_n = -1,$$

$$= \quad \sqrt{2}\delta_{\Omega_p-\frac{1}{2}}\delta_{\Omega_n\frac{1}{2}}\sum_{Nn_z} b^{(+)}_{Nn_z\Omega_p}b^{(+)}_{Nn_z\Omega_n} \quad for \quad \rho_p = +1, \ \rho_n = (7.67)$$

The overlap of the proton and neutron single particle states of the initial (A, Z) and final $(A, Z + 2)$ nuclei are calculated by assuming that the corresponding sets of basis wave functions do not differ significantly each from other. Then

$$< p_f\rho_{p_f}|p_i\rho_{p_i} > \quad = \quad \delta_{\Omega_{p_f}\Omega_{p_i}} \sum_{Nn_z}[b^{(+)}_{Nn_z\Omega_{p_f}}b^{(+)}_{Nn_z\Omega_{p_i}} - b^{(-)}_{Nn_z\Omega_{p_f}}b^{(-)}_{Nn_z\Omega_{p_i}}],$$

$$< n_f\rho_{n_f}|n_i\rho_{n_i} > \quad = \quad \delta_{\Omega_{n_f}\Omega_{n_i}} \sum_{Nn_z}[b^{(+)}_{Nn_z\Omega_{n_f}}b^{(+)}_{Nn_z\Omega_{n_i}} - b^{(-)}_{Nn_z\Omega_{n_f}}b^{(-)}_{Nn_z\Omega_{n_i}}]. \quad (7.68)$$

The index i (f) denotes that proton and neutron single particle states are defined with respect to the initial (final) nucleus.

7.6.2   Analytical expression for the overlap factor

As a consequence of considered many-body approximations the two sets of intermediate nuclear states generated from the initial and final ground states are not identical within the QRPA theory. Thus it is necessary to introduce the overlap factor of these states, which can be expressed with the help of intrinsic phonon operators as follows:

$$< 1(K), m_f|1(K), m_i > = < rpa_f|\ Q^{m_f}_K\ Q^{m_i\dagger}_K\ |rpa_i > . \qquad (7.69)$$

Here, the index i (f) indicates that the excited states of the nucleus are defined with respect to the initial (final) nuclear ground state $|rpa_i > (|rpa_f >)$.

In order to evaluate $< 1(K), m_f | 1(K), m_i >$ the phonon creation operator $Q_K^{m_i \dagger}$ is expressed in terms of creation and anninhilation phonon operators associated with the final nucleus.

$$Q_K^{m_i \dagger} = \sum_{m_f} (a_{m_i m_f} Q_K^{m_f \dagger} + b_{m_i m_f} \tilde{Q}_K^{m_f}). \qquad (7.70)$$

The coefficients of expansion $a_{m_i m_f}$ and $b_{m_i m_f}$ will be determined below. By inserting Eq. (7.70) into Eq. (7.69) one gets

$$
\begin{aligned}
< 1(K), m_f | 1(K), m_i > &= \sum_{m'_f} [< rpa_f | Q_K^{m_f} Q_K^{m'_f \dagger} | rpa_i > a_{m_i m'_f} \\
&\quad + < rpa_f | Q_K^{m_f} Q_{-K}^{m'_f} | rpa_i > b_{m_i m'_f}] \\
&\approx a_{m_i m'_f} < BCS_f | BCS_i > .
\end{aligned}
\qquad (7.71)
$$

Here, the overlap matrix element between the final ground state is neglected and also the two-phonon state generated from the initial nucleus, which is considered to be small and should be not related with the studied quantity. In addition, the overlap of initial and final RPA ground state is approximated with the BCS ones. Thus the overlap factor of the intermediate nuclear states generated from the initial and final ground states is proportional to the overlap of initial and final BCS vacua.

The next step is the calculation of $a_{m_i m'_f}$ and $b_{m_i m'_f}$ coefficients. The quasiparticle creation and anninhilation operators $(a^{(i) \dagger}, a^{(i)})$ $[(a^{(f) \dagger}, a^{(f)})]$ of the initial [final] nucleus are connected with the particle creation and annihilation operators $(c^{(i) \dagger}, c^{(i)})$ $[(c^{(f) \dagger}, c^{(f)})]$ by the BCS transformation. In addition there is a unitary transformation between particle operators associated with initial and final nuclei

$$
\begin{aligned}
c_{\tau \rho_\tau}^{(i) \dagger} &= \sum_{\tau' \rho_{\tau'}} < \tau \rho_\tau | \tau' \rho_{\tau'} > c_{\tau' \rho_{\tau'}}^{(f) \dagger} \\
\tilde{c}_{\tau \rho_\tau}^{(i)} &= \sum_{\tau' \rho_{\tau'}} < \tau \rho_\tau | \tau' \rho_{\tau'} > \tilde{c}_{\tau' \rho_{\tau'}}^{(f)}
\end{aligned}
\qquad (7.72)
$$

The overlap factors of the single particle wave functions of the initial and final nuclei $< \tau \rho_\tau | \tau' \rho'_{\tau'} >$ is given explicitly in the Appendix A. The above mentioned transformations allow us, by using the quasiboson approximation, to rewrite the boson operators of the initial nucleus with the help of the boson operators of the final nucleus:

$$
\begin{aligned}
A^{(i) \dagger}(l, K) &= \sum_{l'} [\mathcal{R}_{ll'} A^{(f) \dagger}(l', K) + \mathcal{S}_{ll'} A^{(f)}(\bar{l}', K)], \\
A^{(i)}(\bar{l}, K) &= \sum_{l'} [\mathcal{R}_{ll'} A^{(f)}(\bar{l}', K) - \mathcal{S}_{ll'} A^{(f) \dagger}(l', K)].
\end{aligned}
\qquad (7.73)
$$

Assuming the definition of the quasiparticle pairs operator in Eq. (3.44) the factors $\mathcal{R}_{ll'}$ and $\mathcal{S}_{ll'}$ can be expressed as

$$
\begin{aligned}
\mathcal{R}_{ll'} &= \; <p\rho_p|p'\rho_{p'}> (u_p^{(i)}u_{p'}^{(f)} + v_p^{(i)}v_{p'}^{(f)}) <n\rho_n|n'\rho_{n'}> (u_n^{(i)}u_{n'}^{(f)} + v_n^{(i)}v_{n'}^{(f)}), \\
\mathcal{S}_{ll'} &= \; <p\rho_p|p'\rho_{p'}> (u_p^{(i)}v_{p'}^{(f)} - u_p^{(i)}v_{p'}^{(f)}) <n\rho_n|n'\rho_{n'}> (u_n^{(i)}v_{n'}^{(f)} - u_n^{(i)}v_{n'}^{(f)})
\end{aligned}
\tag{7.74}
$$

It is worthwhile to notice that in the limit initial and final states are indentical $\mathcal{R}_{ll'} = 1$ and $\mathcal{S}_{ll'} = 0$.

By inserting Eq. (7.73) into the expression for the phonon operator of the initial nucleus [see Eq. (3.46)] and by exploiting the relations

$$
\begin{aligned}
A^{(f)\dagger}(l,K) &= \sum_{m_f}[X_{i,K}^{m_f}Q_K^{m_f\dagger} + Y_{i,K}^{m}\tilde{Q}_K^{m}], \\
A^{(f)}(\bar{l},K) &= \sum_{m_f}[X_{i,K}^{m_f}\tilde{Q}_K^{m_f} + Y_{i,K}^{m_f}Q_K^{m_f\dagger}],
\end{aligned}
\tag{7.75}
$$

we find [170]

$$
\begin{aligned}
a_{m_im_f} &= \sum_{ll'}[X_{l'K}^{m_f}\mathcal{R}_{l'l}X_{lK}^{m_i} - Y_{l'K}^{m_f}\mathcal{R}_{l'l}Y_{lK}^{m_i} \\
&\quad + Y_{l'K}^{m_f}\mathcal{S}_{l'l}X_{lK}^{m_i} - Y_{l'K}^{m_f}\mathcal{S}_{l'l}Y_{lK}^{m_i}].
\end{aligned}
\tag{7.76}
$$

By neglecting the terms proportional to $\mathcal{S}_{ll'}$ due to their smallness we end up with the overlap factor of the intermediate nuclear states given in Eq. (3.62).

The overlap factor of the initial and final BCS vacua can be written as product of proton and neutron BCS overlap factors for a given anular momentum projection quantum number Ω:

$$
\begin{aligned}
<BCS_f|BCS_i> &= \; <BCS_f(p)|BCS_i(p)><BCS_f(n)|BCS_i(n)> \\
&= \prod_{\Omega_p} <BCS_f(\Omega_p)|BCS_i(\Omega_p)> \prod_{\Omega_n} <BCS_f(\Omega_n)|BCS_i(\Omega_n)>
\end{aligned}
\tag{7.77}
$$

where

$$
<BCS_f(\Omega)|BCS_i(\Omega)> = \; <|\prod_{k=1}^{N_\Omega}\left(u_k^{(f)} + v_k^{(f)}c_{\bar{k}}^{(f)}c_k^{(f)}\right) \prod_{l=1}^{N_\Omega}\left(u_l^{(i)} + v_l^{(i)}c_l^{(i)\dagger}c_{\bar{l}}^{(i)\dagger}\right)|> .
\tag{7.78}
$$

N_Ω is the number of single particle states with the same value of quantum number Ω. The same model space for protons and neutrons is assumed. By a direct calculation of the above matrix element one finds

$$
<BCS_f(\Omega)|BCS_i(\Omega)> = \prod_{k=1}^{N_\Omega}u_k^{(f)} \prod_{l=1}^{N_\Omega}u_l^{(f)}
$$

$$+ \quad \sum_{m_1,n_1=1}^{N_\Omega} v_{m_1}^{(f)} v_{n_1}^{(i)} \left(D^{(1)}(m_1;n_1) \right)^2 \prod_{k=1}^{N_\Omega(m_1)} u_k^{(f)} \prod_{l=1}^{N_\Omega(n_1)} u_l^{(i)}$$

$$+ \quad \sum_{m_1,m_2,n_1,n_2=1}^{N_\Omega} v_{m_1}^{(f)} v_{m_2}^{(f)} v_{n_1}^{(i)} v_{n_2}^{(i)} \left(D^{(2)}(m_1,m_2;n_1,n_2) \right)^2 \prod_{k=1}^{N_\Omega(m_1,m_2)} u_k^{(f)} \prod_{l=1}^{N_\Omega(n_1,n_2)} u_l^{(i)}$$

$$+ \quad \cdots \quad + \quad \left(D^{(N_\Omega)}(1,2,...,N_\Omega;1,2,..,N_\Omega) \right)^2 \prod_{k=1}^{N_\Omega} v_k^{(f)} \prod_{l=1}^{N_\Omega} v_l^{(i)}. \tag{7.79}$$

Here, $\prod_{k=1}^{N_\Omega(m_1,m_2)}$ means that index k runs the values from 1 to N_Ω except the values $k = m_1$ and $k = m_2$ ($1 \le m_1 \le N_\Omega$ and $1 \le m_2 \le N_\Omega$). $D^r(m_1,m_2,...,m_r;n_1,n_2,...,n_r)$ denotes the determinant of matrix of rank r constructed of elements of the unitary matrix of the transformation between the initial and final single particle states with row indices $m_1, m_2, ..., m_r$ and column indices $n_1, n_2, ..., n_r$. It is worthwhile to notice that by replacing all determinants in Eq. (7.79) with unity, i.e. the matrix of the transformation between the single particles associated with both nuclei is just unity matrix, we obtain a compact expression [90]

$$< BCS_f(\Omega)|BCS_i(\Omega) >= \prod_{k=1}^{N_\Omega} (u_k^{(f)} u_k^{(i)} + v_k^{(f)} v_k^{(i)}). \tag{7.80}$$

However, this approximation is not justified and can lead to a significant inaccuracy in the calculation of $M_{GT}^{2\nu}$ especially if there is a strong difference in deformations of the intial and final nuclei.

7.6.3   The BCS and RPA overlap factors

Table 7.6: Three sets of nuclear structure input parameters (A, B, and C) for which the calculated nuclear matrix elements $M_{GT}^{2\nu}$ reproduces the experimental $2\nu\beta\beta$-decay half-life of ^{76}Ge. v.o.f. denotes overlap factor of the initial and final BCS vacua.

par. set	mean field of ^{76}Ge			mean field of ^{76}Se			v.o.f.	H_{int}		g_A	$M_{GT}^{2\nu}$
	Def.	Pairing		Def.	Pairing						
	β_2	Δ_p MeV	Δ_n MeV	β_2	Δ_p MeV	Δ_n MeV		χ MeV	κ MeV		MeV^{-1}
A	0.0	1.561	1.535	0.0	1.751	1.710	0.842	0.25	0.060	1.25	0.138
B	0.10	1.561	1.535	0.266	1.751	1.710	0.403	0.25	0.028	1.25	0.138
C	0.10	1.561	1.535	0.216	1.751	1.710	0.587	0.25	0.028	1.00	0.216

Bibliography

[1] C. E. Aalseth et al., Phys. Rev. C **59**, 2108 (1999).

[2] E. G. Adelberger and W. C. Haxton, Ann. Rev. Nucl. Part. Sci. **35**, 501 (1985).

[3] B.D. Anderson, T. Chittrakarn, A.R. Baldwin, C. Lebo, R. Madey, P.C. Tandy, J.W. Watson, B.A. Brown and C.C. Foster, Phys. Rev. C **31** (1985) 1161.

[4] H. Akimune, H. Ejiri, M. Fujiwara, I. Daito, T. Inomata, R. Hazama, A. Tamii, H. Toyokawa, M. Yosoi, Phys. Lett. **B394** (1997) 23.

[5] W.P. Alford, R.L. Helmer, R. Abegg, A. Celler, D. Frekers, P. Green, O. Hausser, R. Henderson, K. Hicks, K.P. Jackson, R. Jeppesen, C.A. Miller, A. Trudel, M. Vetterli, S. Yen, R. Pourang, J. Watson, B.A. Brown and J. Engel, Nucl. Phys. **A514** (1990) 49.

[6] R. Arnold et al, Z. Phys. **C72**, 239 (1996).

[7] R. Arnold et al., Nucl. Phys. **A636**, 209 (1998).

[8] G. Audi and A.H. Wapstra, Nucl. Phys. A **595** (1995) 409; G. Audi, O. Bersillon, J. Blachot, and A.H. Wapstra, Nucl. Phys. A **624** (1997) 1.

[9] N. Auerbach, D.C. Zheng, L. Zamick and B.A. Brown, Phys. Lett. B **304** (1993) 17; D. Troltenier, J.P. Draayer and J.G. Hirsch, Nucl. Phys. A **601** (1996)89.

[10] A. Balysh et al., Phys. Rev. Lett. **77**, 5186 (1996).

[11] S. Balraj, Nucl. Data Sheets 74 (1995) 63.

[12] A. S. Barabash , Phys. Lett. **B216**, 257 (1989).

[13] A. S. Barabash et al. , Phys. Lett. **B345**, 408 (1995).

[14] A.S. Barabash, Czech. J. Phys. 52 (2002) 567.

[15] V. Barger and K. Whisnant, Phys. Lett. **B456**, 194 (1999).

[16] L. Baudis et al., Phys. Rev. Lett. **83**, 41 (1999).

[17] M. Beiner, H. Flocard, N. Van Giai, and P. Quentin, Nucl. Phys. A **238**, 29 (1975).

[18] G.F. Bertsch and S.F. Tsai, Phys. Rep. 18 (1975) 127.

[19] T. Bernatowicz et al., Phys. Rev. Lett. **69**, 2341 (1992).

[20] M. Beck et al., Phys. Rev. Lett. **70**, 2853 (1993).

[21] S.M. Bilenky, C. Giunti, W. Grimus, B. Kayser, and S.T. Petcov, Phys. Lett. B 465 (1999) 193; H.V. Klapdor-Kleingrothaus, H. Päs, A.Y. Smirnov, Phys. Rev. D 63 (2001) 073005.

[22] S. M. Bilenky et al., hep-ph/9907234.

[23] A. Bobyk, W.A. Kaminski, P. Zareba, Nucl. Phys. A **669**, 221 (2000); P. Zareba, PhD thesis, 2000, unpublished.

[24] D. Bogdan, A. Faessler, A. Petrovici, and S. Holan, Phys. Lett. B 150 (1985) 29.

[25] J. Beacom and P. Vogel, Phys. Rev. Lett. **83**, 5222 (1999).

[26] A. Bohr and B. Mottelson, *Nuclear Structure* (Benjamin, New York, 1975).

[27] Buchmüller W, Rückl R and Wyler D, Phys. Lett. **B191**, 442 (1987)

[28] F. Boehm and P. Vogel, *Physics of Massive Neutrinos* Cambridge University Press, Cambridge, 1992 (Second Edition).

[29] C. Caso et al, Eur. Phys. J. **3**, 1 (1998).

[30] L. De Braeckeleer et al, preprint, September 1999.

[31] D. O. Caldwell and R. N. Mohapatra, Phys. Rev. D**48**, 3259 (1993).

[32] E. Caurier, A. Poves, and A. P. Zuker, Phys. Lett. **B252**, 13 (1990).

[33] E. Caurier, F. Nowacki, A. Poves, and J. Retamosa, Phys. Rev. Lett. **77**, 1954 (1996), and E. Caurier, private communication.

[34] D. Cha, Phys. Rev. C **27**, 2269 (1987).

[35] M.K. Cheoun, A. Bobyk, A. Faessler, F. Šimkovic, G. Teneva, Nucl. Phys. A **561**, 74 (1993); Nucl. Phys. A **564**, 329 (1993); M.K. Cheoun, A. Faessler, F. Šimkovic, G. Teneva, and A. Bobyk, Nucl. Phys. **A587**, 301 (1995).

[36] Y. Chikashige, R. N. Mohapatra and R. D. Peccei, Phys. Rev. Lett, **45**, 1926 (1980).

[37] Y.Chikashige ,R. N. Mohapatra and R.D. and Peccei, Phys.Lett, **B98**, 265 (1981)

[38] O. Civitarese, A. Faessler, and T. Tomoda, Phys. Lett. B **194**, 11 (1987).

[39] O. Civitarese, and M. Reboiro, Phys. Rev. C **56**, 1179 (1997); O. Civitarese, M. Reboiro, and P. Vogel, Phys. Rev. C **56**, 1840 (1997).

[40] H.T.Chen, A.L. Goodman, Phys. Lett. **B24**, 257 (1967).

[41] J. Damgaard, H.C. Pauli, V.V. Pashkevich, and V.M. Strutinski, Nucl. Phys. A 135 (1969) 432.

[42] F. A. Danevich et al., Nucl. Phys. **A643**, 317 (1998).

[43] D.S. Delion, J. Dukelsky and P. Schuck, Phys. Rev. **C 55** , 2340 (1997).

[44] A. De Silva et al., Phys. Rev. C **56**, 2451 (1997).

[45] B.M. Dixit, P.K. Rath, and P.K. Raina, Phys. Rev. C 65 (2002) 034311.

[46] J. Dobaczewski, I. Hamamoto, W. Nazarewicz, and J.A. Sheikh, Phys. Rev. Lett. **72**, 981 (1994).

[47] J. Engel, M. Bender, J. Dobaczewski, W. Nazarewicz, and R. Surnam, Phys. Rev. C **60** (1999) 014302; M. Bender, J. Dobaczewski, J. Engel, and W. Nazarewicz, Phys. Rev. C **65** (2002) 054322.

[48] J. Dobeš, Phys. Lett. B **413**, 239 (1997); J. Dobeš, S. Pittel, Phys. Rev. C **57**, 688 (1998).

[49] M. Doi, T. Kotani and E. Takasugi, Prog. Theor. Phys., Suppl. **83** (1985) 1.

[50] E. Moya de Guerra, Phys. Rep. **138** (1986) 293.

[51] H. Ejiri et al., Nucl. Phys. **A611**, 85 (1996).

[52] H. Ejiri, Phys. Rep. 338 (2000) 265.

[53] H. Ejiri et al., nucl-ex/9911008.

[54] J. Ellis and S. Lola, Phys. Lett. **B458**, 310(1999).

[55] J. Engel, P. Vogel, and M. R. Zirnbauer, Phys. Rev. C **37**, 731 (1988).

[56] J. Engels, K. Langanke, and P. Vogel, Phys. Lett. B **389**, 211 (1996).

[57] J. Engel, S. Pittel, M. Stoitsov, P. Vogel, and J. Dukelsky, Phys. Rev. C **55**, 1781 (1997).

[58] J. Engels, K. Langanke, and P. Vogel, Phys. Lett. B **429**, 215 (1998).

[59] S. R. Elliott et al., Phys. Rev. C **46**, 1535 (1992).

[60] M. Ericson, T. Ericson, and P. Vogel, Phys. Lett. **B328**, 259 (1994).

[61] M. Danilov et al., Phys. Lett., to be published; hep-ex/0002003

[62] A. Faessler and F. Šimkovic, J. Phys. G **24**, 2139 (1998).

[63] Faessler A, Kovalenko S, Šimkovic F and Schwieger J, Phys. Rev. Lett **78**, 183 (1997); Proceeding of the Int. Workshop on Non-Accelerator New Physics (NANP'97), Dubna, Russia, June 1997, 1998 Phys. Atom. Nucl. **61** 1329

[64] A. Faessler and F. Šimkovic, Prog. Part. Nucl. Phys. 48 (2001) 233; F. Šimkovic, P. Domin, A. Faessler, Preprint hep-ph/0204278. A.

[65] Faessler, S. Kovalenko, F. Šimkovic, and J. Schwieger, Phys. Rev. Lett. **78**, 183 (1997); A. Faessler, S. Kovalenko, and F. Šimkovic, Phys. Rev. **D 58**, 115004 (1998);

[66] E.Fermi, "Versuch einer Theorie der β-Strahlen. I" Z.Phys. **88** (1934)

[67] A.L. Fetter and J.D. Walecka, *Quantum Theory of Many-Particle Systems* (McGraw-Hill, New York, 1971);

[68] R.P. Feynman and M. Gell-Mann, Phys. Rev. **109** (1958) 193

[69] E. Fiorini, Phys. Rep. **307**, 309 (1998).

[70] H. Flocard, P. Quentin and D. Vautherin, Phys. Lett. B **46** (1973) 304; P. Quentin and H. Flocard, Annu. Rev. Nucl. Part. Sci. **28** (1978) 253; P. Bonche, H. Flocard, P.H. Heenen, S.J. Krieger, and M.S. Weiss, Nucl. Phys. A **443** (1985) 39.

[71] H. Flocard, P. Quentin, A.K. Kerman, and D. Vautherin, Nucl. Phys. A **203** (1973) 433.

[72] P. Fisher, B. Kayser, and K. D. McFarland, hep-ph/9906244.

[73] W.H.Furry, "On transition probabilities in Double-Beta Disintegration", Phys. Rev. **56**, 1184-1193 (1939)

[74] G. Gelmini and M. Rondacelli, Phys. Lett. **B99**, 411 (1981).

[75] A. Sh. Georgadze et al., Phys. At. Nucl. **58**, 1093 (1995).

[76] Georgi H M, Glashow S L and Nussinov S Nucl. Phys. **B193**, 297 (1981)

[77] H. Georgi and S. L. Glashow, hep-ph/9808293.

[78] N. Van Giai and H. Sagawa, Phys. Lett. B **106** (1981) 379.

[79] S.L. Glashow, Nucl. Phys. **22** (1961) 597 .

[80] A.L. Goodman, Phys. Rev. C **63**, 044325 (2001).

[81] A.L. Goodman, Adv. Nucl. Phys. **11**, 263 (1979).

[82] A.L. Goodman, G.L. Struble, and A. Goswami, Phys. Lett. B **26**, 260 (1968).

[83] A.L. Goodman, G.L. Strube, J. Bar-Touv, and A. Goswami, Phys. Rev. C **2**, 380 (1970).

[84] A. L. Goodman, Nucl. Phys. A **186**, 475 (1972).

[85] A.L. Goodman, Phys. Rev. C **58**, R3051 (1998); A.L. Goodman, Phys. Rev. C **60**, 014311 (1999).

[86] A.Goswami, Nucl. Phys. **60**, 228 (1964).

[87] H. Grawe, R. Schubart, K. Maier, and D. Seweryniac, Phys. Scr. **56**, 71 (1995).

[88] H. Grawe et al., Highlight of Modern Nuclear Structure, Proceedings of the 6th International Spring Seminar on Nuclear Physics, S. Agata, Italy, 1998, edited by A. Covello (World Scientific, Singapore, 1998).

[89] A. Griffiths and P. Vogel, Phys. Rev. C**46**, 181 (1992).

[90] K. Grotz and H.V. Klapdor, Phys. Lett. B 157 (1985) 242.

[91] K. Grotz and H.V. Klapdor-Kleingrothaus, *The Weak Interactions in Nuclear, Particle and Astrophysics* (Adam Hilger, Bristol, New York, 1990);

[92] M. Günther et al., Phys. Rev. D **55**, 54 (1997).

[93] W.C. Haxton and G.S. Stephenson Prog. Part. Nucl. Phys. 12, 409 (1984).

[94] J.A. Halbleib and R.A. Sorensen, Nucl. Phys. A **98**,542 (1967).

[95] K. Hara, Prog. Theor. Phys. **32**, 88 (1964); D.J. Rowe, Rev. Mod. Phys. **40**, 153 (1968); D. Karadjov, V.V. Voronov, and F. Catara, Phys. Lett. B **306**, 197 (1993); F. Catara, N. Dinh Dang and M. Sambataro, Nucl. Phys. A **579**, 1 (1994).

[96] R.L. Helmer *et al.*, Phys. Rev. C **55** (1997) 2802.

[97] M. Hirsch, A. Staudt, K. Muto, and H.V. Klapdor-Kleingrothaus, Nucl. Phys. A **535** (1991) 62; K. Muto, E. Bender, and H.V. Klapdor, Z. Phys. A **333** (1989) 125; K. Muto, E. Bender, T. Oda and H.V. Klapdor-Kleingrothaus, Z. Phys. A **341** (1992) 407.

[98] M. Hirsch, H. V. Klapdor-Kleingrothaus, and S. G. Kovalenko, Phys. Lett. **B372**, 181 (1996).

[99] Hirsch M, Klapdor-Kleingrothaus H V, Kovalenko S G, Phys. Rev. **D54**, 4207 (1996)

[100] J.G. Hirsch, O. Castanos, P.E. Hess, Rev. Mex. Fis. 38 Suppl. 2 (1992) 66; O. Castanos, J.G. Hirsch, P.E. Hess, Rev. Mex. Fis. 39 Suppl. 2 (1993) 29.

[101] O. Castanas, J.G. Hirsch, O. Civitarese, and P.O. Hess, Nucl. Phys. A 571 (1994) 276; J.G. Hirsch, O. Castanas, P.E. Hess and O. Civitarese, Nucl. Phys. A 589 (1995) 445; Phys. Rev. C 51 (1995) 2252.

[102] H. Homma, E. Bender, M. Hirsch, K. Muto, H.V. Klapdor-Kleingrothaus and T. Oda, Phys. Rev. C **54**, 2972 (1996).

[103] K. Ikeda, Prog. Theor. Phys. **31**, 434 (1964).

[104] W.A. Kaminski and A. Faessler, Nucl. Phys. A 529 (1991) 605.

[105] A. Kawashima, K. Takahashi, and A. Masuda, Phys. Rev. C **47**, 2452 (1993).

[106] Kayser B, Gibrat-Debu F, and Perrier F, *The Physics of Massive Neutrinos*, World Scientific, Singapore, 1985

[107] B. Kayser, Nucl. Phys. B, Proc. Suppl. **19**, 177 (1991).

[108] H.V. Klapdor-Kleingrothaus, *Springer Tracts in Modern Physics*, Vol. 163 (Springer-Verlag, 2000), pp. 69-104.

[109] H. V. Klapdor-Kleingrothaus, preprint hep-ex/9907040.

[110] H.V. Klapdor-Kleingrothaus et al., Eur. Phys. J. A 12 (2001) 147.

[111] Kobzarev IYu, *et al.*, *Sov. J. Nucl. Phys.* 32:823 (1980)

[112] J. Krumlinde and P. Möller, Nucl. Phys. A **417** (1984) 419.

[113] G.A. Lalazissis, S. Raman and P. Ring, At. Data and Nucl. Data Tables **71** (1999) 1.

[114] P. Langacker and J. Wang, Phys. Rev. D **58** 093004.

[115] The LSND Collaboration, Phys. Rev. Lett. **77**, 3082 (1996) and Phys. Rev. Lett. **81**, 1774 (1998).

[116] R. Luescher et al., Phys. Lett. **B434**, 407 (1998).

[117] R. Madey, B.S. Flanders, B.D. Anderson, A.R. Baldwin, J.W. Watson, S.M. Austin, C.C. Foster, H.V. Klapdor and K. Grotz, Phys. Rev. C **40** (1989) 540.

[118] D.G. Madland and J.R. Nix, Nucl. Phys. A **476**, 1 (1988).

[119] E.Majorana, Nuovo Cim. (1937) 14.

[120] Goeppert-Meyer M, Phys. Rev. **48**, 512 (1935).

[121] A.B. Migdal, Theory of Finite Systems (Interscience, New York, 1967).

[122] M. Moe and P. Vogel, Ann. Rev. Nucl. Part. Sci. **44**, 247 (1994).

[123] R.N. Mohapatra Phys. Rev. D **34**, (1986) 3457.

[124] R.N. Mohapatra and P.B. Pal, *Massive Neutrinos in Physics and Astrophysics* (World Scientific, Singapore, 1991);

[125] P. Moller and J. Randrup, Nucl. Phys. A **514** (1990) 1.

[126] P. Möller, and J.R. Nix, Nucl. Phys. A **536**, 20 (1992).

[127] P. Möller, J.R. Nix, W.D. Myers and W.J. Swiatecki, At. Data Nucl. Data Tabl. 59 (1995) 185.

[128] A. Morales, Nucl. Phys. B, Proc. Suppl. **77**, 335 (1999).

[129] E.M. Muller, K. Muhlhans, K. Neergard, and U. Mosel, Nucl. Phys. A **383**, 233 (1982).

[130] K. Muto, E. Bender and H.V. Klapdor, Z. Phys. A **334**, 177 (1989).

[131] W. Nazarewicz, T.R. Werner, and J. Dobaczewski, Phys. Rev. C **50**, 2860 (1994).

[132] X. Sarazin et al., Nucl. Phys. **B70** (Proc. Suppl), 239 (1999).

[133] R. Nojarov, Z. Bochnacki, and A. Faessler, Z. Phys. A 324 (1986) 289.

[134] L.Pacearescu, A.Faessler, F.Šimkovic "Nuclear deformation and the double beta decay" to appear in Yadernaya Fizika.

[135] L.Pacearescu, V.Rodin, F.Šimkovic, A.Faessler, Phys.Rev.C**68** (2003) 064310

[136] Y.V. Palchikov, J. Dobeš, and R.V. Jolos, Phys. Rev. C **63**, 034320 (2001).

[137] G. Pantis, F. Šimkovic, J.D. Vergados, and A. Faessler, Phys. Rev. C **53**, 695 (1996).

[138] Paes H, Hirsch M, Klapdor-Kleingrothaus HV, and Kovalenko SG, *Phys. Lett. B* 453:194 (1999);ibid 498:35 (2001)

[139] W.Pauli "Brief an die Gruppe der Radioactiven...", Zürich, 4 Dezember, 1930

[140] B. Pontecorvo, J. Exptl. Theoret. Phys. **34** (1958) 247 [Sov. Phys. JETP **7** (1958) 172].

[141] B. Pontecorvo, Phys. Lett. **B26**, 630 (1968).

[142] H. Primakoff and S. P. Rosen, Rep. Prog. Phys. **22**, 121(1959).

[143] A.A. Raduta, V. Ceausescu, A. Gheorghe, and M. Popa, Nucl. Phys. A 427 (1984) 1.

[144] A.A. Raduta, A. Faessler, S. Stoica, and W.A. Kaminski, Phys. Lett. B 254 (1991) 7; Nucl. Phys. A 534 (1991) 149.

[145] A.A. Raduta, A. Faessler, and D.S. Delion, Nucl. Phys. A **564** (1993) 185; Phys. Lett. B **312** (1993) 13; Nucl. Phys. A **617** (1997) 176.

[146] A.A. Raduta, F. Šimkovic, A. Faessler, J. Phys. **G 26**, 793 (2000);

[147] P. Raghavan, At. Data Nucl. Data Tables **42** (1989) 189; N.J. Stone, Oxford University, preprint (2001).

[148] S. Raman, C.H. Malarkey, W.T. Milner, C.W. Nestor Jr. and P.H. Stelson, At. Data Nucl. Data Tables **36** (1987) 1.

[149] V. Rodin and A. Faessler, Phys. Rev. C **66** 051303(R) (2002).

[150] V. Rodin, M.H. Urin, A. Faessler, nucl-th/0311101

[151] O.A. Rumyantsev and M.H. Urin, Phys. Lett. **B443** (1998) 51.

[152] A. Salam, Proc. of the 8th Nobel Symposium on *Elementary Particle Theory, Relativistic Groups and Analyticity*, edited by N. Svartholm, 1969.

[153] T.S. Sandhu, M.L. Rustgi, and A.L. Goodman, Phys. Rev. C **12**, 1340 (1975).

[154] T,S. Sandhu, and M.L. Rustgi, Phys. Rev. C **14**, 675 (1976).

[155] P. Sarriguren, E. Moya de Guerra, R. Nojarov and A. Faessler, J. Phys. G: Nucl. Part. Phys. **20** (1994) 315; J.M. Udias, R. Nojarov and A. Faessler, J. Phys. G: Nucl. Part. Phys. **23** (1997) 1673.

[156] P. Sarriguren, E. Moya de Guerra, and R. Nojarov, Phys. Rev. C **54** (1996) 690; P. Sarriguren, E. Moya de Guerra, and R. Nojarov, Z. Phys. A **357** (1997) 143.

[157] P. Sarriguren, E. Moya de Guerra, A. Escuderos, and A.C. Carrizo, Nucl. Phys. A **635** (1998) 55; P. Sarriguren, E. Moya de Guerra, and A. Escuderos, Nucl. Phys. A **658** (1999) 13; Nucl. Phys. A **691** (2001) 631; Phys. Rev. C **64** (2001) 064306.

[158] P. Sarriguren, E. Moya de Guerra, L. Pacearescu, A. Faessler, F. Šimkovic, and A.A. Raduta, Phys. Rev. C **67**, 044313 (2003).

[159] P. Sarriguren, R. Alvarez-Rodriquez, E. Moya de Guerra, L. Pacearescu, A. Faessler, F. Šimkovic submitted to Phys. Rev. C.

[160] W. Satula, and R. Wyss, Phys. Lett. B **393**, 1 (1997).

[161] W. Satula, and R. Wyss, Nucl. Phys. A **676**, 12 (2000).

[162] W. Satula and R.A. Wyss, Acta Phys. Polon. B **32**, 2441 (2001).

[163] J. Schechter and J. W. F. Valle, Phys. Rev. D **25** (1982) 2951.

[164] Schepkin M G Sov. Phys. Usp.**27** 555 (1984)

[165] K.W. Schmid, F. Grümmer, and A. Faessler, Ann. Phys. (NY) **180**, 1 (1987).

[166] M. D. Shuster and M. Rho, Phys. Lett. **B42**, 54 (1972).

[167] J. Schwieger, F. Šimkovic, and A. Faessler, Nucl. Phys. A 600 (1996) 179.

[168] J. Schwieger, F. Šimkovic, A. Faessler, W.A. Kamiński. Phys. Rev. **C 57**, 1738 (1998);

[169] F. Šimkovic, G. Pantis, and A. Faessler, Phys. Atom. Nucl. **61**, 218 (1998).

[170] F. Šimkovic, G. Pantis, A. Faessler, Prog. Part. Nucl. Phys. 40 (1998) 285;

[171] F. Šimkovic, G. Pantis, and A. Faessler, Phys. Atom. Nucl. **61**, 218 (1998). F. Šimkovic, G. Pantis, J.D. Vergados, and A. Faessler, Phys. Rev. **C 60**, 055502 (1999);

[172] F. Šimkovic, G. Pantis, J.D. Vergados, and A. Faessler, Phys. Rev. **C 60**, 055502 (1999);

[173] F. Šimkovic, N. Nowak, W.A. Kamiński, A.A. Raduta and A. Faessler, Phys. Rev. **C 64**, 035501 (2001).

[174] F. Šimkovic, A.A. Raduta, M. Veselský, and A. Faessler, Phys. Rev. **C 61** , 044319 (2000).

[175] F. Šimkovic, P. Domin, S.V. Semenov, J. Phys. G 27 (2001) 2233.

[176] F. Šimkovic, Ch. Moustakidis, L. Pacearescu and A. Faessler, Phys. Rev. **C 68** (2003) 054319.

[177] F. Šimkovic, L. Pacearescu and A. Faessler, to appear in Nucl. Phys. A.

[178] V.G. Soloviev, *Theory of complex nuclei*, Pergamon press, 1976.

[179] A. Staudt, K. Muto, and H. V. Klapdor-Kleingrothaus, Europ. Lett. **13**, 31 (1990).

[180] S. Stoica and H.V. Klapdor-Kleingrothaus, Eur. Phys. J. A **9**, 345 (2000); Phys. Rev. **C 63**, 064304 (2001); Nucl. Phys. A **694**, 269 (2001).

[181] E.C.G. Sudarshan and R. Marshak, Phys. Rev. **109** (1958) 1860 .

[182] J. Suhonen and O. Civitarese, Phys. Rep. **300**, 123 (1998).

[183] J. Suhonen, J. Taigel, and A. Faessler, Nucl. Phys. A 486 (1988) 91.

[184] J. Suhonen, Phys. Lett. B 477 (2000) 99.

[185] The Super-Kamiokande Collaboration, Phys. Rev. Lett. **81**, 1562 (1998); the K2K Collaboration, Phys. Rev. Lett. **90**, 041801 (2003); the SNO Collaboration, Phys. Rev. Lett. **87**, 071301 (2001) and Phys. Rev. Lett. **89**, 011301 (2002); the KamLAND Collaboration, Phys. Rev. Lett. **90**, 021802 (2003).

[186] Y. Tanaka, Y. Oda, F. Petrovich, and R.K. Sheline, Phys. Lett. B **83**, 279 (1979).

[187] N. Takaoka, Y. Motomura, K. Nagao, Phys. Rev. C **53**, 1557 (1996).

[188] T.Tomoda and A. Faessler, Phys. Lett. B **199**, 475 (1987).

[189] T. Tomoda, Rep. Progr. Part. Phys. **54**, 53 (1991).

[190] J. Toivanen, J. Suhonen, Phys. Rev. Lett. 75 (1995) 410.

[191] J. Toivanen and J. Suhonen, Phys. Rev. **C 55**, 2314 (1997)

[192] V. I. Tretyak and Yu. Zdesenko, At. Data Nucl. Data Tables **61**, 43 (1995).

[193] V.I. Tretyak, Yu.G.Zdesenko, At.Data Nucl.Data Tables **80**, 83 (2002).

[194] A. L. Turkevich, T. E. Economou, and G. A. Cowan, Phys. Rev. Lett. **67**, 3211 (1991).

[195] M. Vallières and D.W.L. Sprung, Can. J. Phys. **56** (1978) 1190.

[196] D. Vautherin and D. M. Brink, Phys. Rev. C **5** (1972) 626; D. Vautherin, Phys. Rev. C **7** (1973) 296.

[197] J. D. Vergados, Phys. Rev. C**24**, 640 (1981).

[198] J.D. Vergados Phys. Lett. **184B**, (1987) 55.

[199] J. D. Vergados, *Beyond the Desert 99*, Ringberg Castle, June 99; hep-ph/9907316.

[200] J.D. Vergados, Phys. Rep. 361 (2002) 1.

[201] P. Vogel, B. Jonson, and P.G. Hansen, Phys. Lett. B **139**, 227 (1984).

[202] P. Vogel and M.R. Zirnbauer, Phys. Rev. Lett. **57**, 3148 (1986);

[203] P. Vogel, M. Ericson, and J. D. Vergados, Phys. Lett. **B212**, 259 (1988); K. Muto, Phys. Lett. **B277**, 13 (1992).

[204] S.R. Elliott and P. Vogel, Ann. Rev. Nucl. Part. Sci. 52 (2002) 115.

[205] H. de Vries, C.W. de Jager and C. de Vries, At. Data Nucl. Data Tables **36** (1987) 495; G. Fricke, C. Bernhardt, K. Heilig, L.A. Schaller, L. Schellenberg, E.B. Shera, C.W. de Jager, At. Data and Nucl. Data Tables **60** (1995) 177.

[206] L. Zamick and N. Auerbach, Phys. Rev. C 26 (1982) 2185.

[207] Yu. Zdesenko, Rev. Mod. Phys. 74 (2002) 663.

[208] S. Weinberg, Phys. Rev. Lett. **19** (1967) 1264 .

[209] H.H. Wolter, A. Faessler, P.U. Sauer, Phys. Lett. B **31**, 516 (1970); Nucl. Phys. A **167**, 108 (1971).

[210] C.S. Wu *et al.*, Phys. Rev. **105** (1957) 1413.

[211] K. E. You et al., Phys. Lett. **B265** 53 (1991).

[212] Yanagida T, *Proc. Workshop on Unified Theory* Sawada and Sugamoto eds., KEK, (1979); Gell-Mann M, Ramond P, and Slansky R, *Supergravity*, van Nieuwenhuizen and Freedman eds., North Holland, Amsterdam (1979)

CURRICULUM VITAE

PERSONAL INFORMATION

Address: Institute fuer Theoretische Physik,
Auf der Morgenstelle 14, 72076 Tuebingen, Germany
Place and date of birth: November 9, 1974 in Târgu-Jiu, Romania
Citizenship: Romanian

EDUCATION

1989 - 1993   "Tudor Vladimirescu" high-school,   Târgu Jiu
  ●*Baccalaureate Diploma* (Summer 1993)
1993 - 1998 University of Bucharest,   Faculty of Physics
  ●*Bachelor of science and engineer title* (Summer 1998)
  ●Physics Major in Theoretical and Applied Nuclear Physics
1998 - 2000   University of Bucharest,   Faculty of Physics
  ●*Master of Science* (Summer 2000)
  ●Physics Major in Elementary Particle and High Energy
2001-present   University of Tuebingen
   ●Ph.D at "Institute fuer Theoretische Physik", Uni-Tuebingen, (Theoretical
Physics)
  Thesis: "Single and Double Beta Decay in Deformed Nuclei"

WORK EXPERIENCE

1998-2001 *Research Assistant*
"National Institute for Physics and Nuclear Engineering - Horia Hulubei", Bucharest
  Research Topic
  ●Theoretical aspects concerning coherent states and group theory applied in
  Nuclear Theoretical Physics
Jan, Feb 2003
"Bartol Research Institute", University of Delaware, Newark, USA
  Research Topic
  ●Shell-Model calculations, J-DMRG method
6-16 Nov. 2003
Dept. fuer Physik und Astronomie, University of Basel, Switzerland
  Research Topic
  ●Nuclear Astrophysics